WATEREUSE FOUNDATION

Leaching of Metals from Aquifer Soils during Infiltration of Low-Ionic-Strength Reclaimed Water

Determination of Kinetics and Potential Mitigation Strategies

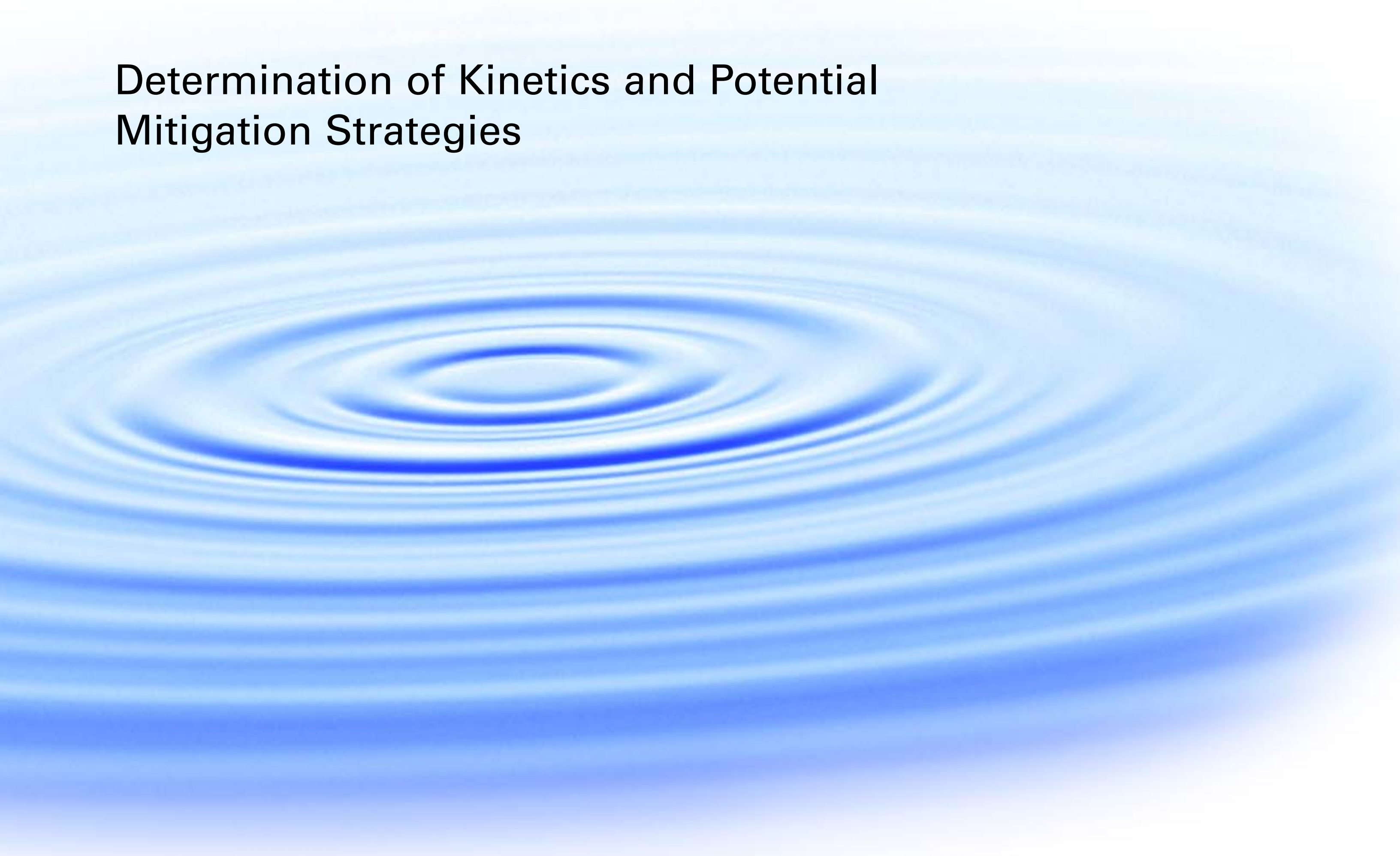

Leaching of Metals from Aquifer Soils during Infiltration of Low-Ionic-Strength Reclaimed Water

About the WateReuse Foundation

The mission of the WateReuse Foundation is to conduct and promote applied research on the reclamation, recycling, reuse, and desalination of water. The Foundation's research advances the science of water reuse and supports communities across the United States and abroad in their efforts to create new sources of high quality water through reclamation, recycling, reuse, and desalination while protecting public health and the environment.

The Foundation sponsors research on all aspects of water reuse, including emerging chemical contaminants, microbiological agents, treatment technologies, salinity management and desalination, public perception and acceptance, economics, and marketing. The Foundation's research informs the public of the safety of reclaimed water and provides water professionals with the tools and knowledge to meet their commitment of increasing reliability and quality.

The Foundation's funding partners include the Bureau of Reclamation, the California State Water Resources Control Board, the Southwest Florida Water Management District, the California Energy Commission, and the California Department of Water Resources. Funding is also provided by the Foundation's Subscribers, water and wastewater agencies, and other interested organizations.

Leaching of Metals from Aquifer Soils during Infiltration of Low-Ionic-Strength Reclaimed Water

Determination of Kinetics and Potential Mitigation Strategies

Qilin Li, Ph.D.
Mason Tomson, Ph.D.
Philip Bedient, Ph.D.
Department of Civil and Environmental Engineering,
Rice University

Cosponsor
Bureau of Reclamation

Published by the WateReuse Foundation
Alexandria, VA

Disclaimer

For more information, contact:
WateReuse Foundation
1199 North Fairfax Street, Suite 410
Alexandria, VA 22314
703-548-0880
703-548-5085 (fax)
www.WateReuse.org/Foundation

WateReuse Foundation Project Number: WRF-06-005
WateReuse Foundation Product Number: 06-005-01

ISBN: 978-1-934183-25-0

Library of Congress Control Number: 2009940466

Printed in the United States of America

♻Printed on Recycled Paper

CONTENTS

Chapter 6. Groundwater Flow and Reactive Transport Models

FIGURES

TABLES

FOREWORD

The WateReuse Foundation, a nonprofit corporation, sponsors research that advances the science of water reclamation, recycling, reuse, and desalination. The Foundation funds projects that meet the water reuse and desalination research needs of water and wastewater agencies and the public. The goal of the Foundation's research is to ensure that water reuse and desalination projects provide high-quality water, protect public health, and improve the environment.

A Research Plan guides the Foundation's research program. Under the plan, a research agenda of high-priority topics is maintained. The agenda is developed in cooperation with the water reuse and desalination communities including water professionals, academics, and Foundation Subscribers. The Foundation's research focuses on a broad range of water reuse research topics including:

- Definition and addressing of emerging contaminants;
- Public perceptions of the benefits and risks of water reuse;
- Management practices related to indirect potable reuse;
- Groundwater recharge and aquifer storage and recovery;
- Evaluation and methods for managing salinity and desalination; and
- Economics and marketing of water reuse.

The Research Plan outlines the role of the Foundation's Research Advisory Committee (RAC), Project Advisory Committees (PACs), and Foundation staff. The RAC sets priorities, recommends projects for funding, and provides advice and recommendations on the Foundation's research agenda and other related efforts. PACs are convened for each project and provide technical review and oversight. The Foundation's RAC and PACs consist of experts in their fields and provide the Foundation with an independent review, which ensures the credibility of the Foundation's research results. The Foundation's Project Managers facilitate the efforts of the RAC and PACs and provide overall management of projects.

The Foundation's primary funding partners include the Bureau of Reclamation, California State Water Resources Control Board, the Southwest Florida Water Management District, the California Energy Commission, Foundation Subscribers, water and wastewater agencies, and other interested organizations. The Foundation leverages its financial and intellectual capital through these partnerships and funding relationships.

This research project assesses the potential for metal leaching during surface infiltration operations using reverse osmosis (RO)-treated wastewater and evaluates strategies for mitigating risks associated with metal leaching. The report is intended to inform utilities of major water quality parameters that contribute to leaching of metals of public health concern and to suggest strategies that may be used to mitigate the associated risk.

David L. Moore
President
WateReuse Foundation

G. Wade Miller
Executive Director
WateReuse Foundation

ACKNOWLEDGMENTS

This project was funded by the WateReuse Foundation in cooperation with the Bureau of Reclamation.

This study would not have been possible without the insights, efforts, and dedication of many individuals and organizations. These include the members of the research team and Project Advisory Committee members (identified below); the WateReuse Foundation's project manager, Burnett King; and key individuals at the participating utilities.

The research team thanks the WateReuse Foundation for funding this applied research project, as well as the following organizations for making in-kind contributions: Groundwater Services, Inc. (TX), the Scottsdale Water Campus (AZ), and the Lake Havasu City Island Wastewater Treatment Plant (AZ).

Principal Investigator and Project Manager
Qilin Li, Ph.D., Rice University

Co-Principal Investigators
Mason Tomson, Ph.D., Rice University
Philip Bedient, Ph.D., Rice University

Research Project Team
Xianhuai Huang, Ph.D., Rice University
Birnur Guven, Ph.D., Rice University
Jianwei Ma, Rice University
Diego Gomez, Rice University

Project Advisory Committee
Bob Arnold, University of Arizona
Gordon Treweek, Chino Basin Watermaster
Don Phipps, Orange County Water District (CA)
James Yahnke, Bureau of Reclamation

EXECUTIVE SUMMARY

Leaching of metals with a negative health impact from vadose zone soil and aquifer materials is a major concern when one is choosing reverse osmosis (RO)-treated water for artificial groundwater recharge because of the low total-dissolved-solid (TDS) concentration in RO-treated water. This report is intended to inform recharge utilities of major water quality parameters that contribute to leaching of metals of public health concern and to suggest strategies that may be used to mitigate the associated risk.

The research project assesses the potential for metal leaching during surface infiltration operations using RO-treated wastewater and evaluates strategies for mitigating risks associated with metal leaching.

By use of vadose zone soils and aquifer materials from two existing recharge sites (the Water Campus Project [WCP] in Scottsdale, AZ, and the Island Wastewater Treatment Plant [IWWTP] at Lake Havasu City, AZ), the effects of solution pH, TDS, ionic composition, and redox condition on desorption equilibrium and kinetics of major metal species were studied. Arsenic was identified as the major contaminant of concern at the WCP site. Contamination mitigation by mixing RO water with a local surface water with a higher Ca concentration and alkalinity was evaluated both through column experiments and through groundwater transport model simulation. The major findings of the study are:

- Arsenic desorption increases slightly with pH because of the higher solubility of arsenic species at higher pH; this effect is, however, largely negated by the lower solubility of carbonate minerals, the main source of desorbable arsenic in the soil samples tested. The buffering capacity of dissolved carbonates stabilizes pH.
- TDS of the recharge water strongly impacts the ion-exchangeable metals, with metal desorption increasing with TDS; arsenic desorption does not change significantly with TDS because of the undetectable amount of ion-exchangeable arsenic in the soil samples.
- Ionic composition of the recharge water has great impact on metal desorption. With the soil samples tested, arsenic desorption decreases with the Ca concentration in the recharge water because of the reduced calcite dissolution, suggesting that lime or soda ash conditioning may be an effective strategy to mitigate arsenic leaching during the recharge.
- Desorption of all metals is biphasic, with a fast and a slow desorption site, and can be well described by a two-first-order-reaction model.
- Both column experiments and groundwater transport model simulation demonstrate that mixing the RO water with a recharge water of a higher Ca concentration and alkalinity can effectively mitigate the metal leaching problem.

CHAPTER 1

INTRODUCTION AND RESEARCH OBJECTIVES

Rapid growth of the world population and the consequent water supply depletion as well as water quality deterioration have caused serious concerns for human and environmental sustainability. At present, one-third of the world's population lives in water-stressed countries, and this figure is predicted to double by 2025 (Simon, 1998). The worldwide water shortage poses an urgent demand for means of producing drinking water from untraditional sources, including domestic wastewater, contaminated surface water, urban runoff, and irrigation return flow. Artificial groundwater recharge using reclaimed water provides an alternative source of potable water. It helps restore depleted groundwater levels, provides a barrier to saline intrusion in coastal areas, and facilitates water storage during times of high water availability to mitigate water shortage problems during dry periods in areas with inconsistent natural recharge of aquifers.

Artificial groundwater recharge can be achieved by three methods: surface spreading or infiltration, vadose zone injection, and direct aquifer injection. Surface spreading is the most widely used method for artificial groundwater recharge (Todd, 1980). In a surface-spreading operation, reclaimed water is spread over surface channels (in-channel systems) or basins (off-channel systems), percolates through the unsaturated or vadose zone, and recharges unconfined aquifers. During the percolation through the vadose zone and storage in the aquifer, the reclaimed water undergoes a series of physical, chemical, and biological processes such as filtration of suspended solids, adsorption and biodegradation of organic matter, adsorption and precipitation of metals, deposition and/or deactivation of pathogenic microorganisms, and dilution by native groundwater. As a result, water quality is improved if the reclaimed water is of lower quality than the native groundwater. This process is usually called soil-aquifer treatment (SAT). Organic and clayey soils and clayey sands/gravels and permeable sands (namely, combinations of sand, silt, and clay) are the most suitable subsoils for wastewater effluent disposal and treatment. In contrast, once the recharge water enters the aquifer bedrock, the rate of purification declines.

1.1 MUNICIPAL WASTEWATER AS RECHARGE WATER

The quality and composition of municipal wastewater vary widely from location to location. Depending on the targeted use of the recharge water, treatment of wastewater before recharge may include preliminary, primary, secondary, and advanced (or tertiary) treatment and disinfection.

Preliminary and primary treatment mainly removes suspended solids and the organic matter associated with them. It does not remove total dissolved solids (TDS) or dissolved organic compounds and has little effect on biological contaminants. However, in locations where the extracted water is used for nonpotable purposes, SAT has been successful if one is using primary effluent as the recharge water (Lance et al., 1980; Carlson et al., 1982; Rice and Bouwer, 1984).

Secondary treatment consists of an aerobic biological process where soluble and colloidal biodegradable organic matter and suspended solids are removed. Depending on the operation, removal of microorganisms can be achieved at different levels. Similar to the primary treatment, secondary treatment provides little to no TDS removal. TDS levels of secondarily treated municipal wastewater effluent vary from 210 mg/L to as high as 4580 mg/L in the United States (National Research Council, 1994). Some heavy metals but not all are removed during secondary treatment. Heavy metals usually found in secondary effluent include arsenic (As), boron (B), chromium (Cr), cadmium (Cd), copper (Cu), lead (Pb), zinc (Zn), nickel (Ni), and mercury (Hg) (Treweek, 1985; Crook, 1992).

Advanced treatment processes are used to further remove suspended solids and dissolved organic as well as inorganic substances when higher-quality reclaimed water is necessary. Advanced treatment usually includes nitrification, denitrification, phosphorus removal, and drinking water treatment processes such as coagulation-flocculation, sedimentation, filtration, activated carbon adsorption, and nanofiltration (NF) or reverse osmosis (RO). The recharge water after advanced treatment processes typically has low concentrations of both organic and inorganic species, especially after NF or RO treatment.

RO and NF membranes provide very high removal efficiency for both organic and inorganic species. The use of RO and NF membranes in advanced wastewater reclamation employing secondary treated wastewater effluent to produce water for indirect potable consumption has increased over the past few years (Ang et al., 2006). Salt removal by NF membranes varies from ~50% for loose NF membranes to ~95% for tight NF membranes, whereas salt rejections of most RO membranes are as high as 99%. Therefore, NF- or RO-treated water typically has much lower TDS levels than does the secondary effluent and often even lower than that of local surface water. Moreover, both NF and RO membranes remove divalent and multivalent ions better than they remove monovalent ions. Therefore, NF- or RO-treated water has a higher ratio of monovalent ions to multivalent ions, reflected by the higher sodium adsorption ratio (SAR). Both the TDS level and the SAR are very important parameters to consider when selecting source water for artificial recharge. The TDS level and SAR of a water determines whether a water tends to disperse flocculated clay (Bouwer, 1978). The combination of low TDS levels and high SAR usually indicates a strong tendency toward clay dispersion.

1.2 POTENTIAL FOR GROUNDWATER CONTAMINATION BY TRACE METALS

Artificial recharge using source waters of impaired quality can potentially introduce microbial, inorganic, and organic contaminants into groundwater. Meanwhile, biochemical and geochemical reactions between the recharge water and the aquifer materials may lead to mobilization of inorganic species that are part of the mineral framework of the aquifer. In addition, contaminants previously immobilized in the vadose zone may leach out and be carried into the groundwater by the recharge water during infiltration of the recharge water. The adverse impacts of these mobilized contaminants on groundwater quality and consequently on human health are of concern.

Metals, unlike hazardous organics, cannot be degraded. In addition to the primary metals Al, Fe, and Mn, a number of heavy metals are naturally present in soil, such as Zn, Cu, Ba, As, Cr, Pb, Ni, and Co. Many soils in arid areas contain naturally occurring, easily leachable contaminants of relevance to drinking water quality, notably F, B, As, Cr, Pb, and Ba (Baker et al., 1998). Metals can also enter the subsurface with the artificial recharge water. Heavy metal accumulation was found in the top 60-cm horizon of recharge basins by using reclaimed municipal wastewater (Bouwer and Chaney, 1974; Banin et al., 2002). These trace metals are usually associated with clays, hydrous metal oxides and sulfides, and soil organic matter. Such association is heavily influenced by the solution condition of the aqueous milieu, including pH, total ionic strength, redox potential, and the presence of organic or inorganic chelating agents and of competing cations. Immobilization of metals by mechanisms of adsorption and precipitation prevents movement of the metals into groundwater. Usually, metal-soil interaction is such that when metals are introduced at the soil surface, downward transportation does not occur to any great extent unless the metal retention capacity of the soil is overloaded or unless metal interaction with the associated aqueous phase enhances its mobility. The extent of vertical contamination is intimately related to the solution and surface chemistry of the soil matrix with reference to the metal and solution matrix.

1.3 FATE OF METALS IN THE SOIL ENVIRONMENT

In soil, metals exist in the following forms as described by Shuman (1991): dissolved in the soil aqueous phase, occupying exchange sites on inorganic soil constituents, specifically adsorbed on inorganic soil constituents, associated with insoluble soil organic matter, precipitated as pure or mixed solids, present in the structure of secondary minerals, and/or present in the structure of primary minerals. The aqueous fraction and fractions in equilibrium with it, namely, the exchangeable fraction, are of primary importance when one is considering the migration potential of metals associated with soils.

The concentration of metals in the soil aqueous milieu, at any given time, is governed by a number of interrelated processes, including inorganic and organic complexation, oxidation-reduction, precipitation/dissolution, and adsorption/desorption reactions. Most studies of the behavior of metals in soils have been carried out under equilibrium conditions. Equilibrium data indicate which reactions are likely to occur under prescribed conditions but do not indicate the period involved. The kinetics of oxidation-reduction, precipitation/dissolution, and adsorption/desorption reactions in many cases is critical to predict the behavior of metals in soils. Unfortunately, our understanding of the kinetic aspect of metals in the soil matrix suffers from a lack of published data. Without kinetic information, the current accepted approach is to assume that local equilibrium occurs in the soil profile. Thermodynamic equilibrium data are then applied not only to predict which precipitation/dissolution, adsorption/desorption, and/or oxidation-reduction reactions are likely to occur under a given set of conditions but also to estimate the solution composition, namely, metal concentration in solution, at equilibrium (Elprince and Sposito, 1981; Harter and Lehmann, 1983; Sparks, 1989). This approach relies heavily on the accuracy of thermodynamic data that can be found in the literature.

When changes in solution chemistry occurs, trace metals may leach out because of 1) direct dissolution of minerals containing trace metals, 2) desorption from the mineral frame as well as from the soil organic materials, 3) dissolution of hydrous metal oxide and sulfide minerals and consequent release of previously adsorbed trace metals, and 4) dispersion of clay colloids and consequent mobilization of clay-associated trace metals. These processes can occur when the solution chemistry of the recharge water differs significantly from the aqueous phase with which the soil is in equilibrium. Downward displacement of heavy metals during reclaimed wastewater recharge has been reported in several studies (Streck and Richter, 1997; Johnson et al., 1999).

1.3.1 Factors Affecting Metal-Soil Interactions

Interactions between metals and soil mainly involve precipitation/dissolution and sorption/desorption. These processes are influenced by the interplay of various solution chemistry parameters, including pH, total ionic strength, redox potential, and the presence of chelating agents and competing cations. The effect of each parameter is explained below.

1.3.1.1 Solution pH

Solution pH affects mineral solubility, metal speciation in the aqueous environment, and adsorption/desorption equilibrium of metals on oxides and clay minerals. The pH of the soil system is a very important parameter, directly influencing sorption/desorption, precipitation/dissolution, complex formation, and oxidation-reduction reactions. In general, adsorption of cationic metals increases with pH, whereas that of anionic metals decreases with pH. For example, cations such as Cd^{2+}, Cu^{2+}, Pb^{2+}, and Zn^{2+} were found to adsorb more strongly at high pH (Lion et al., 1982; Arias, 2005; Lin et al., 2004), while anionic Cr(VI) and As(V, III) were adsorbed more strongly at low pH (Ghosh et al., 2006; Weng, 1994). In a study of heavy metal retention in a SAT system, good correlation was found between pH and partition coefficients of Cu^{2+}, Ni^{2+}, and Zn^{2+} (Lin et al., 2004). Desorption of metals has also been found to depend on pH (Arias et al., 2005). Desorption of cations from clay and a variety of oxides at low pH has been reported in a number of studies (Davis and Kent, 1990; Murray, 1975; Bradbury and Baeyens, 1999). In a recent study of the impact of acid rain, mobilization of Ni, Be, Cd, and Co was reported when the acidification front moved through the vadose zone and the metal concentration peaks were found to migrate with the acidification front (Kjoller et al., 2004). However, because of the complexity of the soil-waste system with its myriad surface types and with solution composition, such a generalization does not hold true for all cases. For example, cationic metal mobility has been observed to increase with increasing pH because of the formation of metal complexes with dissolved organic matter (Lin et al., 2004; Ghosh et al., 2006).

1.3.1.2 Total ionic strength

Total ionic strength is related to the TDS concentration in water. It directly affects mineral precipitation/dissolution equilibria. Meanwhile, because of its impact on surface zeta potential, total ionic strength or TDS concentration also has a strong influence on metal adsorption through ion exchange, as well as through filtration of colloidal materials in the recharge water and the associated metals. It affects the coagulation/dispersion behavior of clays and therefore the fate and transport of trace metals associated with them. Water of low ionic strength can cause mobilization of colloid-associated trace contaminants. In a study by Johnson et al. (1999), an RO-treated water with a very low TDS level was found to cause significant leaching of As, F, and Ba. Dissolution of carbonate minerals was indicated.

At specific adsorption sites, trace cationic metals are preferentially adsorbed over the primary cations (Na, Ca, and Mg) and trace anionic metals are preferentially adsorbed over major anions (SO_4^-, NO_3^-, and soluble ionized organic acids) (Ghosh et al., 2006). However, when specific adsorption sites become saturated, exchange reactions dominate and competition for these sites with major ions becomes important. Harter (1992) studied Cu, Ni, and Co sorption by calcium-saturated soils. At a pH of >5.6, the presence of Ca, a common ion in soils, did not affect Cu sorption but limited the sorption of Co and Ni. This fact can have profound implication on development of best management practices. For example, a typical management practice for metal-contaminated soils is to raise the pH to 7, often using a Ca-buffered system. This approach, however, may lead to leaching of Co and Ni according to Harter's results (Harter, 1992).

The presence of competing cations, whether primary or trace metals, can significantly affect the mobility of the metal of interest. Data that do not reflect the complex mixture of metals specific to a site may not be helpful to understanding or accurately predicting metal mobility.

1.3.1.3 Redox potential

The effect of redox potential on metal leaching is very complex. Redox potential determines the oxidation states of metals and therefore the solubility of the mineral. For example, iron oxides undergo reductive dissolution to form Fe(II), which may lead to release of trace metals originally associated with the iron oxides or oxyhydroxides. In anoxic and sulfidic environments, iron oxide and oxyhydroxide phases dissolve and form FeS and FeS_2, which have adsorption properties different from those of iron oxides or oxyhydroxides. Allen (1995) and Kelly (2005) found that arsenic solubility was controlled by oxidation-reduction conditions and that arsenic accumulated in solution only in the most reducing water. In this case, arsenic is likely released from the solid phase as ferric oxide is reduced. However, in an aquifer with abundant sulfide under reductive conditions, arsenic may be strongly bound to the sulfide phase. As a result, arsenic may be released from soil as iron sulfide is oxidized under aerobic conditions. The behavior of chromium also illustrates the importance of redox conditions to metal movement in soils. Hexavalent Cr(VI) is highly toxic and relatively mobile, while trivalent Cr(III) is far less toxic and relatively insoluble and strongly adsorbs to surfaces.

In soils, reducing conditions are brought about by the absence of oxygen (anaerobic). This situation occurs in waterlogged soils or soils contaminated with oxygen-consuming compounds. The consumption of oxygen could be either chemical or biological. The biological consumption of oxygen is the result of microbes utilizing organic contaminants in the soil system. Oxidizing conditions (aerobic) are normally found in well-drained soils as well as in soils that have not been subjected to contamination by spills or leaks.

The degree of oxidation or reduction is indicated by the redox potential measurement. The four general ranges of redox conditions as suggested by Patrick and Mahapatra (1968) that may be encountered in soils at a pH of 7 are oxidized soils (> +400 mV), moderately reduced soils (+400 to +100 mV), reduced soils (+100 to −100 mV), and highly reduced soils (−100 to −300 mV). The redox state of a soil, as discussed above, usually is closely related to the microbial activity and the type of substrate available to the organisms.

1.3.1.4 Chelating agent

Organic ligands such as aquatic humic substances form complexes with a large number of metals. Association of metals to dissolved organic matter in the aqueous phase affects metal speciation and therefore solubility (Morel and Hering, 1993). On the other hand, metal binding to particulate organic matter in soil is a major sorption mechanism. Binding of heavy metals such as Cu, Cr, Ni, Co, Zn, Pb, and U to natural organic matter has been reported in a number of studies (Prado and Airoldi, 2003; Schmitt et al., 2000; Filella and Town, 2001; Glaus et al., 2000). Kelly et al. (2005) reported that high concentrations of arsenic were almost always found in wells with total organic carbon (TOC) of >2 mg/L. Other well-known metal-chelating organic substances are organic phosphonates, a group of compounds widely used in detergents and corrosion and scale inhibition (Bordas and Bourg, 1998). Inorganic ligands that may affect metal speciation and mineral solubility include chloride (Cl^-), carbonate (CO_3^{2-}), sulfide (S^{2-}), and polysulfide (Giblin et al., 1986; Gardner, 1974; Boulegue et al., 1982). Metal-organic complexation is also affected by solution pH and total ionic strength (Bose and Reckhow, 1997; Lippold et al., 2005).

1.3.1.5 Competing cations

Cations in the aqueous phase may compete with each other for sorption sites (Agbenin and Olojo, 2004) as well as for chelating ligands (Zhou et al., 2005). In particular, high concentrations of sodium have been found to displace divalent cations as well as protons from the surface (Backstrom et al., 2004; National Research Council, 1994), both contributing to trace metal mobilization. Displacement of trace metals by competing cations from soil directly results in groundwater contamination. Displacement of Ca^{2+} occurs when the recharge water has a high SAR. The combination of high SAR and low TDS can result in clay dispersion by removing the “cementing” effect of Ca^{2+}. Dispersion of clay colloids may lead to clogging of the soil layer or, more important, mobilization of trace metals associated with clays. Displacement of H^+ by Na^+ can lower solution pH, leading to desorption of metal cations.

1.3.2 Current Knowledge on Behaviors of Individual Metals in Soils

The most important chemical processes affecting the behavior and bioavailability of metals in soils are those involved in adsorption of metals from the liquid phase on to the solid phase and its reverse process, namely, desorption. These processes control the concentrations of metal ions and complexes in the soil solution and thus exert a major influence on the groundwater quality.

1.3.2.1 Zinc

Zinc is readily adsorbed by clay minerals, carbonates, or hydrous oxides. As with all cationic metals, Zn adsorption increases with pH. Zinc hydrolyzes when $pH > 7.7$, and these hydrolyzed species are strongly adsorbed to soil surfaces.

1.3.2.2 Cadmium

Cd may be adsorbed by clay minerals, carbonates, or hydrous oxides of iron and manganese or may be precipitated as cadmium carbonate, hydroxide, and phosphate. As with all cationic metals, the chemistry of Cd in the soil environment is, to a great extent, controlled by pH. Under acidic conditions, Cd solubility increases and very little adsorption of Cd by soil colloids, hydrous oxides, and organic matter takes place. At pH values greater than 6, Cd is adsorbed by the soil solid phase or is precipitated and the solution concentration of Cd is greatly reduced (Benjamin and Leckie, 1981; Alloway, 1990; McLean and Bledsoe, 1992).

1.3.2.3 Lead

Soluble Pb added to the soil reacts with clays, phosphates, sulfates, carbonates, hydroxides, and organic matter such that Pb solubility is greatly reduced. At pH values above 6, Pb either adsorbs on clay surfaces or forms $PbCO_3$. Of all the trace metals in soils, Pb is retained by soils and soil constituents to the greatest extent under typical environmental conditions.

1.3.2.4 Nickel

Ni does not form insoluble precipitates in unpolluted soils, and retention for Ni is, therefore, exclusively through adsorption mechanisms. Ni will adsorb to clays, iron and manganese oxides, and organic matter and is thus removed from the soil solution (Alloway, 1990; Hickey and Kittrick, 1984).

1.3.2.5 Arsenic

In the soil environment arsenic exists as either arsenate, As(V) (AsO_4^{3-}), or arsenite, As(III) (AsO_3^{3-}). Arsenite is the more mobile and toxic form of arsenic. Arsenite compounds are reported to be 4 to 10 times more soluble than arsenate compounds (Griffin and Shimp, 1978; Pierce and Moore, 1980). The behavior of arsenate in soil is analogous to that of phosphate because of their chemical similarity. Like phosphate, arsenate forms insoluble precipitates with iron, aluminum, and calcium (Hingston et al., 1971; Anderson et al., 1976). Iron in soils is most effective in controlling arsenate's mobility. Both pH and redox potential are important in assessing the fate of arsenic in soil. At high redox levels, As(V) dominates and arsenic mobility is low. As the pH increases or the redox potential decreases, As(III) dominates. This reduced form of arsenic is more subject to leaching because of its high solubility. However, the reduction kinetics is usually slow.

1.4 RESEARCH OBJECTIVES

Reclaimed water recharged into aquifers represents a significant source of potable water. Among the high-priority research initiatives surrounding this source of water is the association of metals of public health concern with soil particles during aquifer transportation and storage. These metals are influenced by the aqueous milieu, including ionic strength, pH, and redox potential of the surrounding groundwater. Observations from aquifer storage and recovery (ASR) sites have indicated the potential for metal mobilization in response to shifts in introduced water chemistry. Introduction of reclaimed water with TDS levels significantly lower than those in groundwater may significantly disturb chemical equilibria, possibly resulting in dissociation of some of these metals and subsequent mobilization into the groundwater. Depending on the kinetics of desorption, leached metals may produce regions of unacceptable water quality.

The overall research objective of the proposed study is to evaluate the potential for release of metals of public health concern from surface infiltration operations when reclaimed water of low TDS is used for recharge. Specific goals of the project include the following:

- Evaluate the effects of solution chemistry, for example, ionic strength, pH, and redox potential, on trace metal immobilization;

- Compare the potentials for metal leaching of different soil types and identify key soil characteristics related to metal leaching;

- Obtain trace metal desorption kinetics data for batch and continuous-flow systems; and

- Develop metal transport models for evaluation of contamination mitigation strategies.

CHAPTER 2

COLLECTION AND ANALYSIS OF WATER AND SOIL SAMPLES

2.1 COLLECTION AND ANALYSIS OF WATER SAMPLES

Water samples were collected from two recharge sites: the Water Campus Project (WCP) in Scottsdale, AZ, and the Island Wastewater Treatment Plant (IWWTP) in Lake Havasu City, AZ.

2.1.1 Site Identification and Sample Collection

The WCP site was identified in the proposal development stage. Two recharge waters are used for vadose zone injection at the WCP site: municipal wastewater treated to drinking water quality by using microfiltration (MF) and RO and Colorado River water transported through the Central Arizona Project (CAP) canal and treated by MF. They will be referred to as RO water and CAP water in the rest of the report. These two recharge waters are very good models for low- and high-TDS recharge waters for this study. The RO water has a typical TDS concentration of 40 to 50 mg/L, pH of 6.5, and no detectable heavy metals. The CAP water is the only surface water source nearby and was used to approximate natural recharge in the area. The CAP water was used as both the model surface water and high-ionic-strength recharge water in our study.

The locations of the WCP WWTP and the CAP water treatment plant are shown in the map in Figure 2.1.

The IWWTP recharge site was selected mainly because of its shallow water table and hence ease of obtaining aquifer material samples. Previous groundwater quality data of samples taken from monitoring wells near the recharge facility show some high concentrations of As, Ba, and Cr, indicating the presence of these metals in the aquifer material. The location of the IWWTP is shown in Figure 2.2.

One hundred twenty liters of RO water was collected on August 2, 2007, from the RO permeate line at the WCP wastewater reclamation plant by staff members of the WCP and was shipped overnight to the lab at Rice University. The sampling line was purged with RO permeate water for a few minutes before sample collection. Twenty liters of MF-treated CAP water was collected following the same sampling procedure from the permeate line of the MF process at the CAP treatment plant on August 21, 2007. A groundwater sample was collected on August 23, 2007, from monitoring well 5B at the IWWTP site. The sample site was approximately 500 ft from the eastern border of the IWWTP and more than 1000 ft from the nearest wastewater infiltration pond. The well was installed to a total depth of approximately 30 ft with screened interval from 25 to 30 ft bgs. The static water level measured 24.45 ft below the top of the casing prior to purging. Field measurements for pH, specific conductivity, and temperature were taken periodically (every 5 gal) throughout purging (see Appendix 1 for groundwater sampling record and Appendix 2 for water quality data). After roughly 35 gal was purged, a 20-L sample was taken, put on ice packs, and shipped overnight to the lab at Rice University.

All samples were taken with 25-L high-density polyethylene containers. The containers were rinsed at least twice with the sample water before collection of the sample.

FIGURE 2.1. Area map of water campus. Scottsdale, AZ.

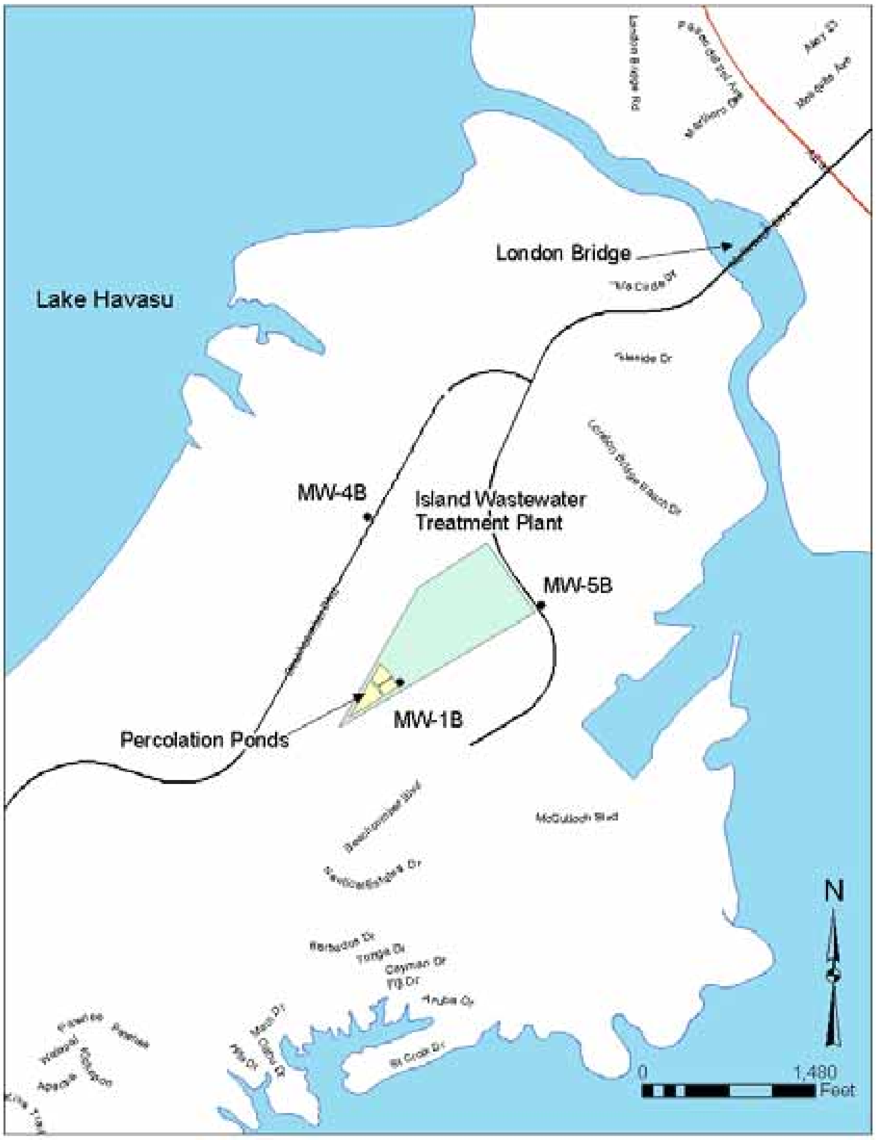

FIGURE 2.2. Location of IWWTP.

2.1.2 Water Sample Analysis

Upon arrival at Rice University, the water samples were immediately stored at 4 °C in an environmental chamber. Water quality analysis was performed within 2 days after sample arrival. The pH, TDS, and conductivity of water samples were measured by using a pH/conductivity meter (pH/CON 510; OAKTON Instruments, IL). TOC concentrations were determined using a combustion-based total organic carbon analyzer (TOC-V_{CSH}; Shimadzu Scientific Instruments, Kyoto, Japan). Heavy metals as well as other relevant metal species were analyzed by using inductively coupled-atomic emission spectrometry (ICP-AES) or ICP-mass spectrometry (ICP-MS) (ELAN9000; Perkin-Elmer,CA), as described later. Table 2.1 lists some water quality parameters relevant to this study. Metals not listed in the table were below the detection limits of our analytical methods. The reporting limit of detection is provided in Table 2.2.

TABLE 2.1. Relevant Water Quality Data for RO and CAP Waters at WCP and for Groundwater at IWWTP[a]

Variable Measured		Mean or SD Measured at:					
		RO		CAP		GW	
		Mean	SD	Mean	SD	Mean	SD
pH		6.24	0.28	7.8	0.02	7.1	0.18
Total alkalinity (mg/L as $CaCO_3$)		19	0.24	110	0.35	287.8	0.49
TOC (mg/L)		0.4	0.13	2.4	0.22	4.7	0.35
TDS (ppm)		25.6	3.2	505.6	9.3	866	0.49
Conductivity (μS)		50.6	0.25	1082.5	14.7	1726	0.62
Metals (mg/L)	K	1.25	0.0376	5.48	0.0261	11.4	0.011
	Na	8.9	0.236	98.5	0.2347	515.6	0.11
	Ca	0.24	0.0059	74.62	0.2063	128.6	0.104
	Mg	0.107	0.004	30.94	0.0721	50.21	0.026
	Fe	ND	—	0.19	0.011	0.321	0.011
	Al	ND	—	ND	—	ND	—
Metals (μg/L)	Mn	ND	—	ND	—	ND	—
	Ba	ND	—	135	3.0	34.6	0.67
	Pb	ND	—	ND	—	ND	—
	As	ND	—	3.887	0.02	5.53	0.09
	Zn	ND	—	ND	—	ND	—
	Cr	ND	—	13.636	2.80	36.152	0.20

[a] GW, groundwater; ND, “not detected.”

TABLE 2.2. RLD for Metals Analyzed

Variable Measured	Primary Metal*									
	K	Na	Ca	Mg	Fe	Al				
RLD (mg/L)	0.15	1.01	0.96	0.07	0.01	0.14				
Trace metal$^{\#}$	Mn	As	Ba	Cr	Cd	Cu	Hg	Ni	Pb	Zn
RLD (µg/L)	3	2	21	2	2	15	14	12	3	9

* analyzed by ICP-AES; #, analyzed by ICP-MS. RLD, reporting limit of detection.

2.2 IDENTIFICATION, COLLECTION, AND ANALYSIS OF SOIL SAMPLES

2.2.1 Sampling Site Identification

The primary criterion for selection of soil sampling site is heavy metal content of the soil. Because of the limited soil characteristic data we found from surface infiltration sites, we did not limit soil sampling to surface infiltration sites.

The same sites for water sample collection, the WCP in Scottsdale and the IWWTP in Lake Havasu City, were chosen for soil sampling. Because metal leaching will most likely occur when the reclaimed water percolates through the vadose zone, the decision was made to take vadose zone soil samples from an uncontaminated site. The vadose zone soil at the WCP recharge site had been found to contain As, Cr, Cd, Ni, and Ba, making it a good candidate soil for this study. Saturated aquifer material samples were needed to evaluate the potential water quality changes in the aquifer. Two criteria were used in selecting the aquifer material sampling site: 1) because of budget constraints, the site needed a shallow aquifer, and 2) the aquifer material contained reasonable amounts of different heavy metals. The recharge site at IWWTP has an average water table of 26 ft bgs. Although soil characteristic data are not available, previous groundwater sample analysis at this site found high concentrations of As, Ba, and Cr, indicating the presence of these metals in the aquifer material. Therefore, the IWWTP recharge site was chosen for sampling of aquifer materials.

2.2.2 Soil Sample Collection

At the WCP site, both the top layer (from the surface to approximately 200 ft) and the aquifer (approximately 550 ft bgs), are sand dominated with silt and gravel, with silt-dominated soils in between. On May 11, 2007, a new well, no. 140, was drilled by using a reverse circulation rotary drilling method near the WCP recharge site. Drill cuttings at depths of 180', 400', 550', and 700' (designated S180, S400, S550, and S700, respectively) were collected in polyethylene freezer bags and kept in new 1-gal paint cans by Maurice Tatlow, the hydrogeologist for the Water Resource Department of Scottsdale. Once sample collection was complete, the samples were packed with blue ice in coolers and shipped by FedEx overnight. Upon arrival, soil samples were immediately stored in an environmental chamber at 4 °C. Between sample collection and transportation, the samples were stored in a refrigerator at 4 °C on the WCP site. The sample from each interval was mixed before packing.

Undisturbed core samples were collected at the IWWTP site on August 23, 2007. Soil sampling was performed using a hollow-stem auger drilling rig operated by Yellow Jacket Drilling Services, based in Phoenix, AZ. A clean 8-in. auger was used to advance the borehole located in the southwest corner of the parking lot south of the main office building and east of the wastewater percolation pond. The boring was advanced initially to 20 ft bgs without collecting samples. Beginning at 20 ft bgs, a sampler sleeve was lowered through the hollow augers, hammered 1 ft into the undisturbed soil below the augers, and retrieved for sample collection. The augers were then advanced 1 ft into the subsurface and the process repeated to a total depth of 36 ft. Each sample collection returned two 2-in. (diameter) by 6-in. (length) undisturbed core samples contained in brass sleeves, and the samples were denoted LHCXX (XX stands for the depth bgs where the sample was collected). The samples were sealed with square Teflon sheets and capped at each end to ensure minimal headspace and to prevent further disturbance or air intrusion during shipping. Samples were placed on ice, shipped overnight to the lab at Rice University, and immediately stored in the environmental chamber at 4 °C. Some samples were sectioned in the lab to provide adequate sample volume for further characterization and subsequent desorption studies. A general description of subsurface stratigraphy was obtained through analysis of the cuttings returned when advancing the augers (see attached boring log SB-1 in Appendix 1). The water table was encountered at the depth of 28 ft bgs.

2.2.3 Sample Pretreatment

Some of the soil samples were processed shortly after arrival in the lab for soil characterization. Since it is difficult to obtain a representative sample with wet or damp materials, wet soil samples are usually dried, crushed, and ground to reduce subsample variability, provided that drying does not affect the extraction of the analytes of interest in the sample. The soil samples were air-dried in a fume hood (Purifier Bio-safety Class II Cabinet) at ambient temperature (~22 °C) to prevent contamination by the environment. Because the soil samples from the WCP site contain a large amount of drilling fluid, the bulk of the drilling fluid was carefully removed before drying of the soil samples. After 120 h, about 98% water was removed from the soil samples. The air-dried samples were mixed thoroughly to achieve homogeneity, sieved using a USS no. 10 sieve (2-mm diameter), and stored in plastic bags before characterization. Soil aggregates were broken by hand and plastic mallet before sieving.

2.2.4 Soil Characterization

Major soil characteristics important to sorption/desorption of heavy metals include mineralogical composition, hygroscopic moisture, soil pH, particle size distribution, specific surface area, pore size distribution, organic matter, cation-exchange capacity (CEC), and total metal load. All soil characterization tests were conducted using a soil fraction smaller than 2 mm in diameter, which was thoroughly mixed before use. Analysis of these soil characteristics is described in detail below.

Soil pH was measured in water suspensions with a 1:1 soil-to-water ratio. For all other characterizations, aliquots of soil samples were oven-dried at 105 °C until constant weight was attained. Analytical methods used for soil characterization are summarized in Table 2.3.

TABLE 2.3. Analytical Methods for Soil Characterization[a]

Soil Characteristic	Analytical Method
Mineralogical composition	XRD to identify major mineral phases
Major element analysis	SEM/EDAX
Hygroscopic moisture	Analysis of weight loss after oven drying at 105 °C
Particle size distribution	Sieve analysis using ASTM standard sieves
BET surface area	N_2 adsorption/desorption
Pore size distribution	N_2 adsorption/desorption
Organic matter	Analysis of weight loss after heating at 400 °C for 4 h (Nelson and Sommers, 1975; Ben-Dor and Banin, 1989)
Metal concn	Wet extraction followed by ICP or ICP-MS analysis
CEC	Polemio and Rhoades method (Polemio and Rhoades, 1977)

[a] XRD, X-ray diffraction; SEM/EDAX, scanning electron microscopy–energy-dispersive analysis of X-rays.

The CEC of soils is an indication of metal fractions that are easily leachable. To determine the soil CEC, a modification of the method developed by Polemio and Rhoades (1977) was adopted. This method is recommended for analysis of soils in arid areas (Page et al., 1982) and is directly applicable to the soil samples collected in this project. The procedure involves three steps: 1) saturation of cation-exchange sites with Na by equilibrating the soil with a 60% ethanol solution containing 0.4 N sodium acetate (NaAc) and 0.1 N NaCl at pH = 8.2, 2) extraction with 0.5 N $Mg(NO_3)_2$ to replace Na^+, and 3) measurement of total Na^+ and Cl^- concentrations in the extracted solution. Measurement of Cl^- is required so that the soluble Na^+ from the excess saturating solution carried over from the saturation step can be deducted from the total Na^+ to obtain exchangeable Na, which is equivalent to the CEC. CEC can be then calculated by the following equation:

$$\mathrm{CEC} = (Na^+_t - Na^+_{sat,sol}) = Na^+_t - (Cl^-_t)(Na^+/Cl^-)_{sat.sol.}$$

where Na^+_t is total Na^+ concentration in the extracted solution, $Na_{sat,sol}$ is the residual Na in the solution from the saturation step, Cl_t is total Cl^- in the extracted solution, and $(Na^+/Cl^-)_{sat\ sol}$ is the ratio of Na and Cl in the saturation solution.

BET surface areas (N_2 physisorption at 77 K) were obtained with an ASAP 2010 analyzer (Micromeritics Instrument Co., GA) using high-purity N_2 (Mittler Supply Inc., IN). Prior to analysis, the catalyst surfaces were degassed to remove physisorbed volatile substances, initially under vacuum at room temperature for 2 h, after which the temperature was ramped to 150 °C (25 °C/min) and held in a vacuum for 4 h. After sample degassing, the sample test tubes were connected to an ASAP 2010 analysis port and N_2 adsorption and desorption curves were obtained, from which the BET surface area and pore size distribution were determined.

Table 2.4 summarizes some general properties of the soil samples collected at the two recharge sites. Only two samples, namely, the top and bottom core samples from the IWWTP site, were characterized. The aquifer materials from the IWWTP site are mostly fine sand, with relatively low hygroscopic moisture and CEC and little BET surface area. The soil samples from the WCP site have higher clay content. As a result, the hygroscopic moisture, CEC, and BET surface area are higher or greater than those found in the IWWTP samples. Among the samples taken from the WCP site, the sample from the 400-ft interval is rich in clay and silt. Consequently, it has the smallest particles and highest hygroscopic moisture, and CEC and most BET surface area.

TABLE 2.4. General Characteristics of Soil Samples

Value Measured	**Values for Location:**					
	WCP				**IWWTP**	
Sample ID	S180	S400	S550	S700	LFC20	LFC36
pH	8.8	8.2	8.8	8.9	8.6	8.5
Hygroscopic moisture (%)	1.2	2.8	1.2	1.0	0.5	0.7
Organic matter (mg/kg)	18.1	13.4	9.7	8.3	-	-
CEC (meq/100 g of soil)	3.3	12.6	2.5	2.3	0.8	0.7
BET surface area (m^2/g)	7.63	18.87	5.4	2.25	1.54	1.42

The particle size distributions of soil samples collected from the WCP site are shown in Figure 2.3. Consistent with the total BET surface area measurement, the S400 sample has significantly larger fractions of fine particles because of its high content of clay and silt. Because of the limited number of soil samples from the IWWTP site, particle size distribution was not tested for these samples.

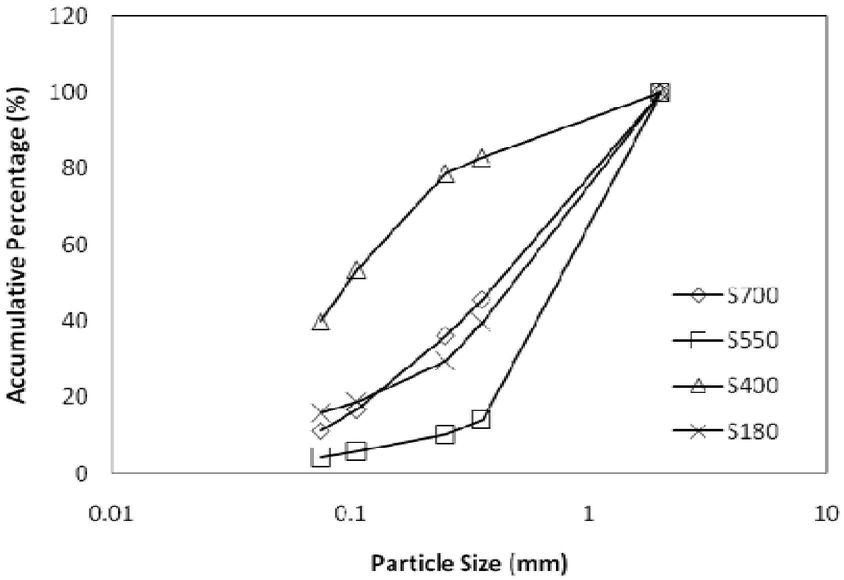

FIGURE 2.3. Particle size distribution of soil samples from the WCP site.

Pore size distributions of soil samples collected from both sites are presented in Figure 2.4. For all soil samples, the majority of the pore volume is located in pores smaller than 10 nm. There is a large fraction of micropores with pore diameters around 3.5 nm.

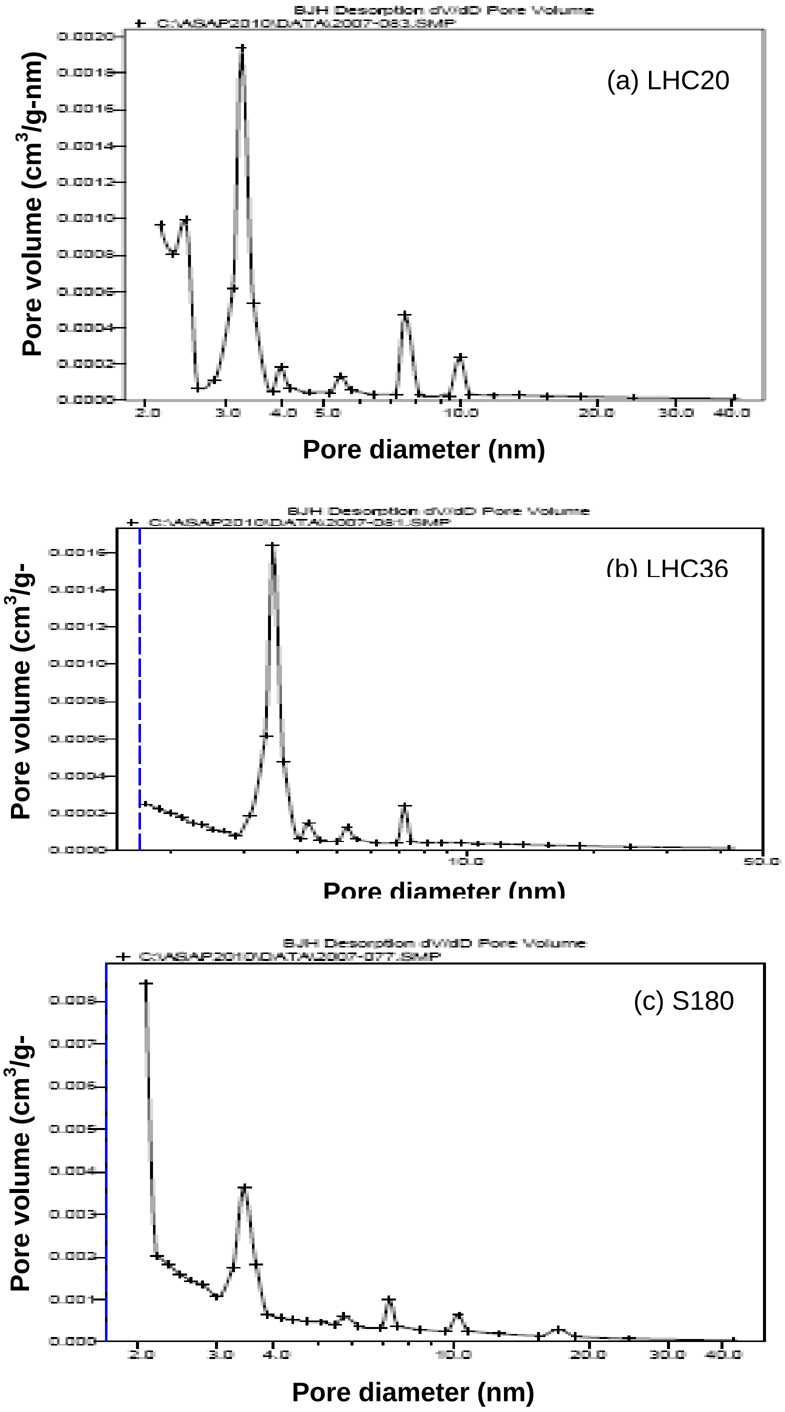

FIGURE 2.4. Pore size distributions of soil samples collected at 20' (a) and 36' (b) from the IWWTP and at 180' (c), 400' (d), 550' (e), and 700' (f) from the WCP.

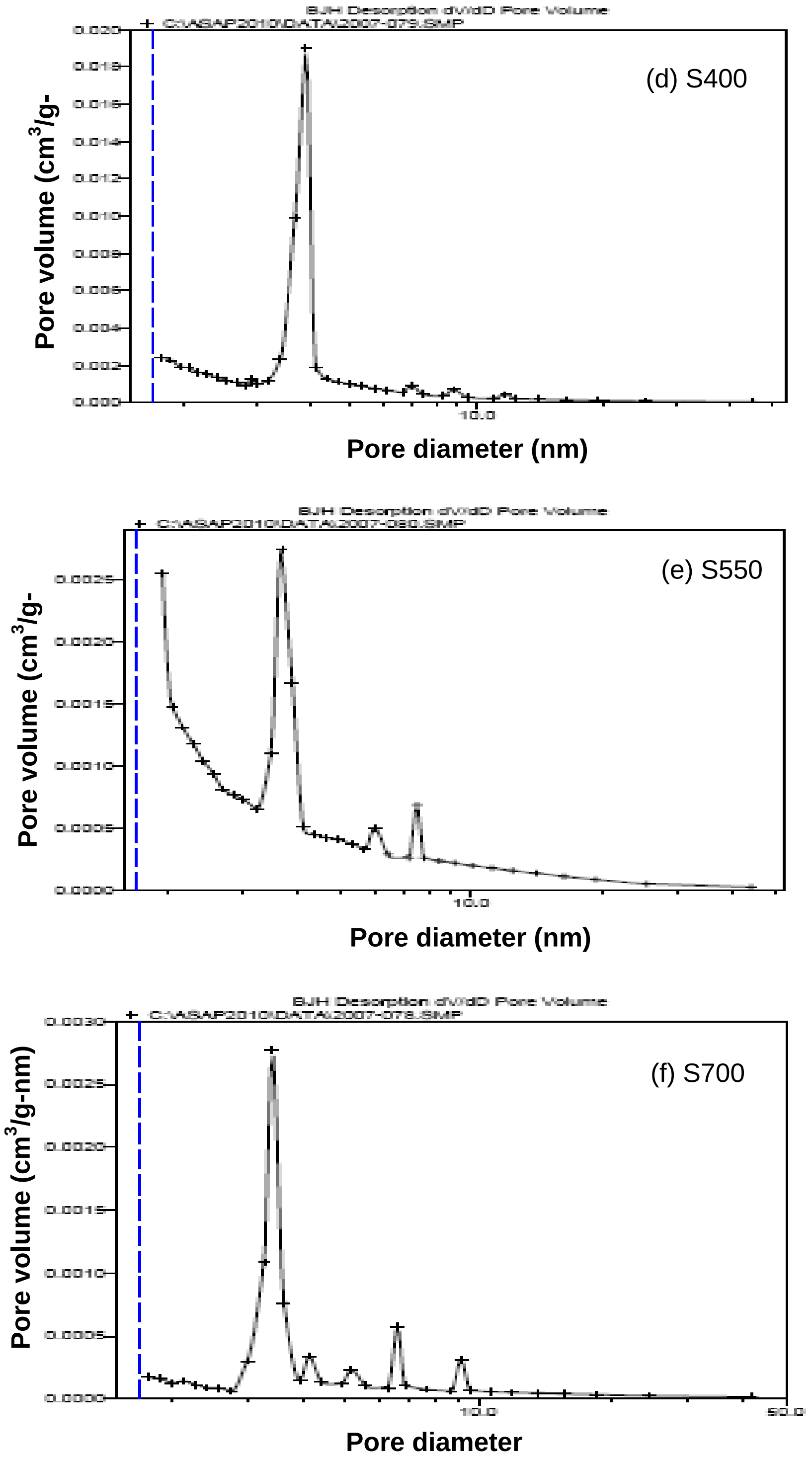

FIGURE 2.4. ***Continued.***

X-ray diffraction (XRD) (Haley et al., 2006; Cengiz et al., 2004) was used to determine the mineralogical composition of soil samples. XRD analyses were performed using a Rigaku® D/Max Ultima II Powder Diffractometer with Cu Kα radiation. The samples were scanned from 2θ of 10° to 80° at a scan rate of 0.02° 2θ/s. The data obtained were processed using JADE 7.5 data-processing software and the ICDD PDF-2 database.

XRD spectra of soil samples taken at different intervals at the WCP and IWWTP sites are included in Appendix 2. XRD analyses show that the primary minerals in the soil samples from the WCP site are quartz and calcite, while quartz is the predominant mineral in aquifer materials at the IWWTP site. Although XRD analysis did not reveal mineralogical sources of heavy metals or primary metals other than Ca, these minerals could have been present at low concentrations and were not detected by XRD analysis.

Scanning electron microscopy (SEM) with energy-dispersive analysis of X-rays (EDAX) was used for analysis of major elements in soil (Righi and Elsass, 1996). SEM/EDAX analyses were performed using a JEOL® 6500 scanning electron microscope equipped with a back-scattered electron detector for compositional and topographical imaging. Samples for SEM/EDAX analyses were prepared by attaching the soil particles on an adhesive tape placed on a sample stub. Coating of the samples with a conductive material (Au) was necessary prior to the analysis. An accelerating voltage of 20 to 25kV was used for all analyses.

SEM/EDAX results (Appendix 3) show a close similarity in elemental compositions of the soils at the WCP and IWWTP sites. The results are summarized in Table 2.5. Aluminum, iron, and magnesium, although abundant in the soil (ca. 4.1 to 8.3 wt %, 2.5 to 5.3 wt % and 0.9 to 2.6 wt %, respectively), were not identified in any of the main crystalline phases from the XRD analysis, indicating their presence in amorphous phases.

TABLE 2.5. Elemental Composition of Soil Samples

	Findings for:											
	WCP								**IWWTP**			
	S180		**S400**		**S550**		**S700**		**LHC20**		**LHC36**	
Element	**Wt %**	**At %**	**Wt %**	**At %**	**Wt %**	**At %**	**Wt %**	**At %**	**Wt %**	**At %**	**Wt %**	**At %**
O	43.3	60.1	41.8	58.4	44.1	60.1	40.2	56.6	45.4	61.2	47.0	62.0
Si	29.1	23.0	31.4	25.0	30.7	24.0	35.9	28.8	36.6	28.0	37.4	28.1
Al	7.83	6.44	8.3	6.8	7.2	5.9	7.3	6.1	4.1	3.3	4.7	3.7
Ca	6.81	3.8	4.9	2.7	6.2	3.4	3.5	2.0	6.9	3.7	3.9	2.1
Fe	4.7	1.9	5.3	2.1	3.9	1.5	5.3	2.1	2.8	1.1	2.5	1.0
Mg	2.3	2.1	2.6	2.4	2.1	1.9	1.7	1.5	1.1	1.0	0.9	0.8
K	2.4	1.4	2.4	1.4	2.4	1.3	2.9	1.7	1.7	0.9	2.1	1.2
Na	1.1	1.1	0.7	0.7	1.1	1.1	0.9	0.9	0.8	0.7	1.4	1.3

Details of analysis of metals in soil are described below.

2.3 SOLID-PHASE AND AQUEOUS-PHASE METAL ANALYSIS

Major metal species analyzed included alkaline metals (Na and K), alkaline earth metals (Ca, Mg, Ba, and Al), and other metals (Mn, Al, Fe, Cu, Zn, As, Cr, Cd, Ni, Hg, and Pb).

2.3.1 Analysis of Metals by ICP-AES or ICP-MS

All aqueous samples including soil extracts were analyzed for target metals as well as other relevant metal species by using ICP-AES or ICP-MS. ICP analysis has the advantage of high speed, low detection limits, and excellent sensitivity and precision.

The standard solutions of metals were prepared by using single-element standards at 1000 µg/mL (CPI International, CA). Prior to measurement, all aqueous samples or soil extracts were filtered with 0.22-µm-pore-size syringe filters followed by acidification with 2% nitric acid. All metals were measured simultaneously by using ICP-AES or ICP-MS. All samples were analyzed in duplicate.

2.3.2 Analysis of Metals in Soil

Concentrations of metals in soil were determined by wet digestion followed by ICP-AES or ICP-MS analysis of the extracts. Upon arrival, aliquots of the soil samples were air-dried, ground, and sieved through a standard USS no. 10 sieve according to standard methods (Page et al., 1982). The soil fraction that passes the no. 10 sieve was used in the subsequent analysis.

Total metal analysis was performed using the EPA 3050B method. This method determines total metal concentrations in soil that are “environmentally available.” Briefly, a representative 1- to 2-g (wet weight) or 1-g (dry weight) sample is digested with repeated additions of nitric acid (HNO_3) and hydrogen peroxide (H_2O_2). For ICP-MS analysis, the extract is reduced in volume by heating and then diluted to a final volume of 100 mL. For ICP-AES analysis, HCl is added to the initial extract and the sample is refluxed. In an optional step to increase the solubility of some metals, the extract is filtered and the filter paper and residues are rinsed, first with hot HCl and then with hot reagent water. Filter paper and residues are returned to the digestion flask, refluxed with additional HCl, and then filtered again. The extract is then diluted to a final volume of 100 mL.

Fractions of trace metals associated with different components of the soil were determined by using a stepwise sequential extraction procedure developed by Han and Banin (1997). This analysis provides information on the sources of metals in the soil. It helps one understand how changes in solution chemistry impact leaching of metals by affecting different soil components. The factions considered include soluble and exchangeable metals, carbonate-associated metals, metals associated with easily reducible oxides (such as Mn-oxides), soil organic matter-associated metals, metals associated with reducible oxides (such as Fe-oxides), and the residual fraction. The extraction reagents used as well as the digestion conditions are summarized in Table 2.6, and the procedure employed is briefly outlined below.

2.3.2.1 Soluble plus exchangeable metals

Twenty-five milliliters of 1 M NH_4NO_3 solution (pH adjusted to 7.0 with NH_4OH) were added to 1.3 g of wet soil (equivalent to 1 g of dry soil) in a 50-mL Teflon centrifuge tube, and the mixture was shaken for 30 min at room temperature. The contents were then centrifuged at 10,000 rpm for 10 min. The supernatant was decanted and filtered through a 0.45-µm-pore-size syringe filter. The soil residue was kept for the next extraction step. The same centrifugation-decantation procedure was used after each of the following extraction steps.

2.2.3.2 Elements bound to carbonate

Twenty-five milliliters of 1 M NaAc-HAc solution at a pH of 5.0 were added to the soil residue from the previous step, and the mixture was shaken for 6 h. Excess CO_2 was released by opening of the tube cap during the first 2 h.

2.2.3.3 Elements bound to easily reducible oxides

Twenty-five milliliters of 0.04 M NH_2OH-HC1 in 25% HAc solution were added to soil residue and agitated for 30 min.

2.2.3.4 Elements bound to organic matter

Three milliliters of 0.01 M HNO_3 and 5 mL of 30% H_2O_2 were added to the soil residue. The contents were digested in a water bath at 80 °C for 2 h. An additional 2 mL of H_2O_2 were added, and the content was heated for another 1 h. Fifteen milliliters of 0.01 M HNO_3 solution were added and agitated for 10 min.

2.2.3.5 Elements bound to reducible oxides

Twenty-five milliliters of 0.04 M NH_2OH-HCl in 25% HAc solution were added to the soil residue, and the mixture was digested in a water bath at 90 °C for 3 h.

2.2.3.6 Elements in the residual fraction

This fraction is calculated as the difference between the total metal determined by the EPA 3050B method and the sum of the five fractions above.

TABLE 2.6. Sequential Extraction Methods for Metal Analysis

Targeted Fraction	Reagent	pH	Soil:Solution Ratio	Temp (°C)	Digestion Time
Soluble and exchangeable	1 M NH_4NO_3	7	1:25	25	30 min
Carbonate associated	1 M NaAc-HAc	5	1:25	25	6 h
Easily reducible oxides associated	0.04 M NH_2OH-HCl, 25% HAc	2	1:25	25	30 min
Organic matter associated	30% H_2O_2, 0.01 M HNO_3	2	1:25	80	3 h
Reducible oxides associated	0.04 M NH_2OH-HCl, 25% HAc	2	1:25	90	3 h

All soil samples were analyzed in duplicate. Blank extraction tests were performed in parallel with the samples for each extraction method following exactly the same procedure for soil samples.

Figure 2.5 presents the total metal concentrations for soil samples from both recharge sites. The total metal concentrations of all soil samples are summarized in Table 2.7. Overall, the soil samples from the WCP site have higher contents of both primary and trace metals than do those from the IWWTP site. In particular, S400 feet bgs has the highest metal contents, presumably because of its small particles and high clay and silt content. In all soil samples, notable amounts of Ba, Mn, Zn, Cr, and Pb were found. The WCP soil samples also contain As, while the IWWTP aquifer materials contain notable amounts of Cu and Ni. The IWWTP aquifer materials contain very little As. This finding is unexpected because elevated concentrations of As have been reported in the groundwater at the IWWTP site.

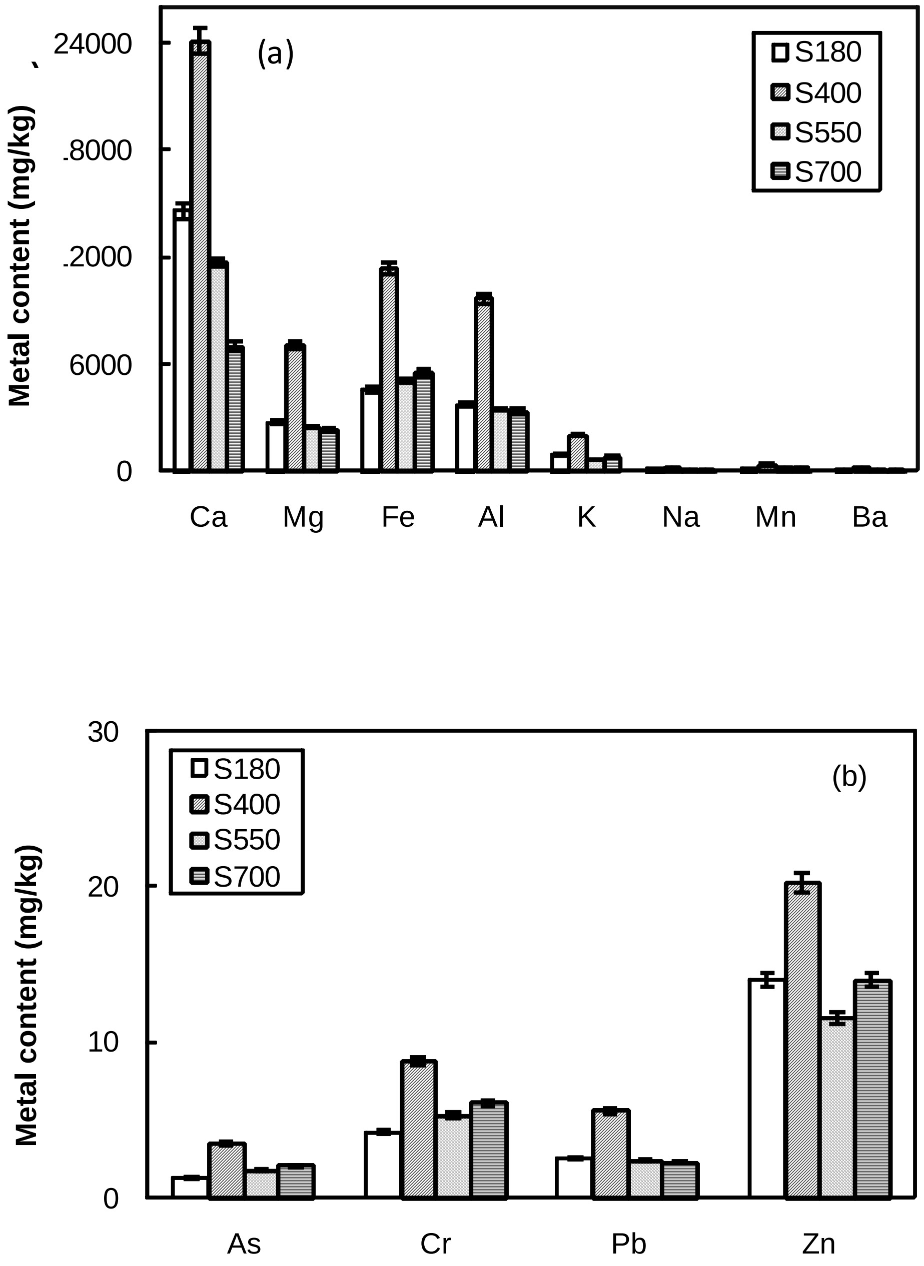

FIGURE 2.5. Primary and trace metal contents of soil samples from the WCP site (a and b) and the IWWTP site (c and d).

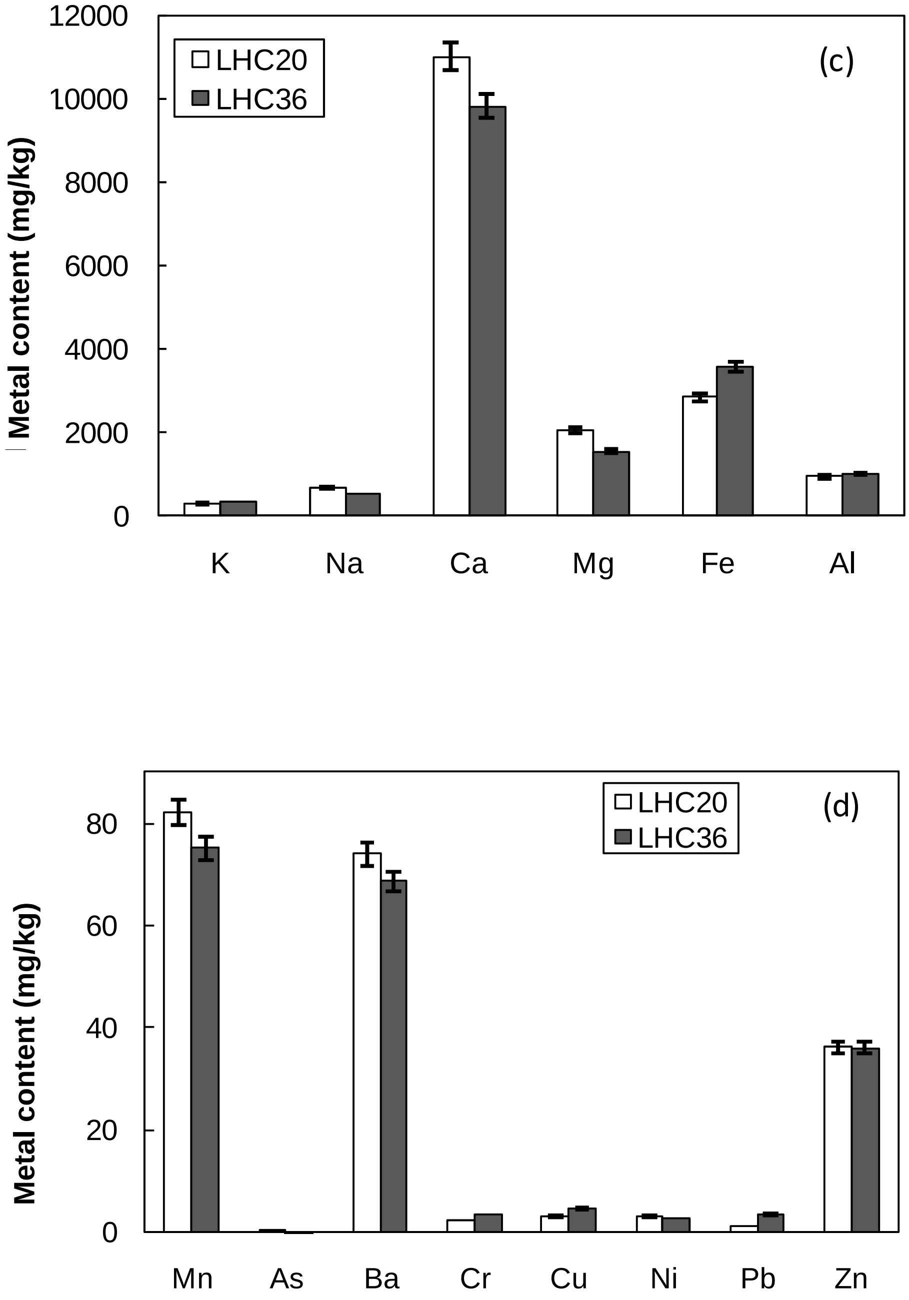

FIGURE 2.5. ***Continued.***

TABLE 2.7. Metal Contents of Soil Samples at WCP and IWWTP Sites

Metal	Site Statistics in mg/kg for:											
	WCP								IWWTP			
	S180		S400		S550		S700		LHC20		LHC36	
	Mean	SD	Mean	SD	Mean	SD	Mean	SD	Mean	SD	Mean	SD
K	920	13.4	2020	74.2	634	44.5	792	23.3	290	6.2	316	7.8
Na	141	5.6	181	10.6	86	2.8	95	4.9	685	13.3	505	13.4
Ca	14,600	410	24,125	757	11,690	560	6997	400	11,020	320	9828	362
Mg	2727	33.2	7092	232	2434	45	2326	133	2040	40	1541	25.6
Fe	4583	139	11,340	339	5051	86	5516	363	2840	52.3	3577	96
Al	3702	85.6	9694	461	3427	118	3369	249	933	16.1	1018	23.3
As	1.3	0.1	3.5	0.1	1.8	0.1	2.1	0.2	0.2	0.1	0.1	-
Cr	4.2	0.1	8.8	0.2	5.3	0.2	6.1	0.1	2.0	0.1	3.6	0.1
Pb	2.5	0.3	5.6	1.2	2.4	0.1	2.3	0.1	1.0	0.1	3.4	0.2
Zn	14	1.3	20.3	1	11.6	1.6	14	0.1	36	0.5	36	2.1
Mn	143	14.8	372	9.2	173	9.9	186	9.6	82	4.8	75	5
Ba	70	5.5	189	3.1	44	4.3	68	5.3	74	3	68.5	3.4

The distribution of metals in different components of the WCP soil samples is presented in Figure 2.6. The metal association with different soil components is in general similar for samples taken at different intervals. Almost all Fe and Al are contained in the residual (RES) fraction. Ca is mainly in the EXC, CARB, and ERO fractions, with a large percentage in the CARB fraction. This finding is consistent with the XRD analysis result that calcite is a major mineral phase in these soils. Although the majority of metals of health concerns reside in the RES fraction, there are notable amounts of As, Ba, Pb, and Zn in the EXC, CARB, and ERO fractions, indicating potential leaching of these metals upon changes in ionic strength, pH, and redox potential.

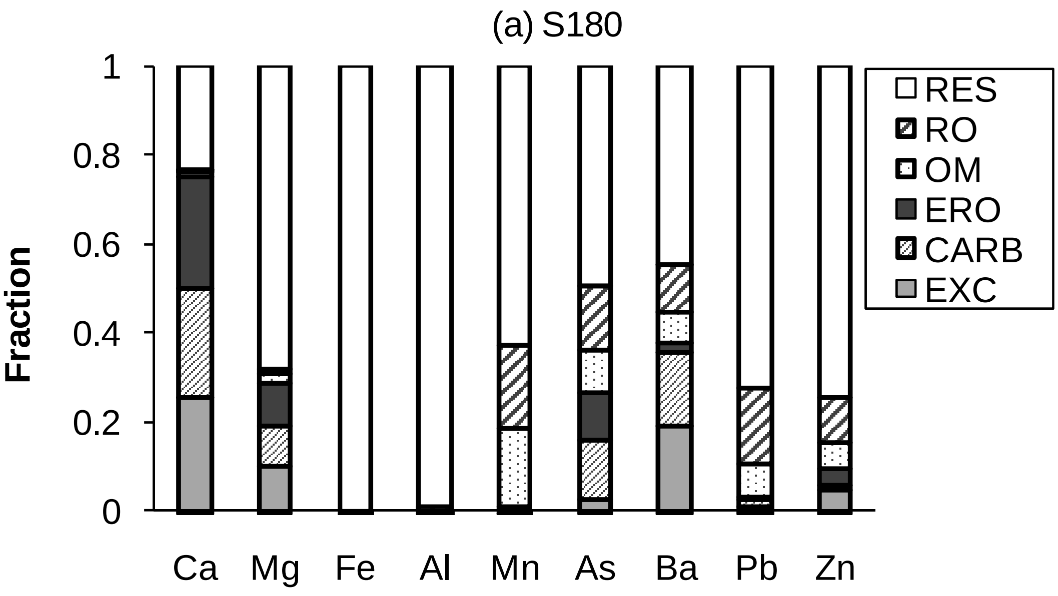

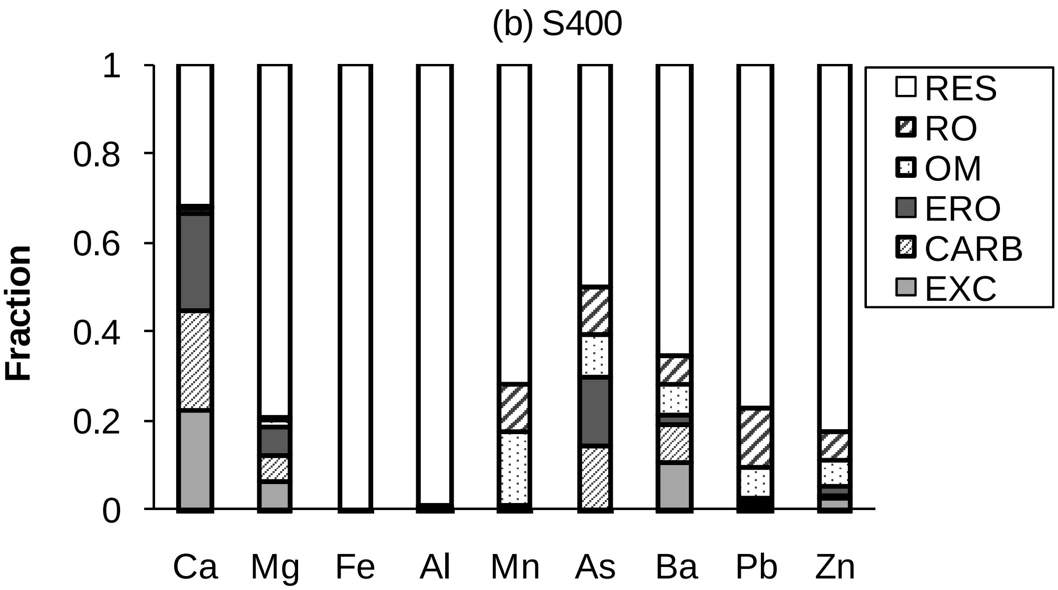

FIGURE 2.6. Distribution of metals with different soil components in S180 (a), S400 (b), S550(c), and S700 (d). EXC = soluble plus exchangeable metals, CARB = elements bound to carbonate, ERO = elements bound to easily reducible oxides, OM = elements bound to organic matter, RO = elements bound to reducible oxides, and RES = elements in the residual fraction.

(c) S550

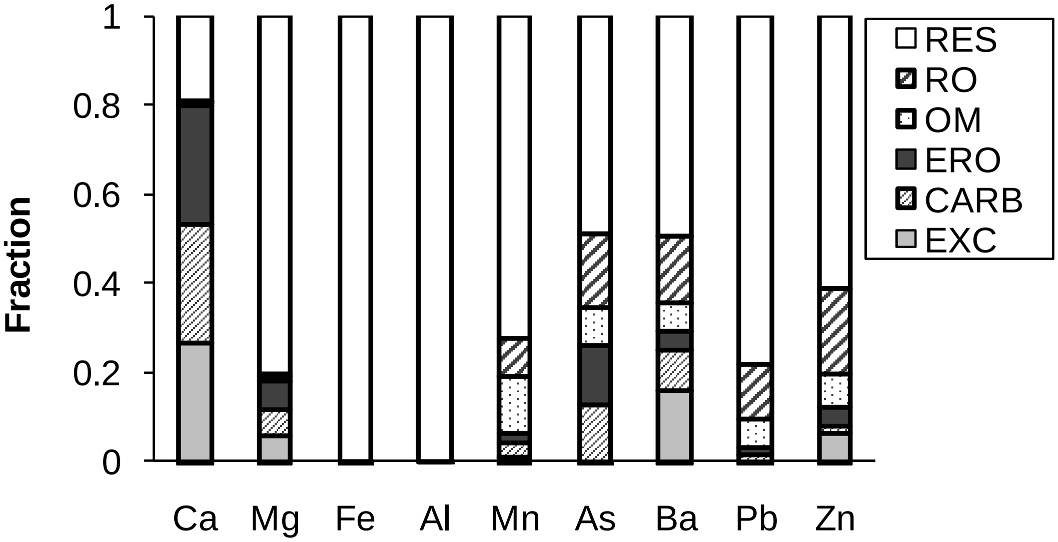

(d) S700

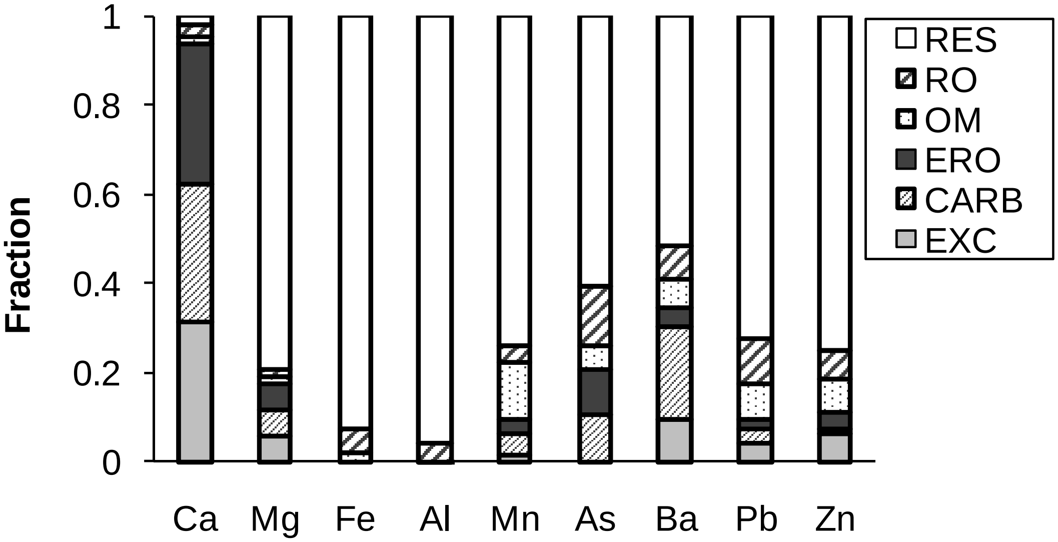

FIGURE 2.6. ***Continued.***

CHAPTER 3

DESORPTION EQUILIBRIUM STUDY

Batch desorption equilibrium experiments were conducted with a vadose soil (S400, collected at 400 ft at the WCP site) and two aquifer material samples (S700 [collected at 700 ft at the WCP site] and LHC30 [core sample collected at 30 to 31 ft at the IWWTP site]). The RO water adjusted to different TDS levels and pHs was used to investigate the effect of the TDS concentration and solution pH on metal desorption from these three soil samples. Because the concentrations of trace metals in these soil samples were relatively low according to our soil analysis results, artificial loading was performed to create higher concentrations of As, Cd, Cr, Ni, and Zn in the S400 and S700 soil samples. Desorption experiments were performed with both the original and the loaded soil samples, providing desorption data for soils with a wide range of metal contents. The effects of solution pH, total ionic strength, redox conditions, and microbiological activities were examined.

3.1 SOIL SAMPLE PRETREATMENT AND CHARACTERIZATION

Because the soil samples from the WCP site had been exposed to air during collection, all experiments and soil pretreatment for S400 and S700 were performed under aerobic conditions. Soil samples were processed shortly after arrival in the lab. The soil samples were air-dried at ambient temperature (~22 °C) in a fume hood (Purifier Bio-safety Class II cabinet) to prevent contamination from the environment. After 120 h, about 98% water was removed from the soil samples according to the moisture analysis. The air-dried samples were mixed thoroughly to achieve homogeneity, sieved with a USS no. 10 sieve (2-mm diameter), and stored in plastic bags before using. Soil aggregates were broken by hand and a plastic mallet before sieving.

The core samples collected from the IWWTP site were stored as received at 4 °C in capped brass sleeves sealed with square Teflon sheets, and the redox condition of the samples was preserved relatively well. A small amount of the IWWTP sample was processed and dried for characterization.

3.2 ARTIFICIAL LOADING OF TARGET METALS

High-metal-content soils were created by an adsorption experiment. In a 2-L polypropylene plastic bottle, 1000 g of each soil sample was mixed with 500 mL of a solution containing 47 mg of As/L, 34.5 mg of Cd/L, 616 mg of Cr/L, 983 mg of Ni/L, and 4452.5 mg of Zn/L. The pH of the adsorption solution was adjusted to 3 before being mixed with the soil. These concentrations and the pH were chosen carefully to obtain medium-level metal loading as well as to ensure that there was no precipitation in the bulk solution based on equilibrium calculations using Visual MINTEQ. No visible precipitation was observed during preparation of the solution. The solution was added very slowly to the soil to avoid surface precipitation.

The mixed suspension was then shaken for 48 h at 30 rpm on a rotary shaker (Vibrax*VXR; VWR). At the end of the mixing period, the pH of the suspensions was recorded. The pH of the S400 suspension was at 6.0, and that of the S700 was 5.9. The increase of pH showed that the soil samples had strong buffering capacity, consistent with the high calcite content of these soil samples.

The suspensions of soils were centrifuged at 9610 × *g* for 15 min by using a refrigerated centrifuge (J2-MC, Beckman, CA). The supernatants were then decanted, but there were still 220-mL and 250-mL solutions remaining in the loaded soils of S400 and S700. Samples were taken from the supernatants, filtered through 0.22-μm-pore-size membrane syringe filters, and analyzed for heavy metals by ICP-AES or ICP-MS. The concentrations of metals in the soil were determined based on mass balance calculations and summarized in Table 3.1.

The metal-loaded soils were aged for 30 days in plastic bottles with covers and were then air-dried and processed following the same sample pretreatment procedure for fresh soil samples. It is noted that the concentrations listed in Table 3.1 include the metals in the pore water after centrifugation and supernatant removal. This fraction of metals is expected to adsorb or precipitate on the soil particles during the drying process.

TABLE 3.1. Calculated Metal Contents of S400 and S700 after Artificial Loading

	Trace Metal Concn (mg/kg of Soil)				
Loaded Soil	**As**	**Cr**	**Cd**	**Ni**	**Zn**
S400	26.72	315.99	13.39	455.88	2058.98
S700	24.25	313.85	10.18	346.68	2034.75

3.3 BATCH DESORPTION EQUILIBRIUM EXPERIMENTS

3.3.1 Desorption solutions

In order to determine the effect of pH and total ionic strength (or TDS) on desorption of the target metals, desorption solutions with a range of TDS levels (58, 280, and 500 mg/L) and pHs (4.0, 6.5, and 9.0) were prepared by adding a predetermined amount of trace-metal-free HNO_3 (or NaOH) and NaCl to the RO water collected from the WCP site.

Because the soil samples from the WCP site were exposed to the atmosphere during sample collection, all desorption experiments with natural and loaded S400 and S700 samples were conducted under ambient (aerobic) conditions. The solution conditions tested for these soil samples are summarized in Table 3.2.

TABLE 3.2. Desorption Equilibrium Experiment Conditions for Natural and Loaded S400 and S700 Samples

Exp. ID	Experimental Variables		
	pH	**TDS (mg/L)**	**Redox Condition**
1	4	58	Aerobic
2	4	280	Aerobic
3	4	500	Aerobic
4	6.5	58	Aerobic
5	6.5	280	Aerobic
6	6.5	500	Aerobic
7	9.0	58	Aerobic
8	9.0	280	Aerobic
9	9.0	500	Aerobic

Desorption equilibrium experiments with the LHC30 sample were performed under both aerobic and anoxic conditions. Table 3.3 summarizes the experimental conditions used in desorption equilibrium experiments with LHC30. For experiments under anoxic conditions, the desorption solution was purged with ultrapure N_2 for 30 min before being added to the soil samples. The centrifuge tubes were filled with the desorption solution to eliminate headspace. The redox potential of the soil-water mixture was monitored after each desorption period to confirm that anoxic conditions were maintained during the desorption experiment.

TABLE 3.3. Desorption Equilibrium Experiment Conditions for the LHC30 Sample

	Experimental Variables		
Exp. ID	**pH**	**TDS (mg/L)**	**Redox Condition**
1	4	58	Aerobic
2	4	280	Aerobic
3	4	500	Aerobic
4	4	58	Anoxic
5	4	280	Anoxic
6	4	500	Anoxic
7	6.5	58	Aerobic
8	6.5	280	Aerobic
9	6.5	500	Aerobic
10	6.5	58	Anoxic
11	6.5	280	Anoxic
12	6.5	500	Anoxic
13	9	58	Aerobic
14	9	280	Aerobic
15	9	500	Aerobic
16	9	58	Anoxic
17	9	280	Anoxic
18	9	500	Anoxic

For all experiments, 1 g of soil was mixed with 15 mL of desorption solution in a 20-mL polypropylene tube. The suspension was equilibrated for 20 h on a rotary shaker (Vibrax*VXR; VWR) at 30 rpm, followed by 10 min of centrifugation. The clear supernatant was decanted, filtered through a membrane syringe filter, and then collected in a 10-mL polypropylene plastic centrifuge tube for analysis of target metal concentrations. Preliminary experiments were performed by using different centrifugation rates (9610 × *g* and 21,000 × *g*) and membrane filters with different pore sizes (0.02, 0.22, and 0.45 µm). Results showed no significant difference (<3% and <5% for As and Ba, respectively) in the measured metal concentrations within the range of centrifugation rates and membrane pore sizes tested. Therefore, 9610 × *g* and 0.22-µm-pore-size membrane filters were used in all subsequent analyses. This desorption process was repeated for a total of over 10 times by adding a fresh batch of desorption solution to the soil sample every time. At the end of the 20-h contact period, the mass of the supernatant extracted was weighed to determine the amount of solution remaining in the interstices of the soil sample so that a mass balance could be performed for the target metals. The pH of the supernatant was measured after the 1st, 5th, 10th, and 15th contacts. Duplicate experiments were run for all experimental conditions.

Overall, no significant desorption of Cr, Cd, Ni, and Hg from the natural S400 and S700 was observed. The aqueous-phase concentrations after the first 20-h desorption period were below the detection limit. For the artificially loaded S400 and S700, very low desorption of Ni, Zn, and Cd was observed only during the first 20-h desorption period, after which the aqueous-phase concentrations dropped to below the detecting limits. Therefore, desorption data were presented below only for As, Ca, Mg, and Ba.

For the LHC30, the desorption equilibrium aqueous-phase concentrations of all trace metals of interest, namely, As, Cr, Pb, Zn, and Ni, after each desorption step were either below or similar to our reporting limit of detection (see Table 2.2). Therefore, desorption of these metals is considered negligible and is not reported here. The negligible desorption of these trace metals is expected because of their extremely low concentrations in this soil (see Table 2.4). Although there is a significant amount of Zn in the LHC soils (36 ± 1.4 mg/kg), most of it is not extractable. However, significant desorption or dissolution of Ca, Mg, and Ba was observed. Each data point in the figures represents a 20-h desorption period using a fresh batch of desorption solution.

3.3.2 Effect of pH

Figures 3.1 to 3.3 present the amount of primary metal cations desorbed from the original and artificially loaded S400 as a function of cumulative desorption solution volume. Note that the cumulative desorption solution volume is equal to the sum of the desorption solution volume added in the consecutive 20-h desorption periods. Each data point in the figures represents a 20-h desorption period. It was found that desorption of Ca, Mg, and Ba decreased with increasing pH. This discovery is consistent with the majority of the findings reported in the literature. This effect of pH can be attributed to two factors: 1) the solubility of these cations increases when pH decreases, and 2) ion exchange by H^+ is more significant at a low pH.

It is noted that the amount of Ca desorbed increases almost linearly with the cumulative desorption solution volume for most solution conditions tested; namely, the equilibrium aqueous-phase concentration of Ca remains constant for each batch of desorption solution. Because calcite is a major mineral in this soil, it is deduced that the release of Ca is controlled by a dissolution process. The equilibrium aqueous-phase concentration is therefore determined by the solubility product of the calcite mineral. Under two sets of conditions, pH = 4 and TDS = 58 mg/L and pH = 4 and TDS = 280 mg/L, the desorption curve shows a second stage with increased desorption. This phenomenon probably stems from the exposure of new desorption sites after dissolution of calcite on the soil particle surface. Similar results were observed for Ba desorption, indicating that dissolution of a Ba mineral may be the major source of Ba release.

On the contrary, desorption of As was found to increase with increasing solution pH (Figure 3.4). This finding is consistent with the lower adsorption of As at high pH values (Ghosh et al., 2006). Typically, arsenic exists in soils as either arsenate (AsO_4^{3-}) or arsenite (AsO_3^{3-}). Because both arsenic acid (H_3AsO_4) and arsenious acid ($As[OH]_3$) are weak acids, their speciation strongly depends on pH. The pK_a values of H_3AsO_4 and $As(OH)_3$ are listed in Table 3.4. When pH increases, proton dissociation proceeds, leading to higher solubility of As and hence to greater desorption of arsenic in the form of oxyanions from the soil. However, the impact of pH was small overall for the fresh S400. Since a notable fraction of arsenic in this soil is associated with carbonate (Figure 2.6b), it is reasonable to assume that part of the arsenic desorption results from dissolution of calcite. The decreased dissolution of calcite and of other carbonate minerals offsets the increased mobility of As at higher pH. This property explains the small effect of pH observed in As desorption. Overall, the desorption behaviors of the natural S400 and the artificially loaded S400 were similar, suggesting that the effect of pH on As desorption is consistent over a wide range of soil As content. The effect of pH is slightly more pronounced for the artificially loaded S400 because of the higher As concentration in the loaded soil. Also, the artificially loaded As may not necessarily be associated with calcite.

TABLE 3.4 Acidity Constants of Arsenic Compounds

As Compound	**p*K*$_{a,1}$**	**p*K*$_{a,2}$**	**p*K*$_{a,3}$**
H_3AsO_4	2.25	6.76	11.60
$As(OH)_3$[a]	9.23	12.13	13.40

[a] National Research Council, 1994.

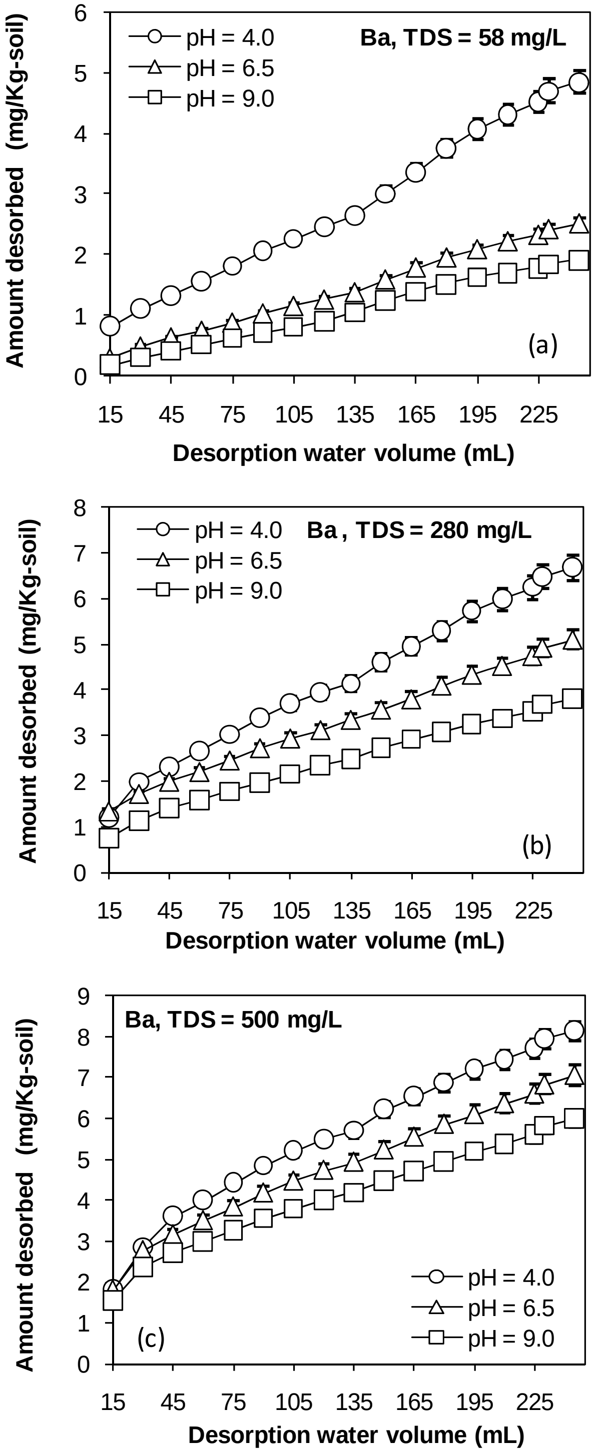

FIGURE 3.1. Effect of pH on cumulative desorption of Ba from natural (a, b, and c) and artificially loaded (d, e, and f) S400.

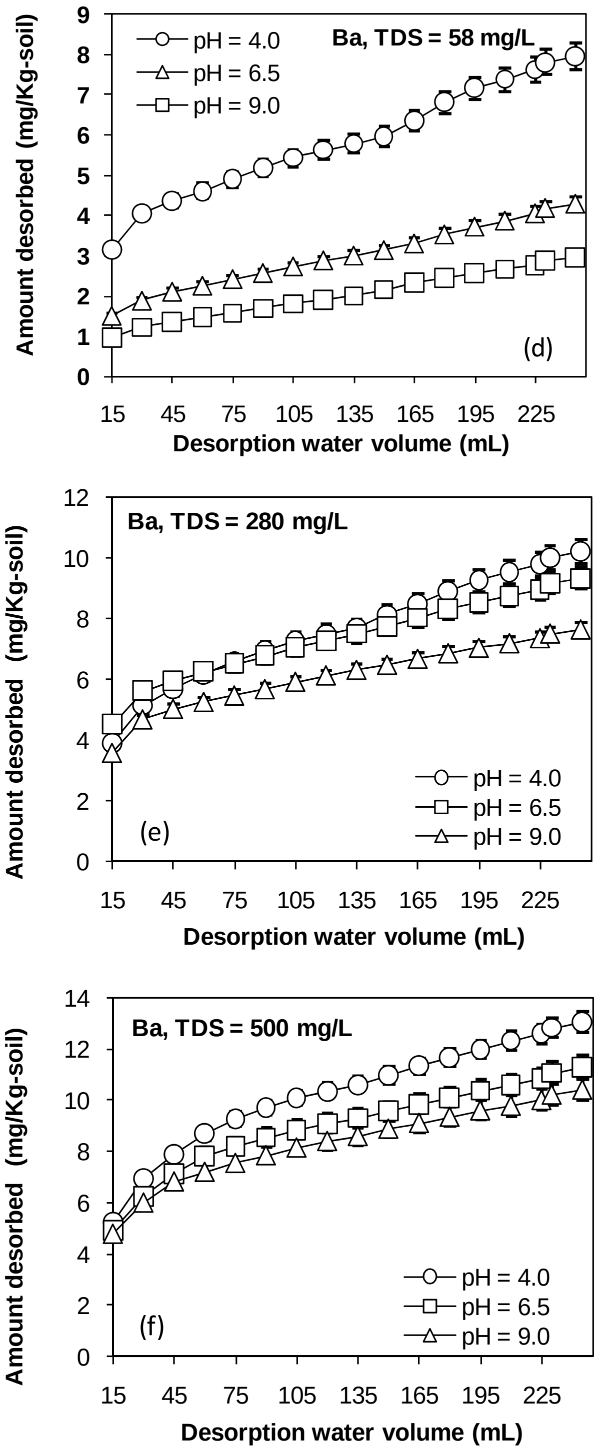

FIGURE 3.1. ***Continued.***

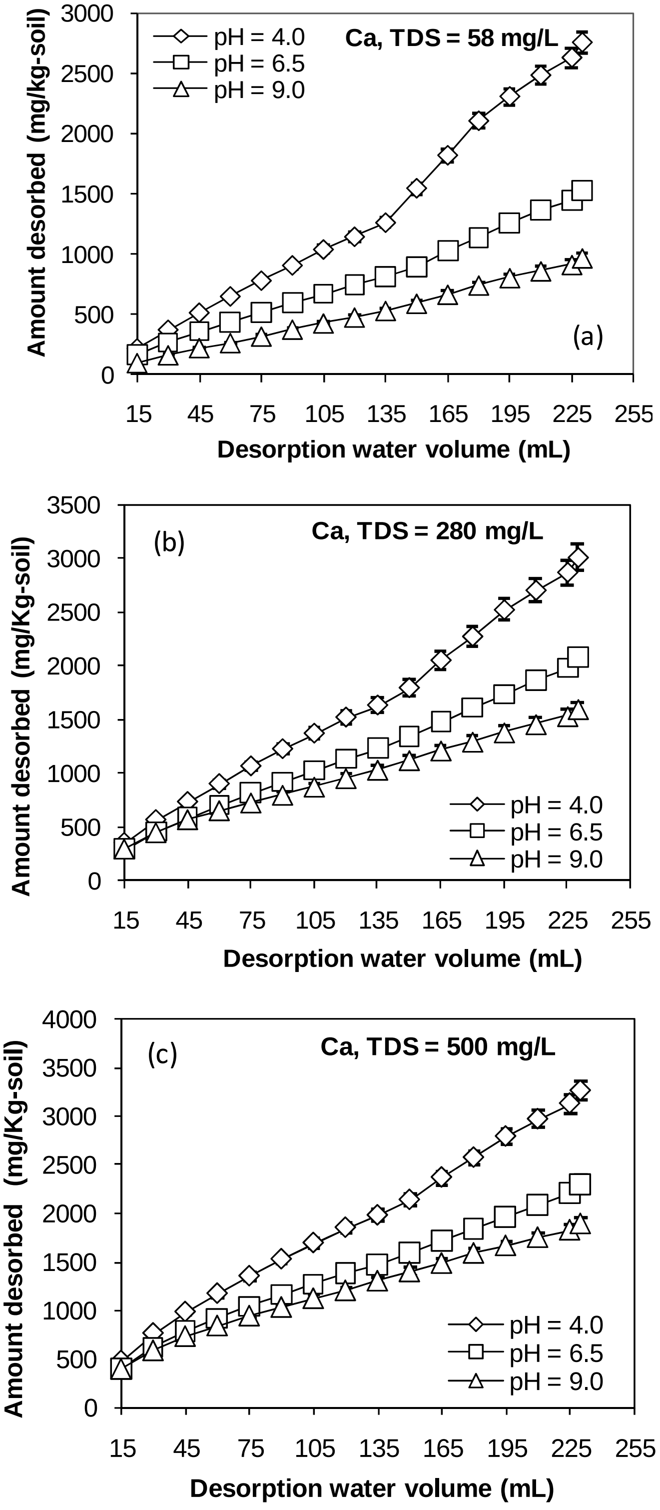

FIGURE 3.2. Effect of pH on cumulative desorption of Ca from fresh (a, b, and c) and artificially loaded (d, e, and f) S400.

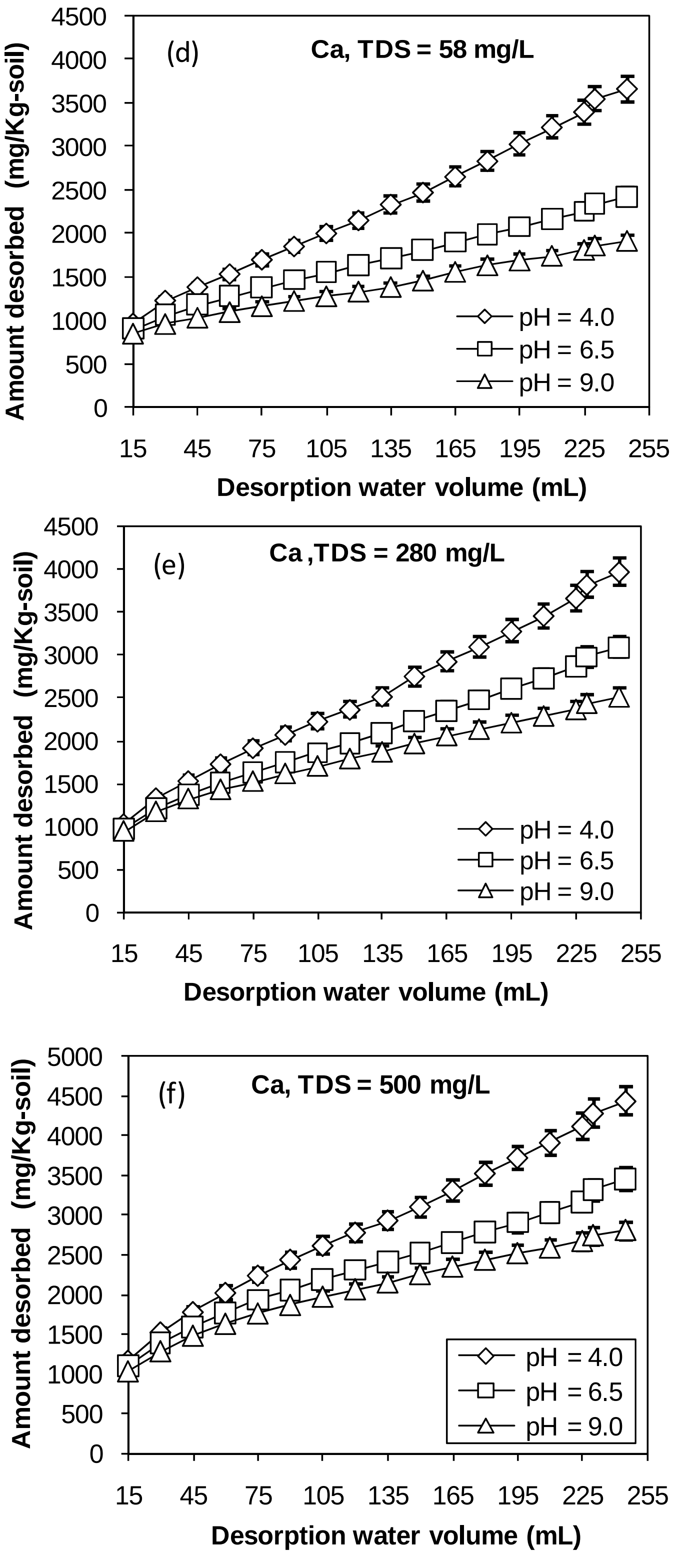

FIGURE 3.2. ***Continued.***

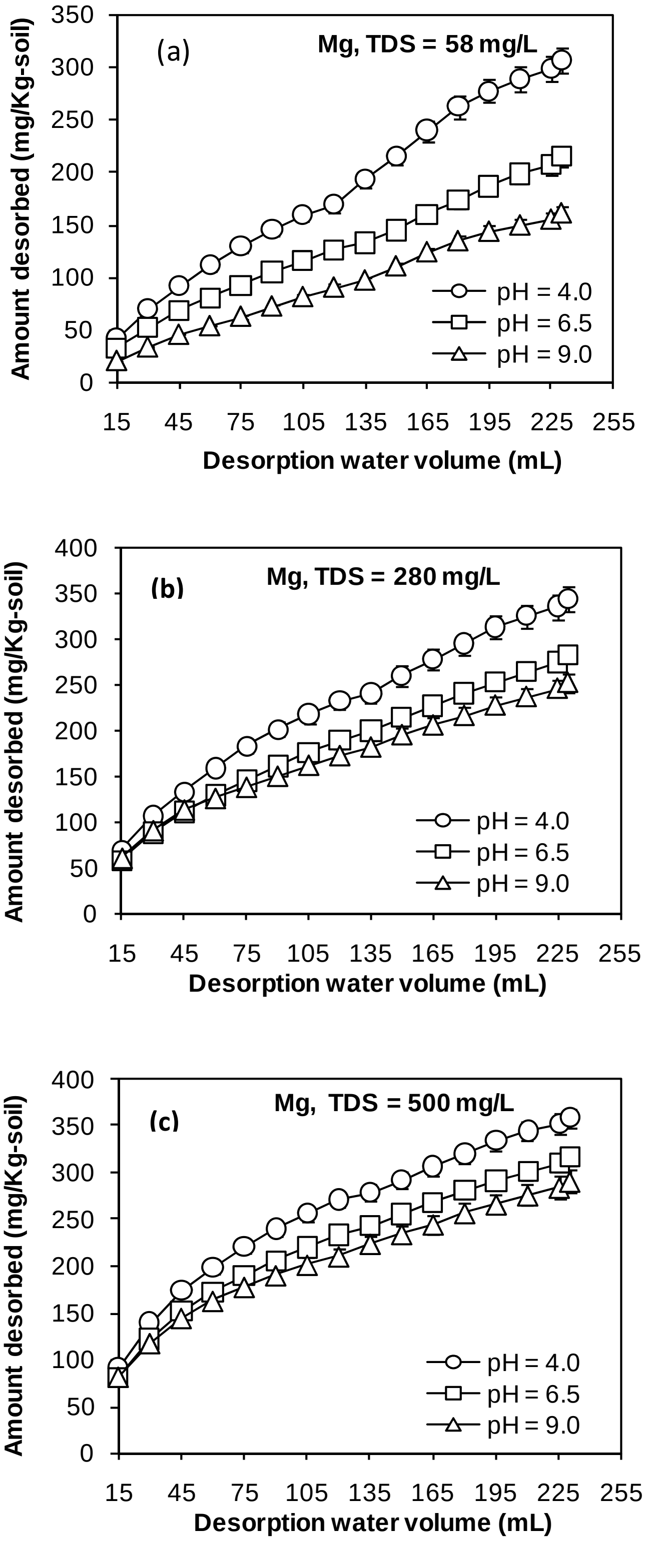

FIGURE 3.3. Effect of pH on cumulative desorption of Mg from natural (a, b, and c) and artificially loaded (d, e, and f) S400.

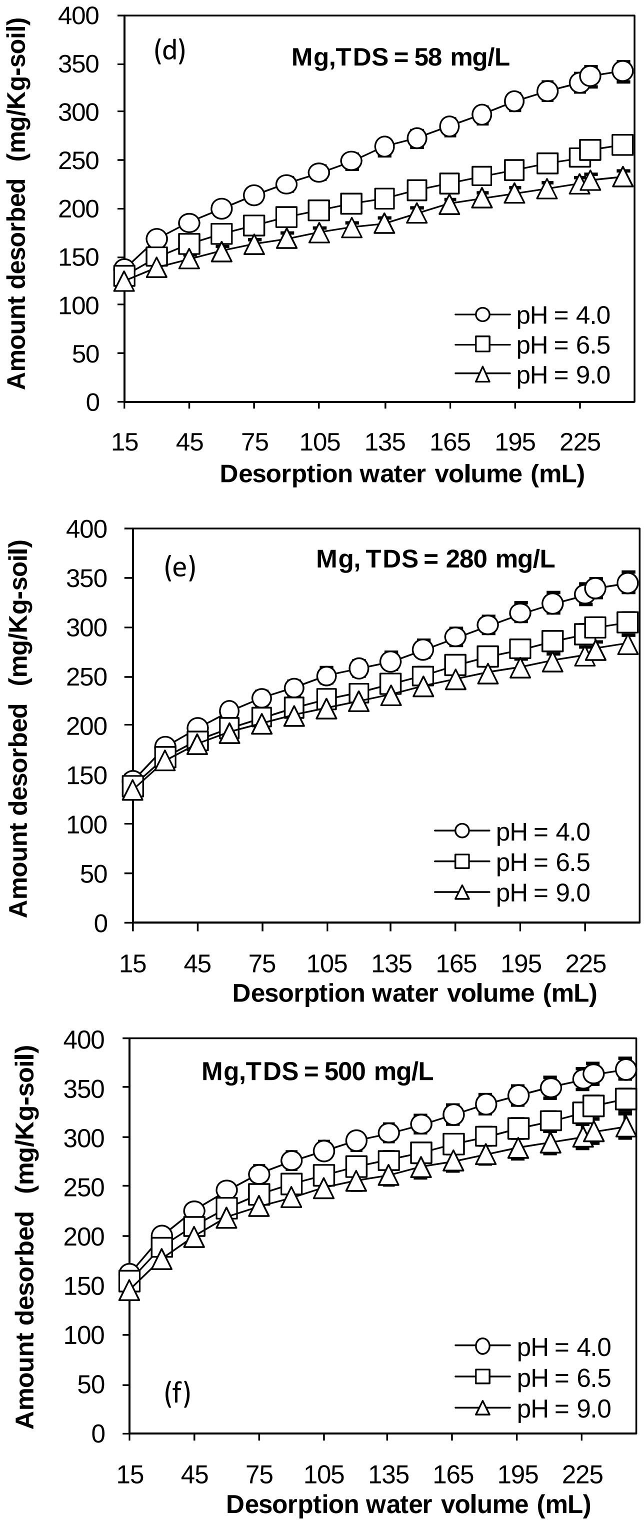

FIGURE 3.3. ***Continued.***

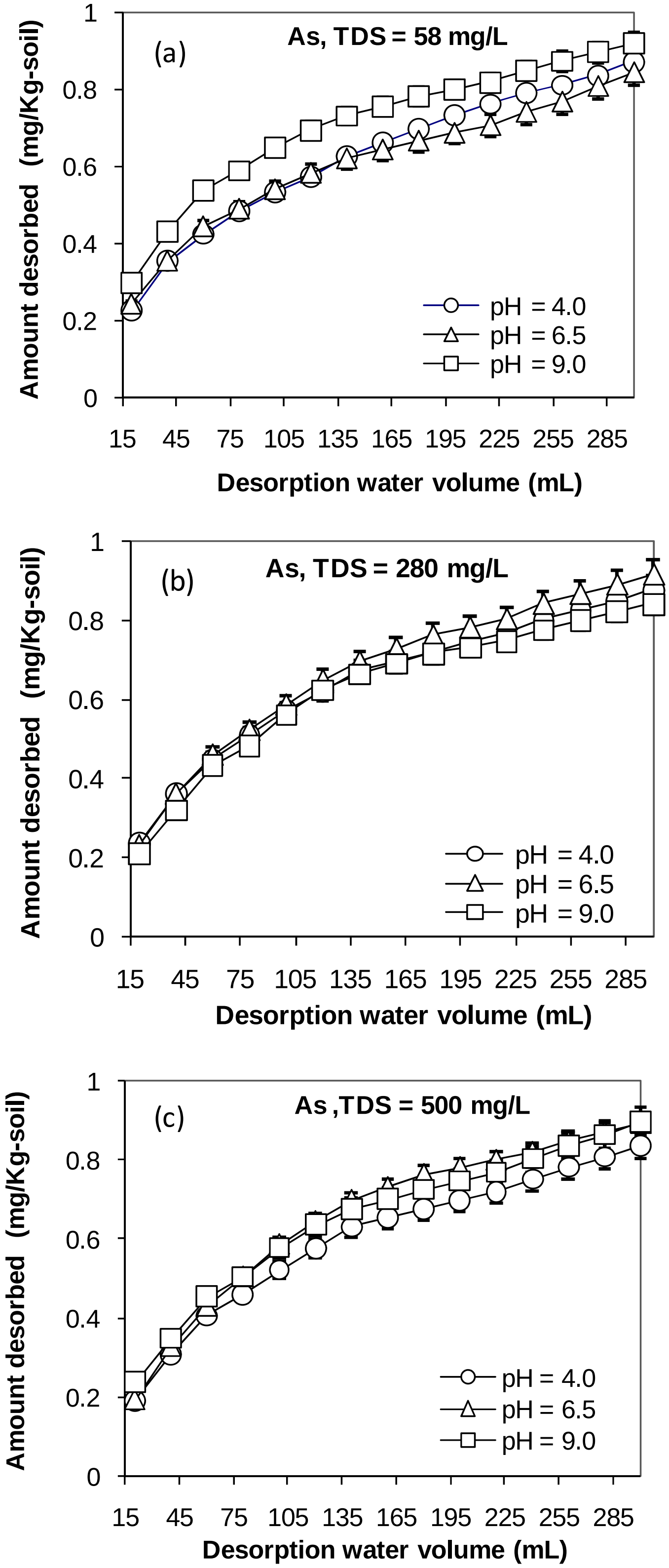

FIGURE 3.4. Effect of pH on cumulative desorption of As from fresh (a, b, and c) and artificially loaded (d, e, and f) S400.

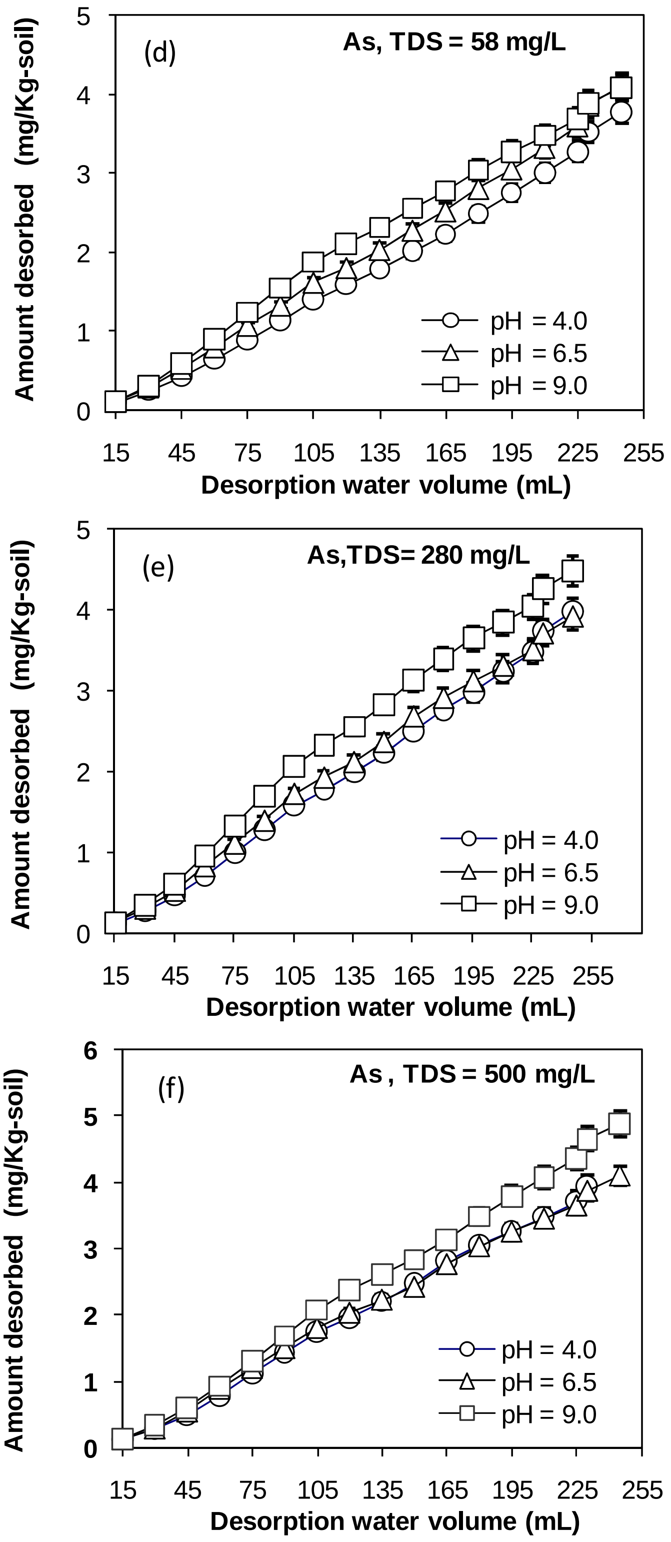

FIGURE 3.4. ***Continued.***

Desorption of target metals from the natural and artificially loaded S700 at different solution pHs is presented in Figures 3.5 to 3.8. Overall, the desorption of all target metals from the S700 soil samples is lower than that from the S400 soil samples because of the smaller surface area and lower CEC and organic carbon concentration, as shown in Table 2.4.

As shown in Figures 3.5 to 3.8, the effect of pH on metal desorption from the natural and artificially loaded S700 is similar to that from the natural and artificially loaded S400: desorption of Ba, Ca, and Mg increases with decreasing pH, while that of As increases with increasing pH.

It is noted that the soil samples from the WCP site have a strong buffering capacity due to the abundance of carbonate. For all three initial pHs of the desorption solution, the pH of the soil-water mixture during 200-h contact periods was within the range of 8.3 to 9.4, 7.7 to 9.4, 7.5 to 9.4, and 7.2 to 9.4 for S400, loaded S400, S700, and loaded S700, respectively. Figure 3.9 shows the evolution of pH during a desorption experiment with fresh S400. It can be seen that the pH was well buffered and remained fairly constant. These results further support the hypothesis that the release of Ca stems mainly from the dissolution of calcite, which offsets the effect of pH on As solubility.

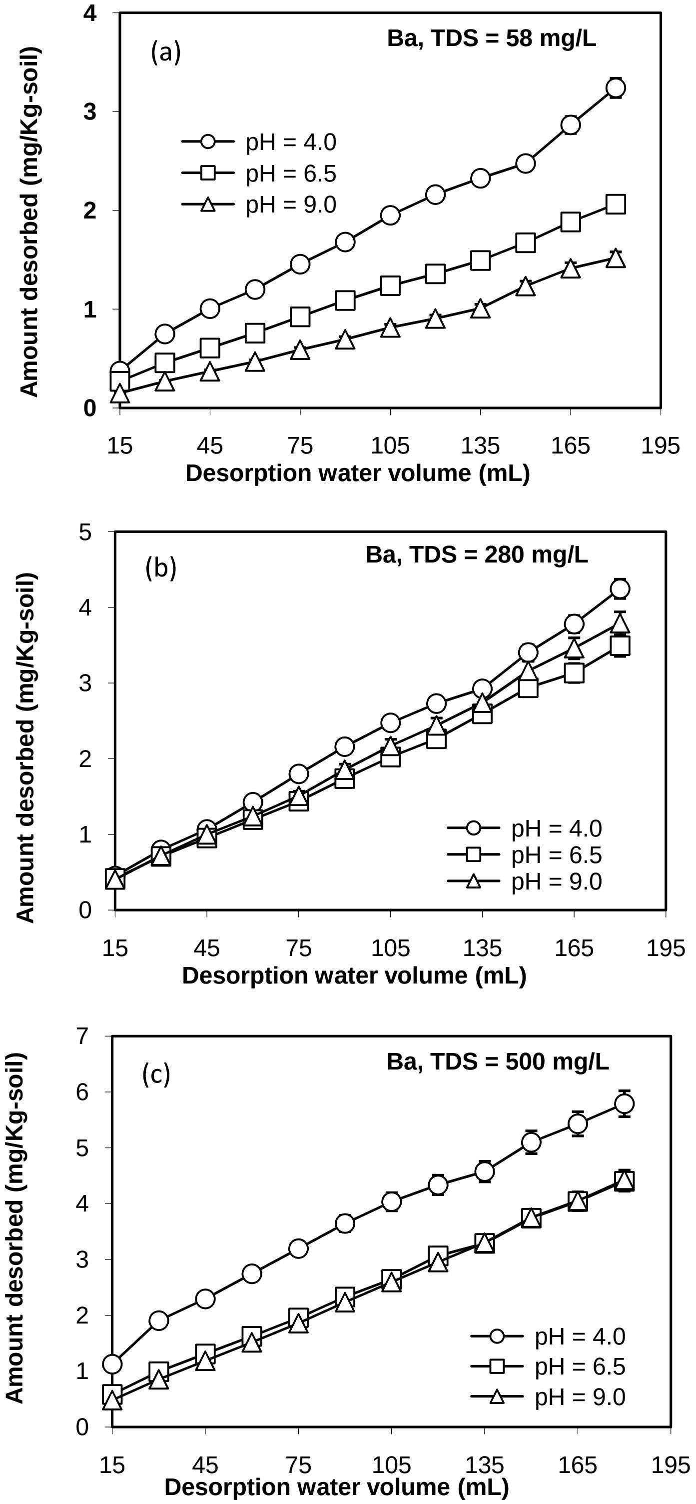

FIGURE 3.5. Effect of pH on cumulative desorption of Ba from fresh and artificially loaded S700.

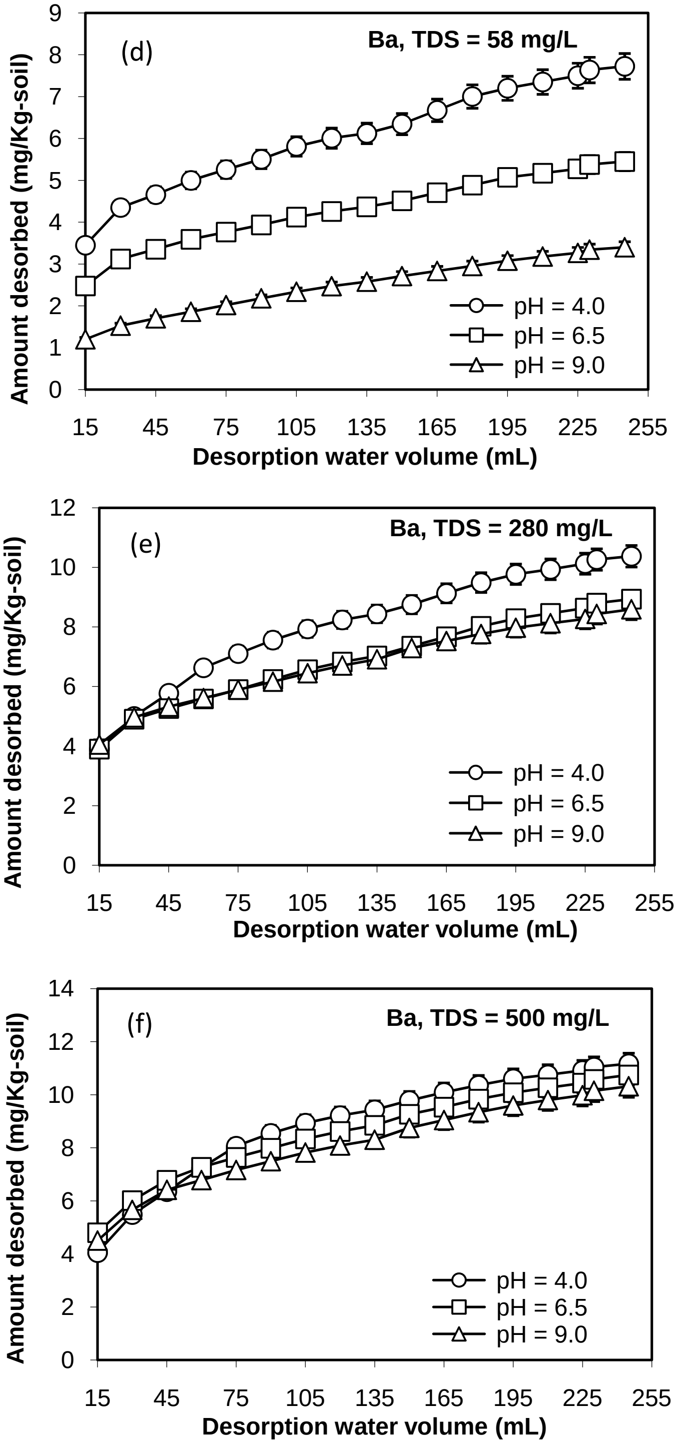

FIGURE 3.5. ***Continued.***

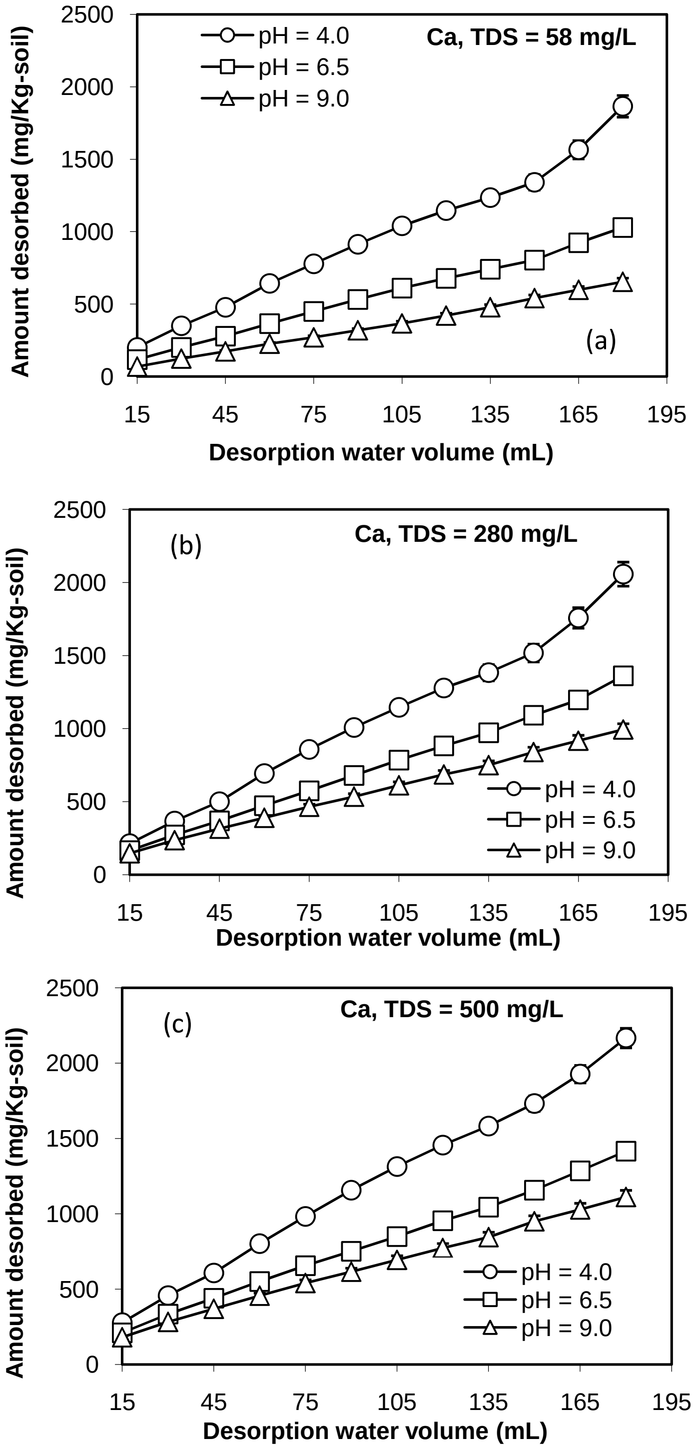

FIGURE 3.6. Effect of pH on cumulative desorption of Ca from fresh and artificially loaded S700.

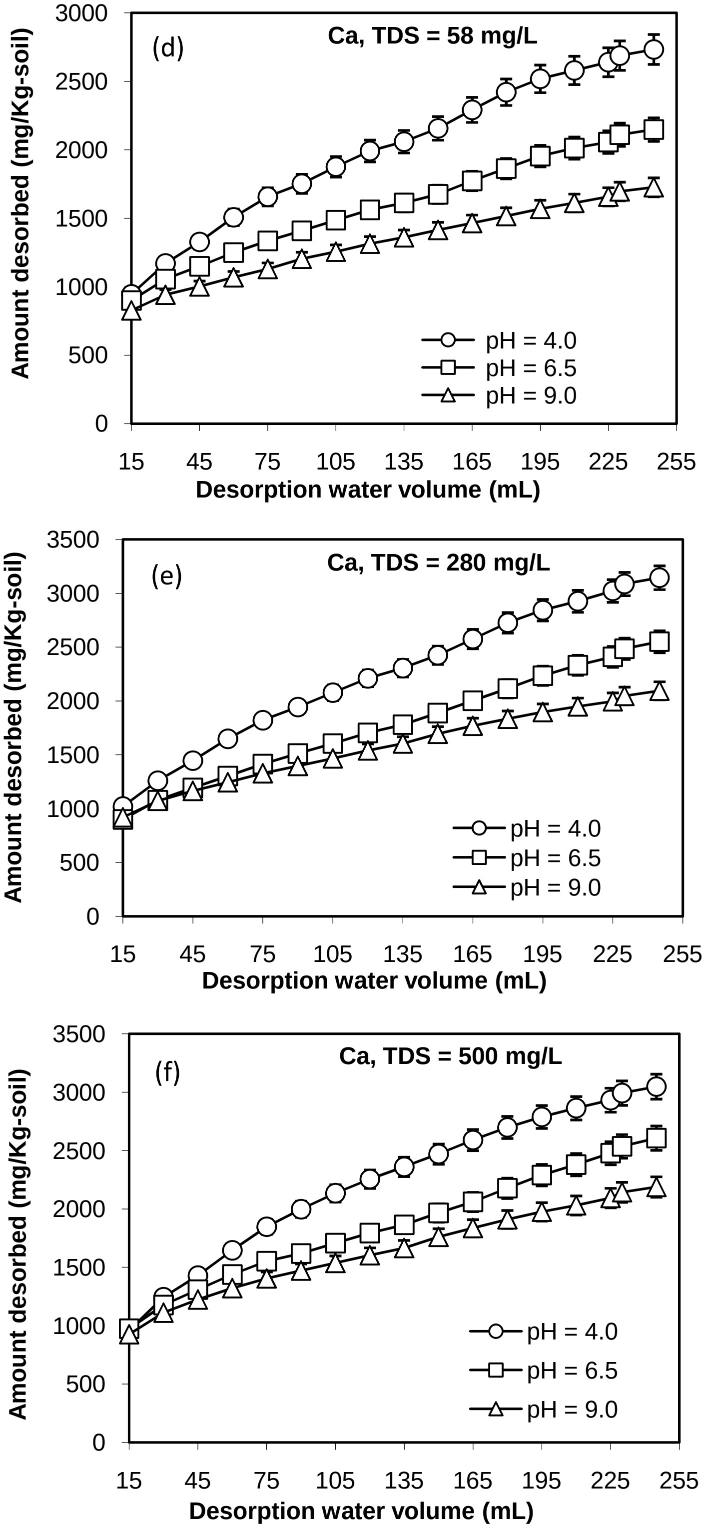

FIGURE 3.6. ***Continued.***

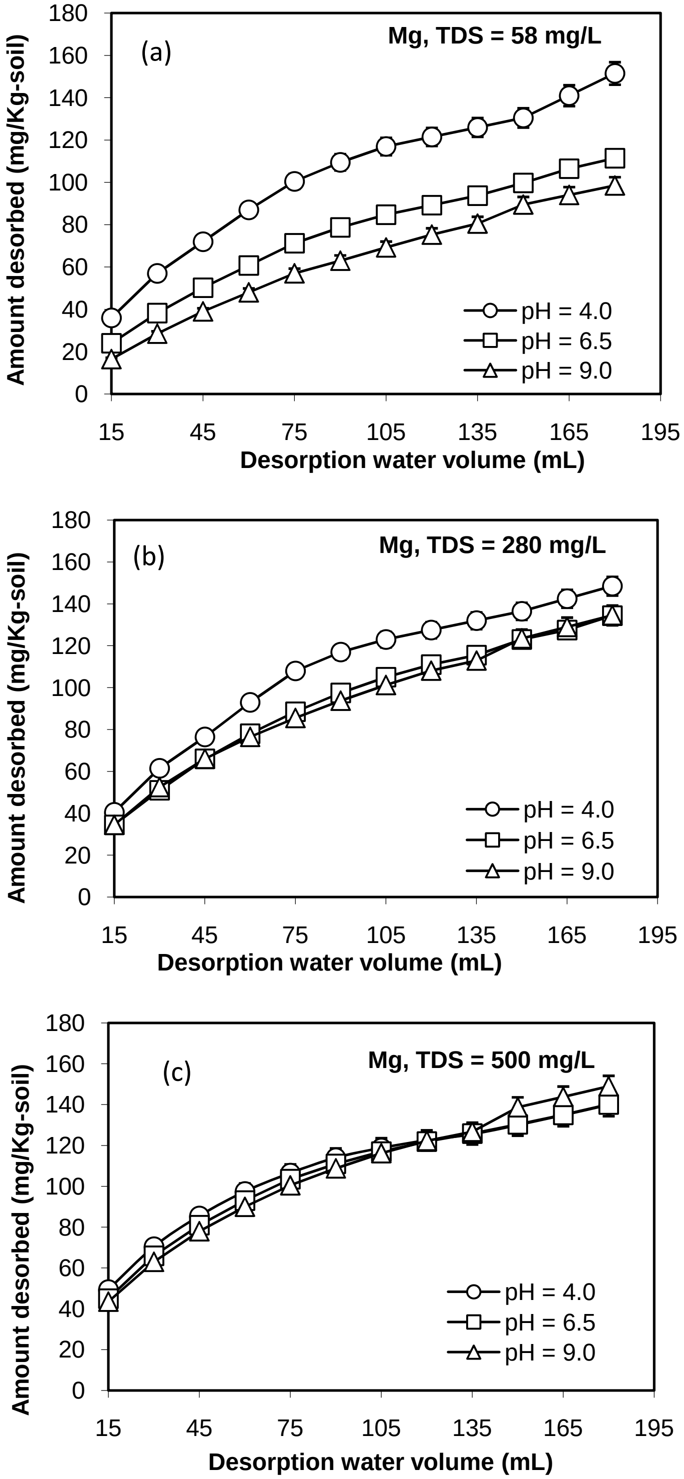

FIGURE 3.7. Effect of pH on cumulative desorption of Mg from fresh and artificially loaded S700.

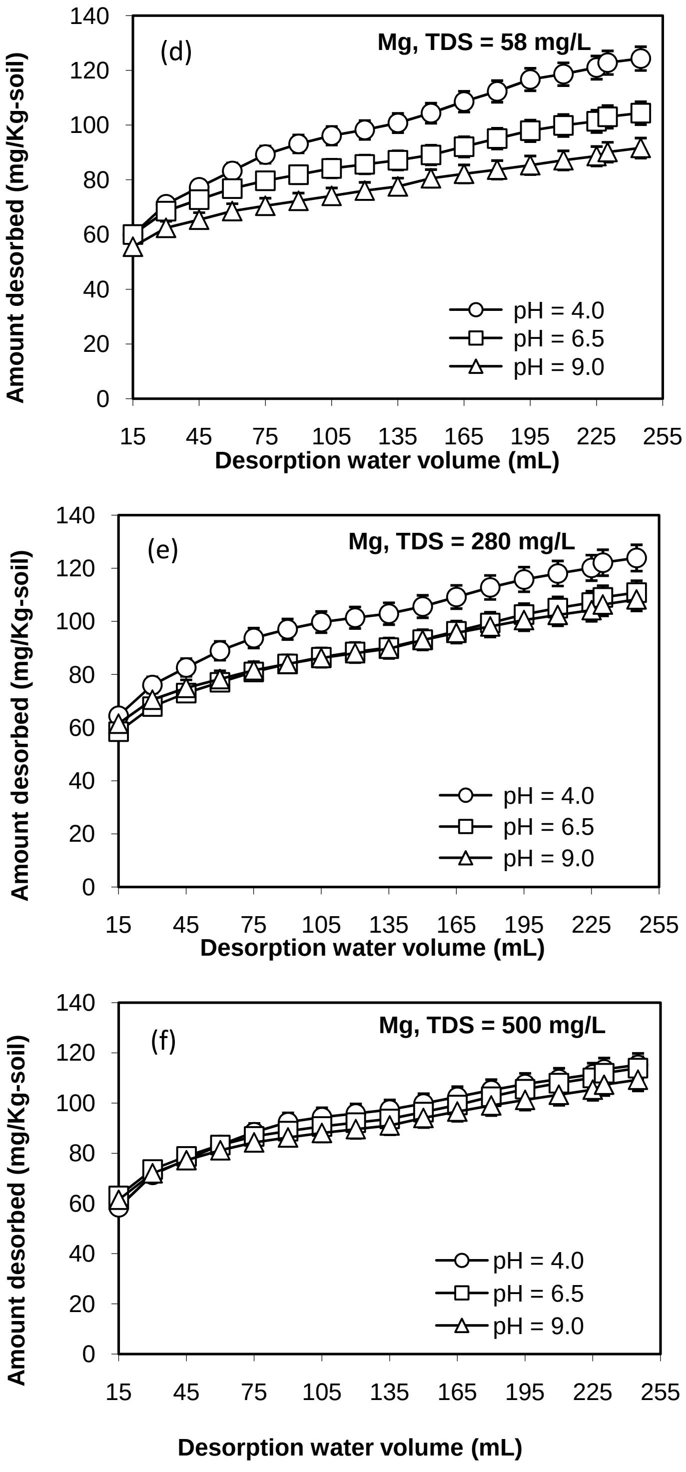

FIGURE 3.7. ***Continued.***

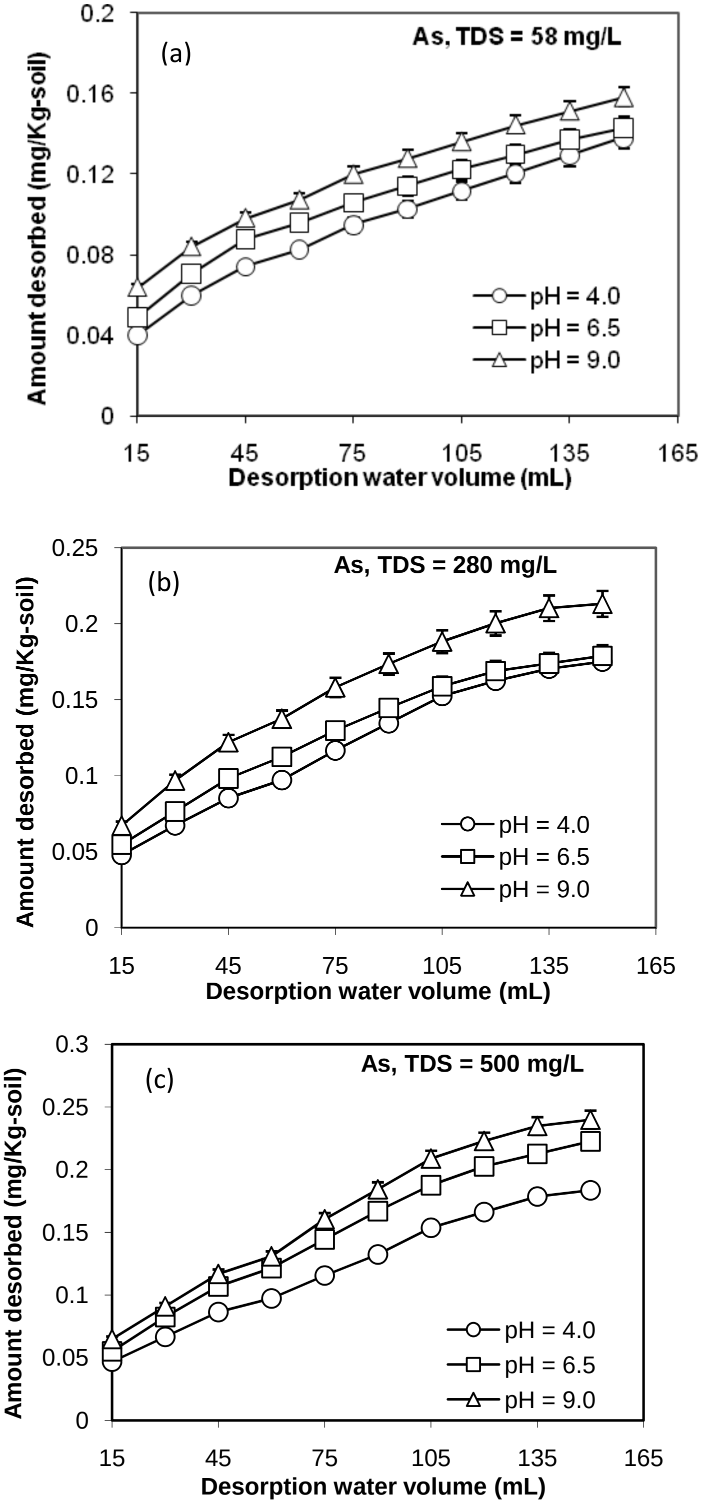

FIGURE 3.8. Effect of pH on cumulative desorption of As from natural (a, b, and c) and artificially loaded (d, e, and f) S700.

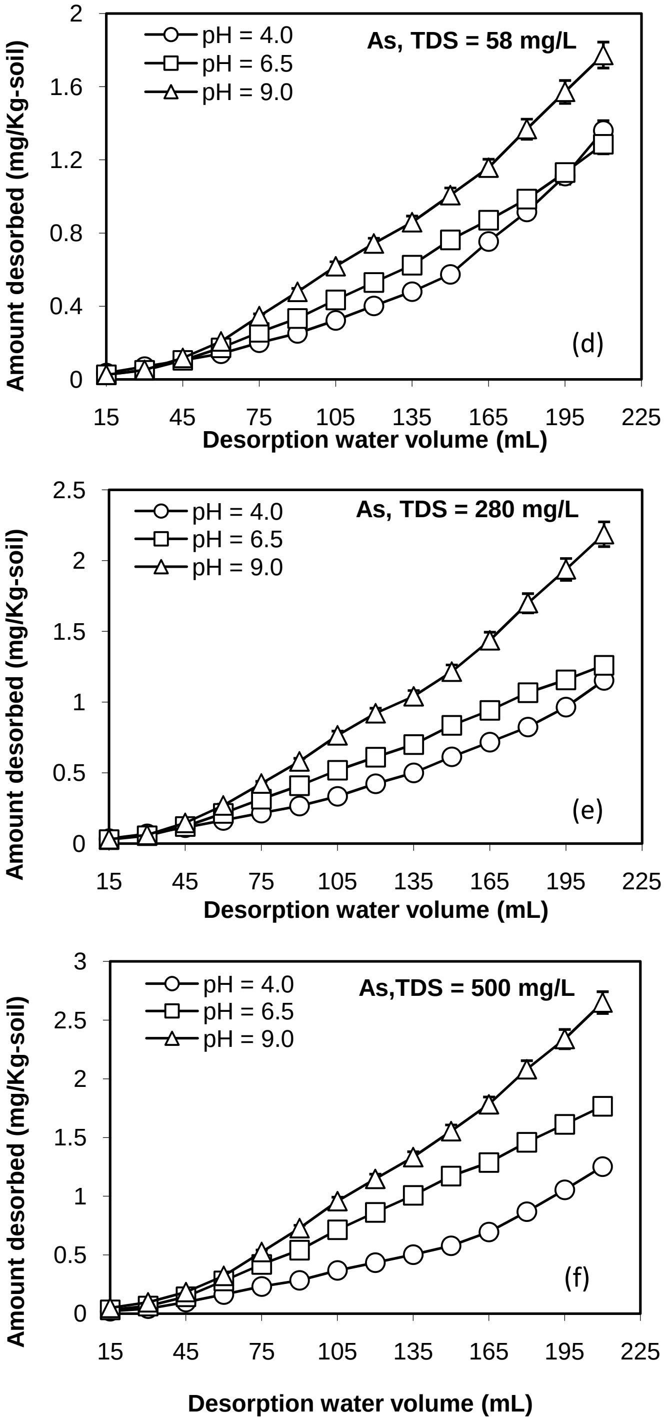

FIGURE 3.8. ***Continued.***

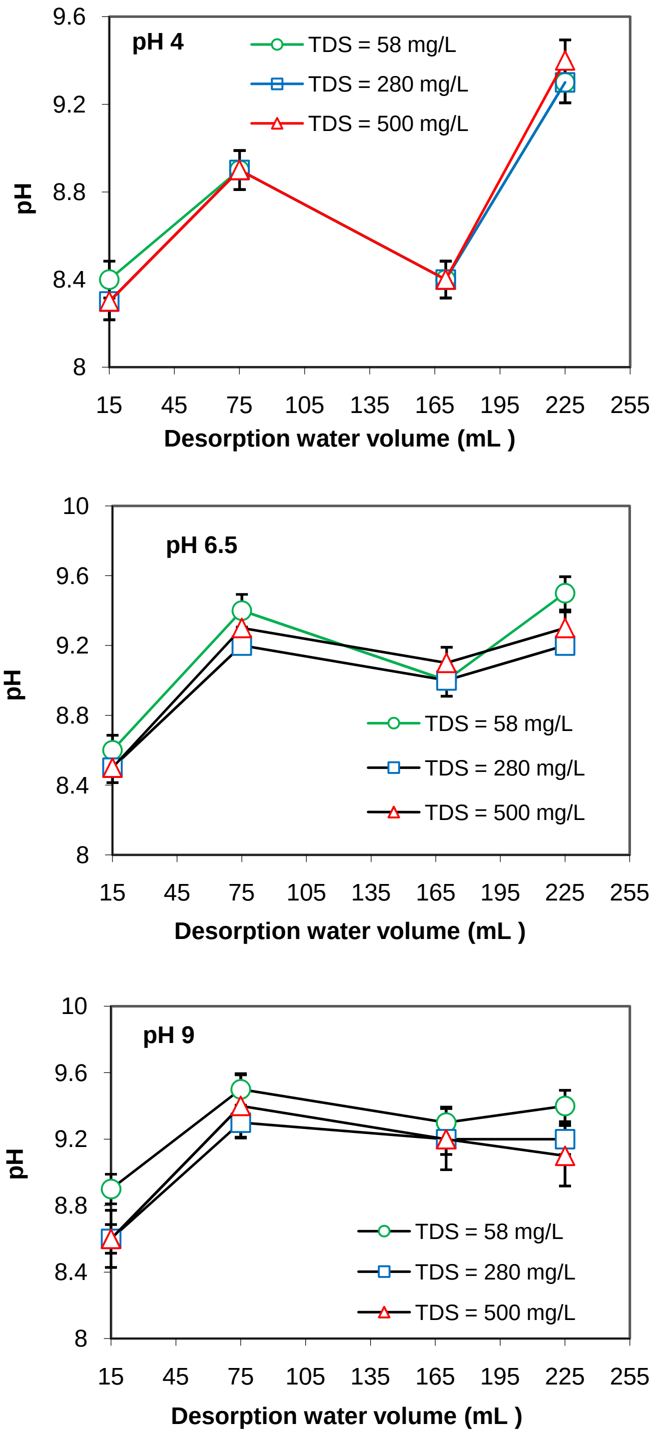

FIGURE 3.9. Evolution of suspension pH during desorption experiments with fresh S400.

Figures 3.10 to 3.12 demonstrate the effect of solution pH on desorption of Ca, Mg, and Ba, respectively, from the LHC30 under both aerobic and anoxic conditions. Similar to that observed with the S400 and S700 soil samples, pH plays a very important role in desorption of Ca, Mg, and Ba from the LHC30. Desorption of all three metals increases with decreasing pH.

It is also noted that the aqueous-phase concentration of Ca after each desorption period stayed relatively constant, as reflected by the linear relationship between cumulative desorption and desorption solution volume in Figure 3.11. This finding strongly suggests that release of Ca is controlled by dissolution of calcium minerals, consistent with the strong effect of pH observed in Ca desorption. Although XRD analysis did not show calcium minerals in a crystalline form, there is relatively high Ca content in the soil samples from the IWWTP site. The calcium minerals may be present as amorphous phases. Release of Mg and Ba, on the other hand, does not seem to be dominated by dissolution.

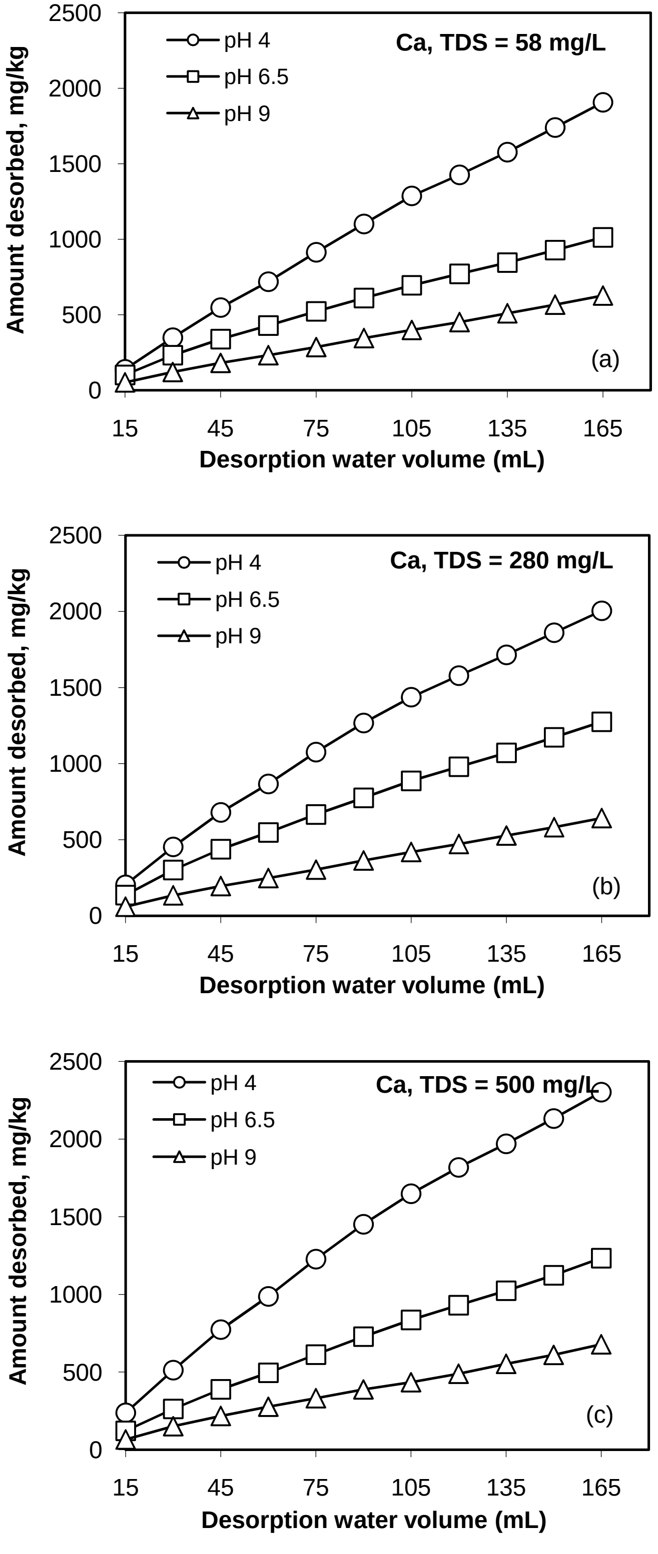

FIGURE 3.10. Effect of solution pH on desorption of calcium from the LHC30 soil sample under aerobic (a, b, and c) and anoxic (d, e, and f) conditions.

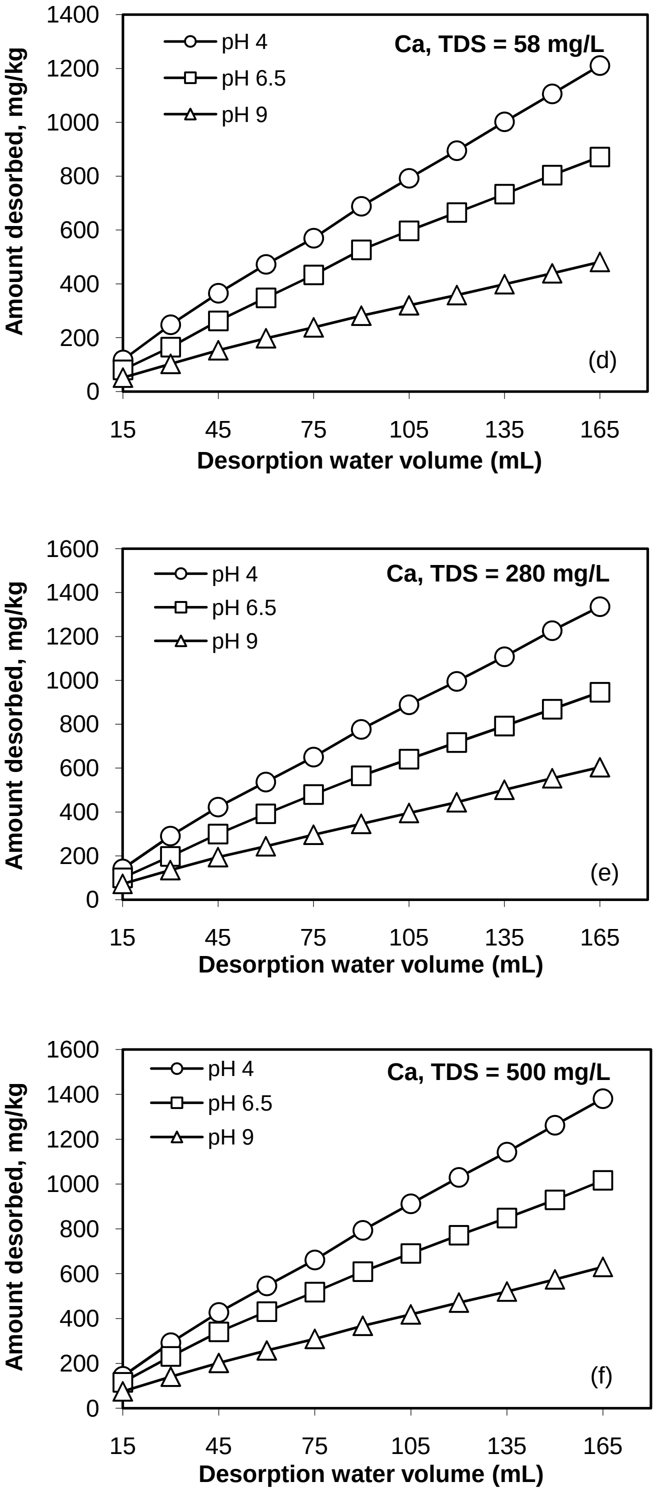

FIGURE 3.10. ***Continued.***

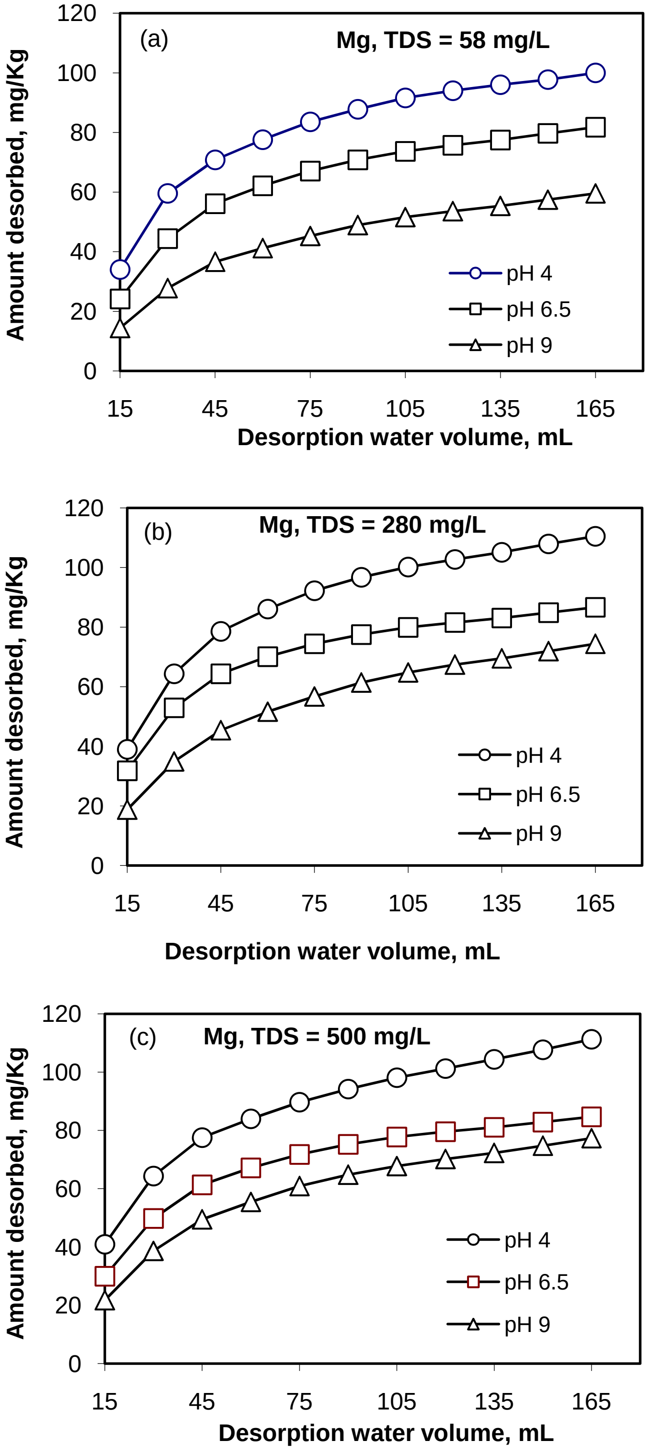

FIGURE 3.11. Effect of solution pH on desorption of magnesium from the LHC30 soil sample under aerobic (a, b, and c) and anoxic (d, e, and f) conditions.

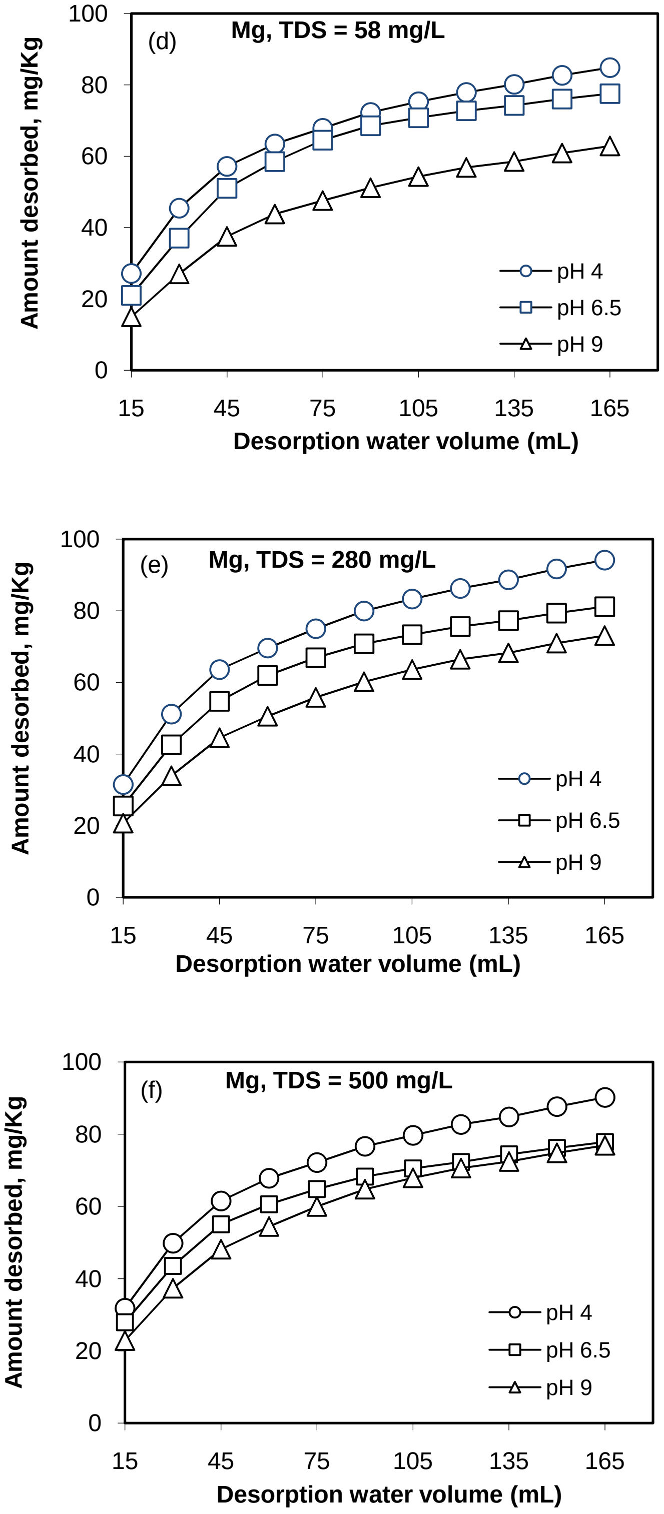

FIGURE 3.11. ***Continued.***

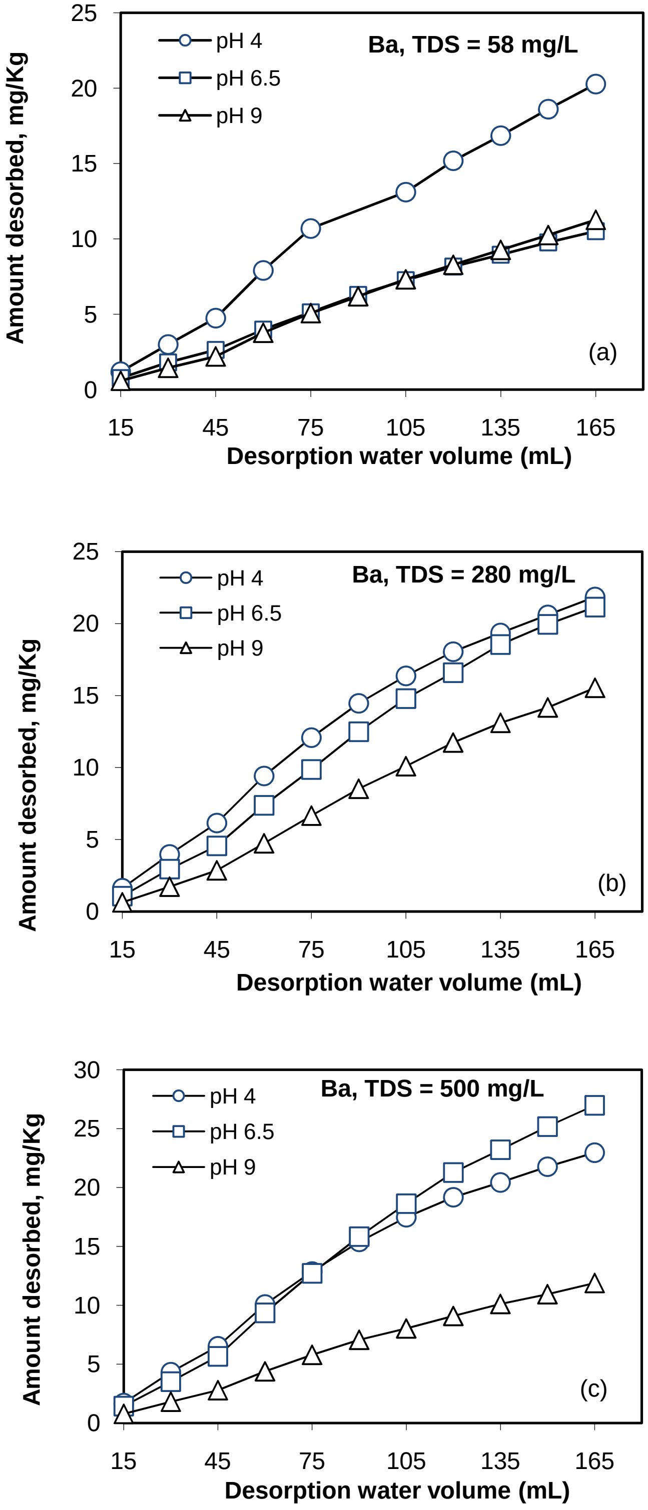

FIGURE 3.12. Effect of solution pH on desorption of barium from the LHC30 soil sample under aerobic (a, b, and c) and anoxic (d, e, and f) conditions.

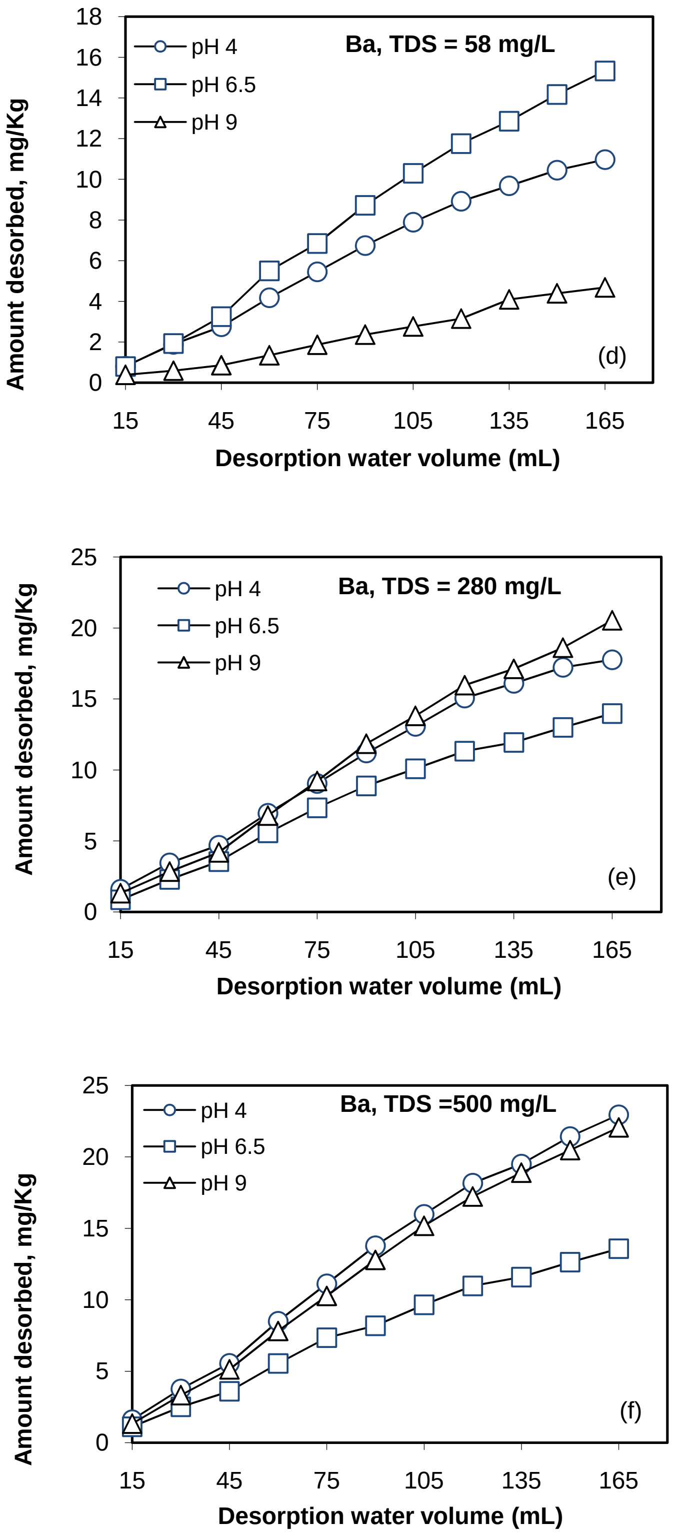

FIGURE 3.12. ***Continued*****.**

3.3.3 Effect of TDS

Figures 3.13 to 3.15 present desorption of Ba, Ca, and Mg, respectively, from natural and artificially loaded S400. It is shown that desorption of Ba, Ca, and Mg increases monotonically with TDS concentration of the desorption water for all the three pHs tested. The significantly higher desorption observed at higher TDS concentrations can be explained by two mechanisms: 1) desorption via ion exchange is greater with higher TDS concentrations, and 2) the lower activity coefficient at higher TDS concentrations results in higher solubility of theses cations, as demonstrated by the equation below:

$$\gamma_M [M^{2+}] \gamma_A [A^{2-}] = K_{so} \tag{3.1}$$

$[M^{2+}]$ = molar concentration of the divalent metal cation, namely, Ca^{2+} (moles/liter)

$[A^{2-}]$ = molar concentration of the associated anion, namely, CO_3^{2-} (moles/liter)

γ_M = activity coefficient of the divalent cation.

γ_A = activity coefficient of the associated anion.

K_{so} = solubility product of the mineral MA.

The effect of the ion-exchange mechanism seems to be more important since the effect of the TDS concentration appears to be greater at higher pH, where dissolution is less important.

Interestingly, the effect of the TDS concentration on the desorption of As from S400 was observed to be minimal. As shown in Figure 3.16, there was no significant difference in the amount of As desorbed over the TDS concentration range of 58 to 500 mg/L at all three pHs tested. These results indicate that ion exchange does not play a major role in As desorption. This finding is consistent with the negligible amount of ion-exchangeable As in the soil (Figure 2.6b).

The effect of the TDS concentration on metal desorption from the S700 soil samples is shown in Figures 3.17 to 3.20. The effect of the TDS concentration on desorption of Ba, Ca, and Mg from the S700 soil samples was similar to that observed with the S400 soil samples. The TDS concentration seems to play a more important role in As desorption from the S700 than from the S400. However, the total amount of As desorbed from the fresh S700 is much smaller than that from the fresh S400. These data indicate that ion exchange is an important mechanism of As desorption for the fresh S700 soil sample, although the amount of ion-exchangeable As in S700 is extremely small. The artificially loaded S700 soil sample showed much higher As desorption because of the high As content in the soil sample. The response of As desorption to changes in TDS concentration is similar to those of Ba, Ca, and Mg. This finding indicates that most of the artificially loaded As is ion-exchangeable.

Figures 3.21 to 3.23 show the effect of the TDS concentration on desorption of Ca, Mg, and Ba, respectively, from the LHC30. In general, desorption of Ca and Mg slightly increases with increasing TDS, but TDS does not affect Ca or Mg desorption as much as the solution pH. Because it is hypothesized that release of Ca is controlled by dissolution of Ca minerals, calculation of the activity coefficient was done to demonstrate the effect of the TDS concentration on Ca desorption: assuming that all the TDS in the desorption solutions are NaCl, the ionic strengths corresponding to the TDS concentration of 58, 280, and 500 mg/L are 1, 4.8, and 8.6 mM, corresponding to activity coefficients of 0.87, 0.74, and 0.68, respectively, for Ca ions. This finding is consistent with the difference in Ca desorption between the TDS levels of 58 and 500 mg/L observed in some experiments, although in other experiments' sets of conditions, for example, pH = 9 (aerobic) and pH = 4 and 6.5 (anoxic), smaller-than-expected differences between the different TDS levels were observed. These observations indicate that the impact of TDS is more complex than simply affecting the activity coefficient of Ca.

The slightly higher desorption of Mg at a higher TDS concentration is attributable to stronger ion exchange by Na^+ in the desorption solution.

TDS plays an important role in Ba desorption; a higher TDS level in general results in more Ba desorption except for at pH = 9 under aerobic conditions. This phenomenon can be explained by a combination of the impacts of TDS on solubility and on ion exchange.

It is noted that no common ion effect exists under the conditions tested since the TDS was adjusted by using only NaCl. The effect of the TDS concentration will be very different if common ions, namely, Ca^{2+}, Mg^{2+}, and Ba^{2+}, are present in the desorption solution. This finding is discussed in more detail later.

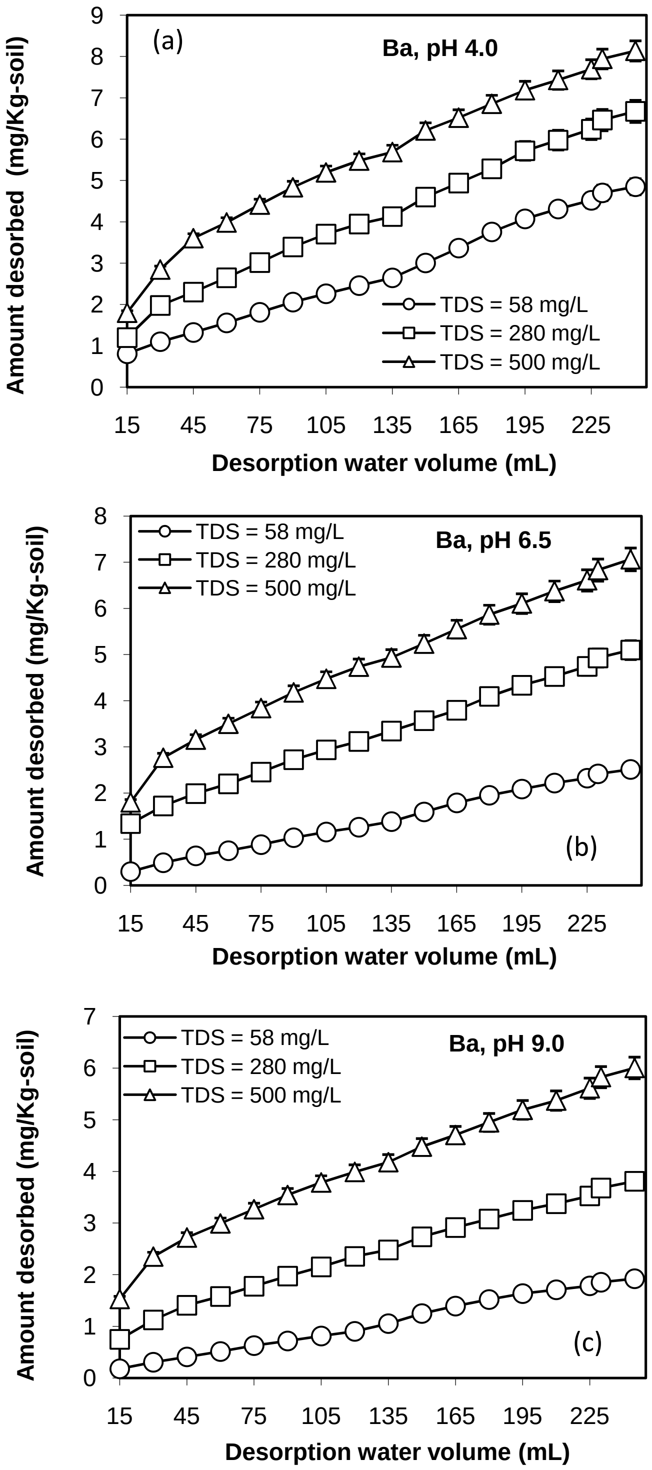

FIGURE 3.13. Effect of TDS on cumulative desorption of Ba from natural (a, b, and c) and artificially loaded (d, e, and f) S400.

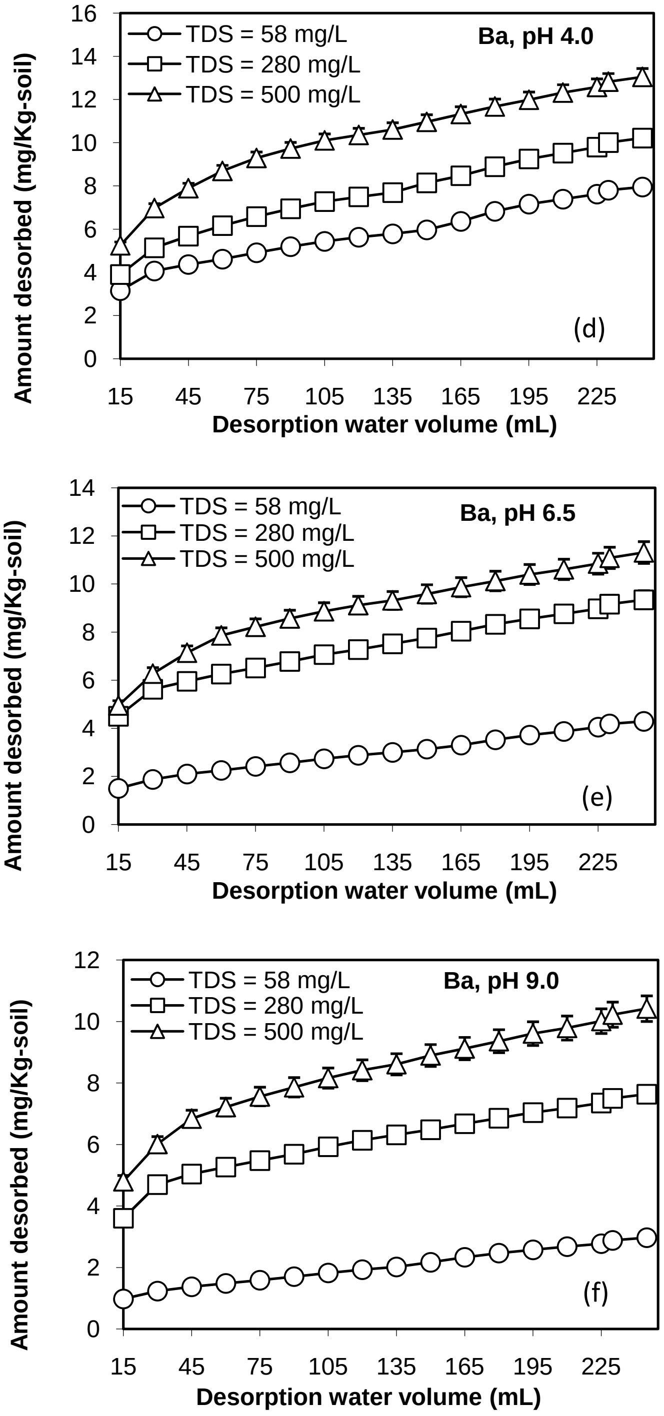

FIGURE 3.13. ***Continued*****.**

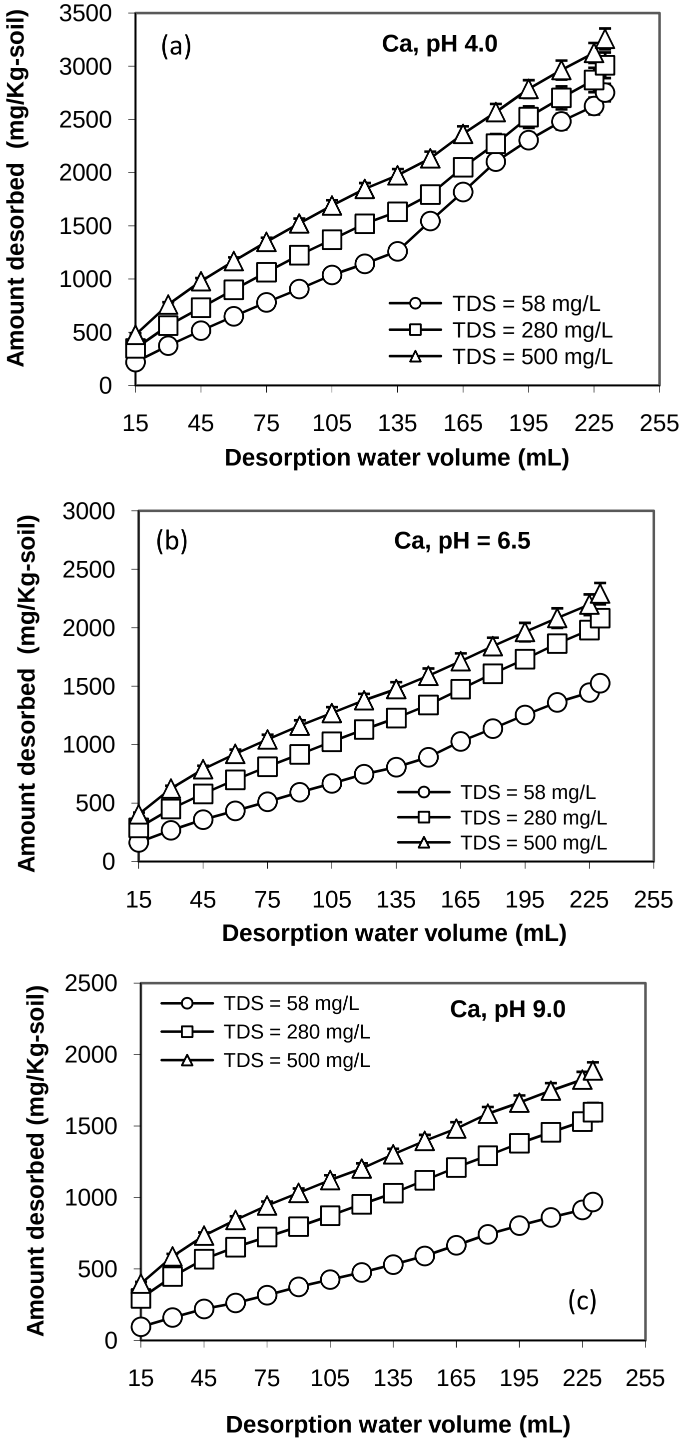

FIGURE 3.14. Effect of TDS on cumulative desorption of Ca from natural (a, b, and c) and artificially loaded (d, e, and f) S400.

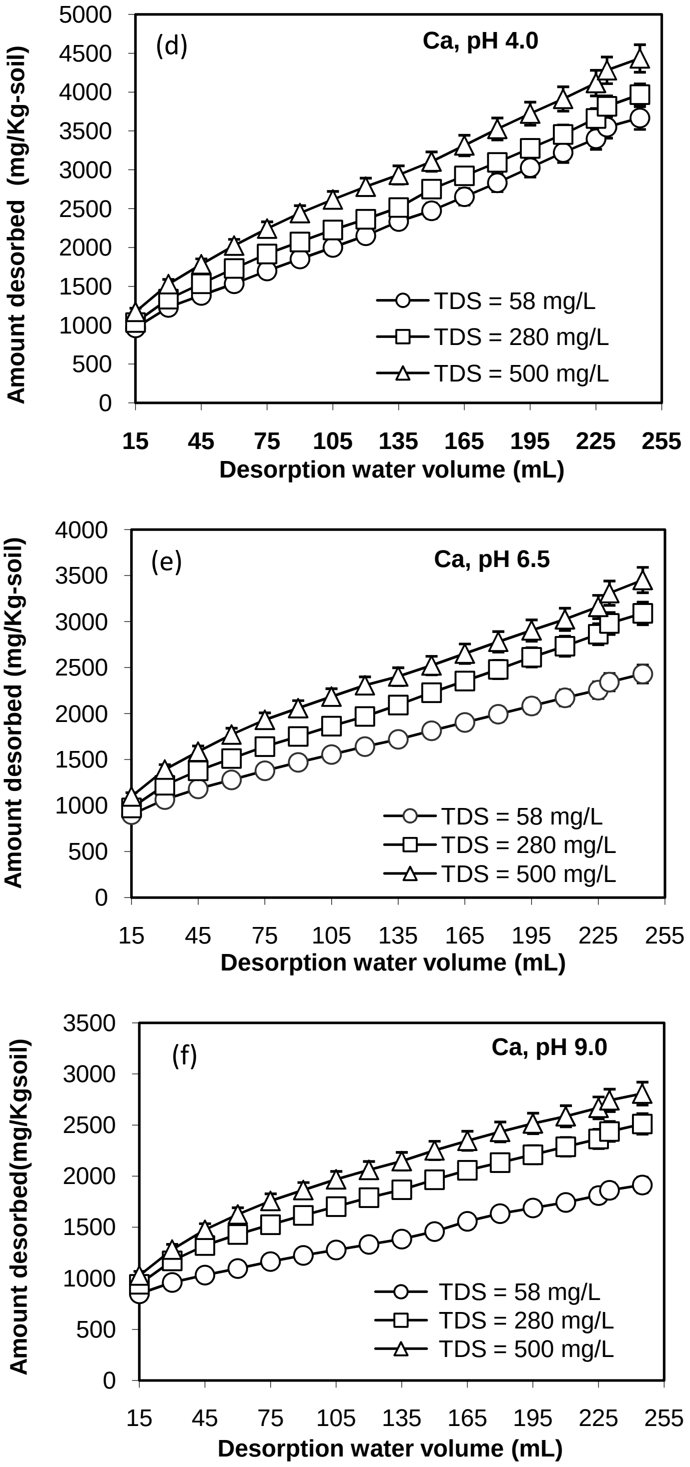

FIGURE 3.14. ***Continued*****.**

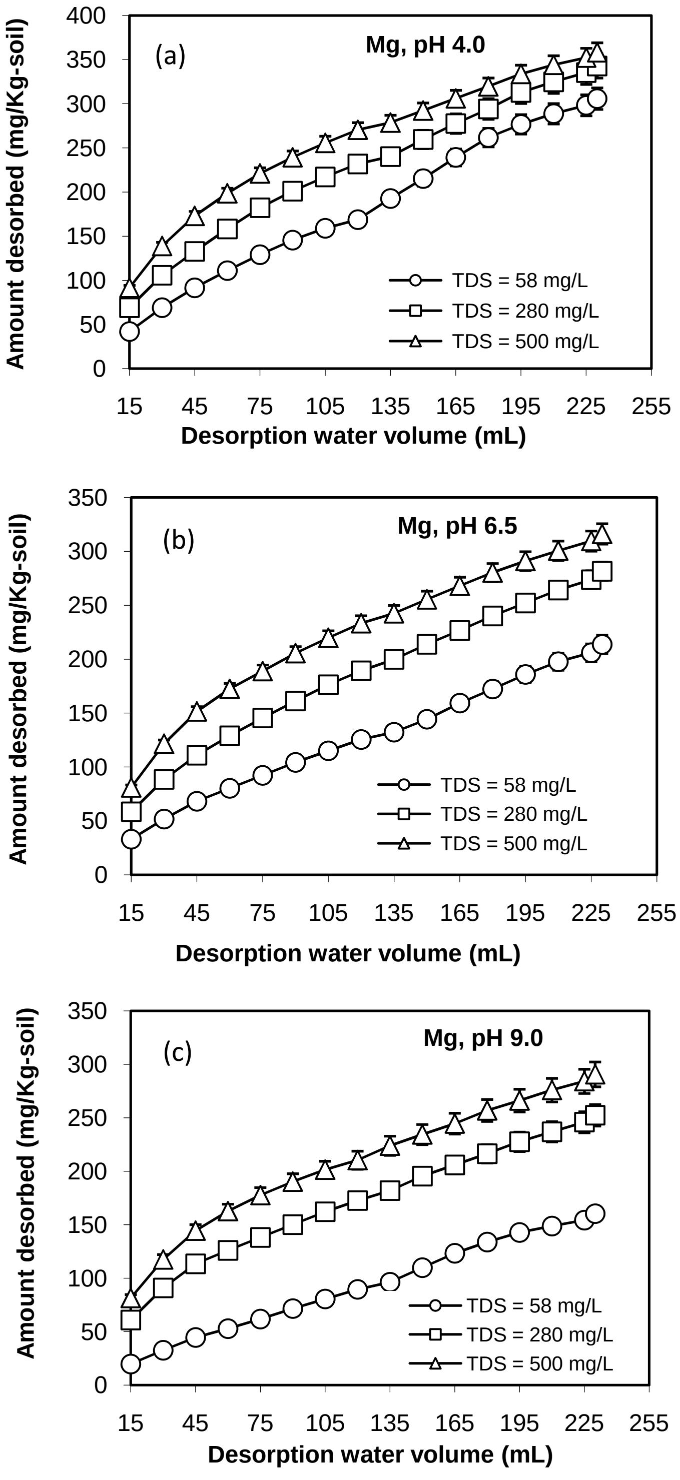

FIGURE 3.15. Effect of TDS on cumulative desorption of Mg from natural (a, b, and c) and artificially loaded (d, e, and f) S400.

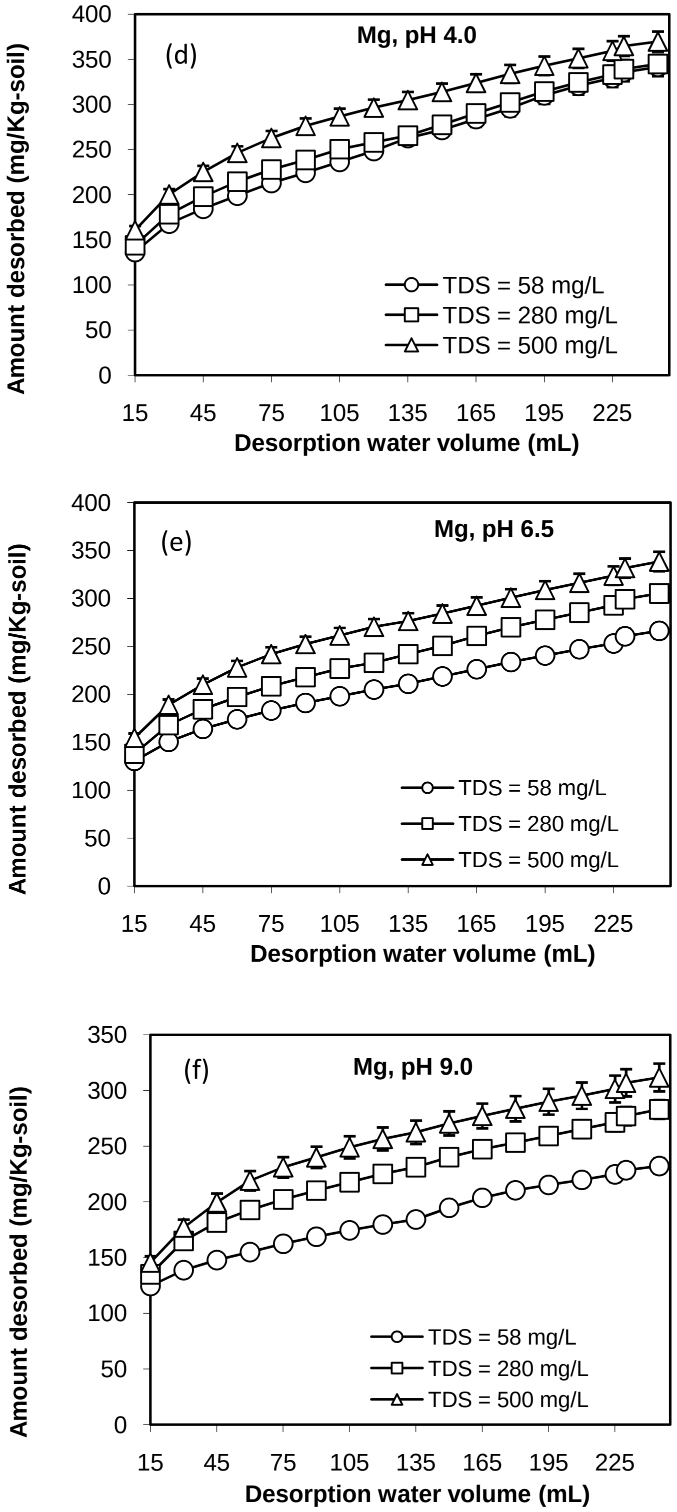

FIGURE 3.15. ***Continued.***

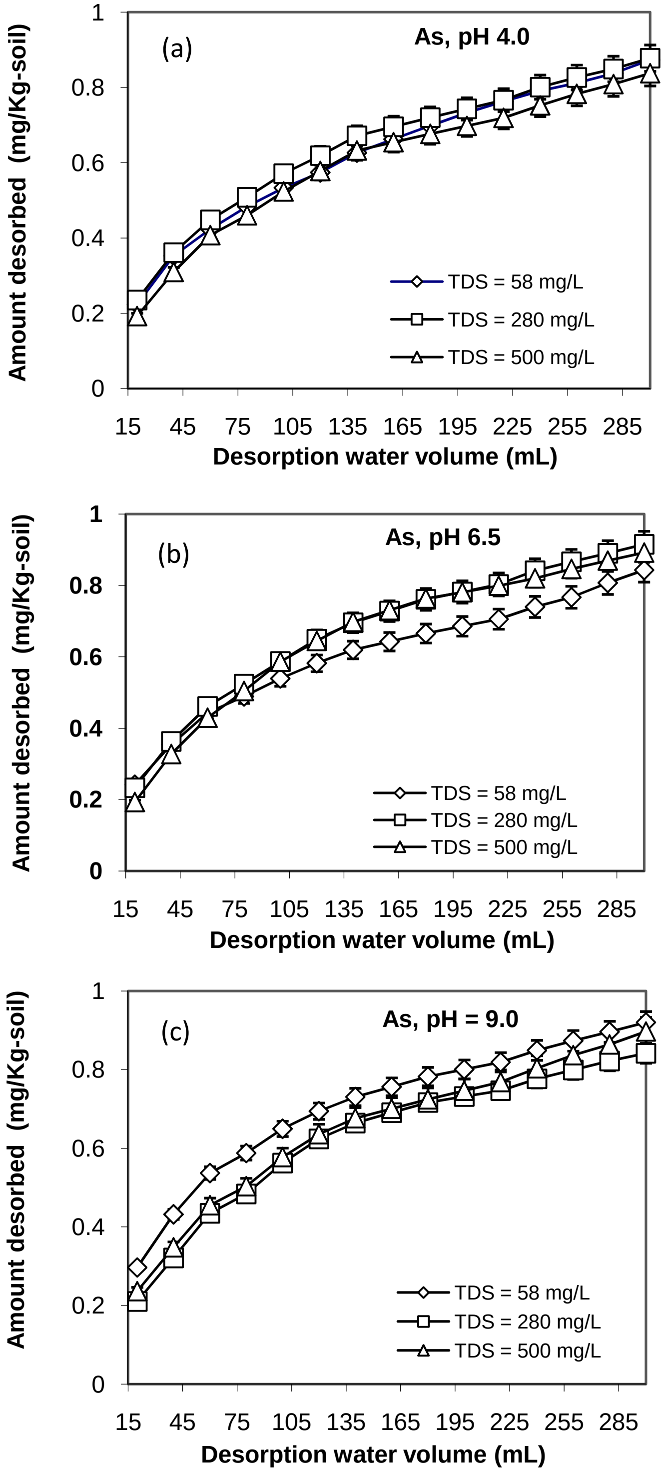

FIGURE 3.16. Effect of TDS on cumulative desorption of As from natural (a, b, and c) and artificially loaded (d, e, and f) S400.

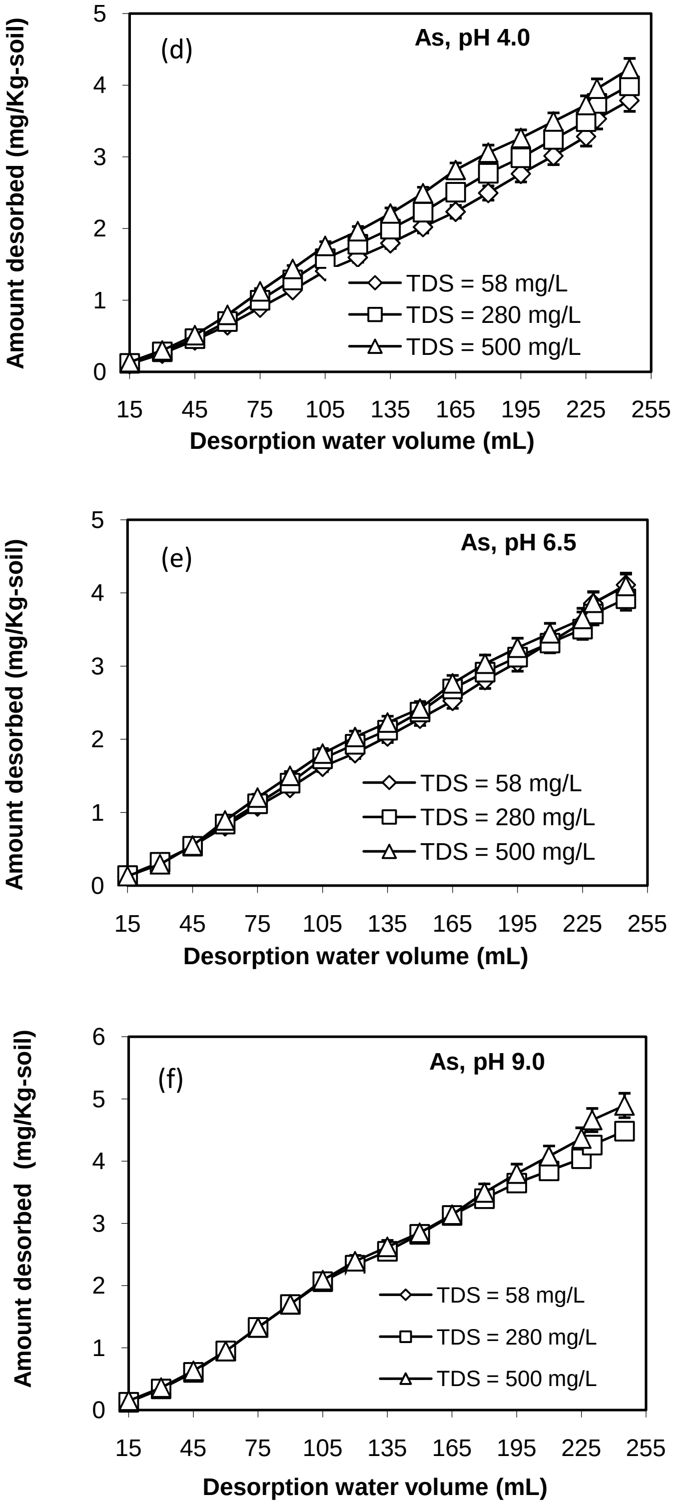

FIGURE 3.16. ***Continued.***

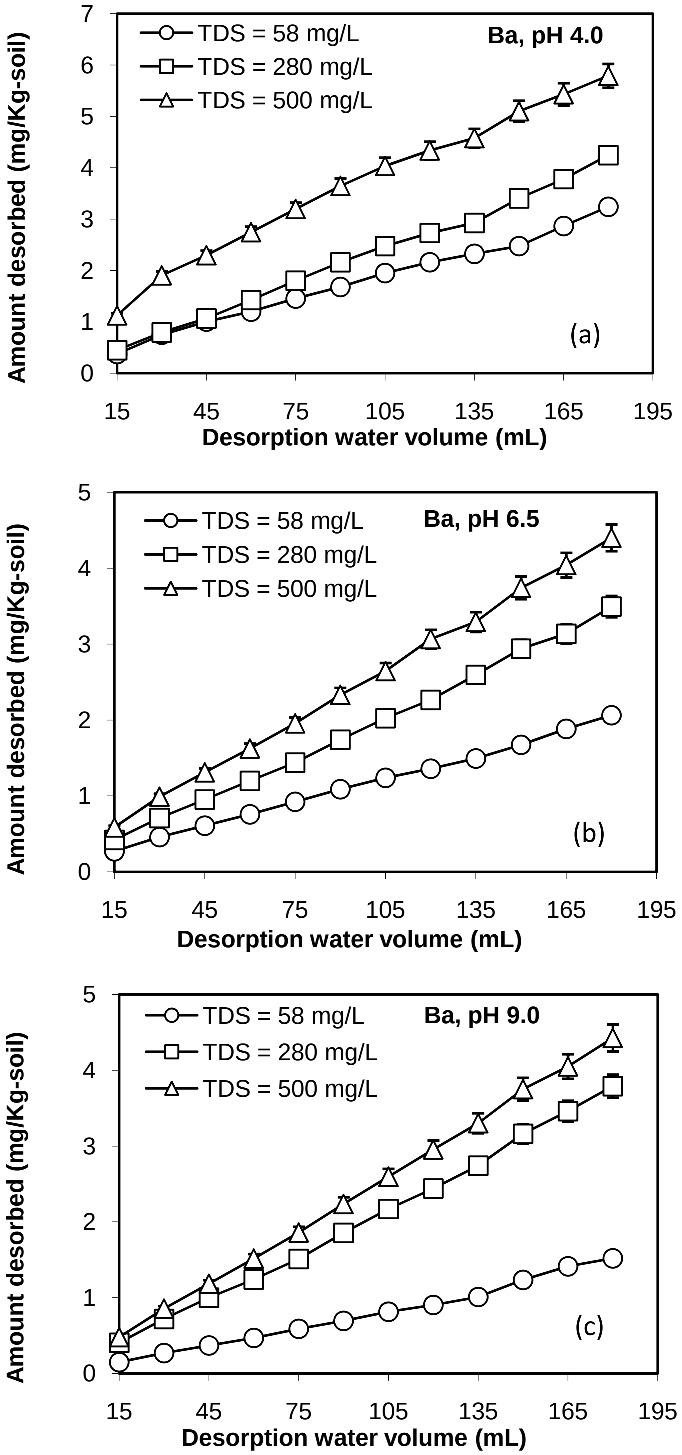

FIGURE 3.17. Effect of TDS on cumulative desorption of Ba from natural (a, b, and c) and artificially loaded (d, e, and f) S700.

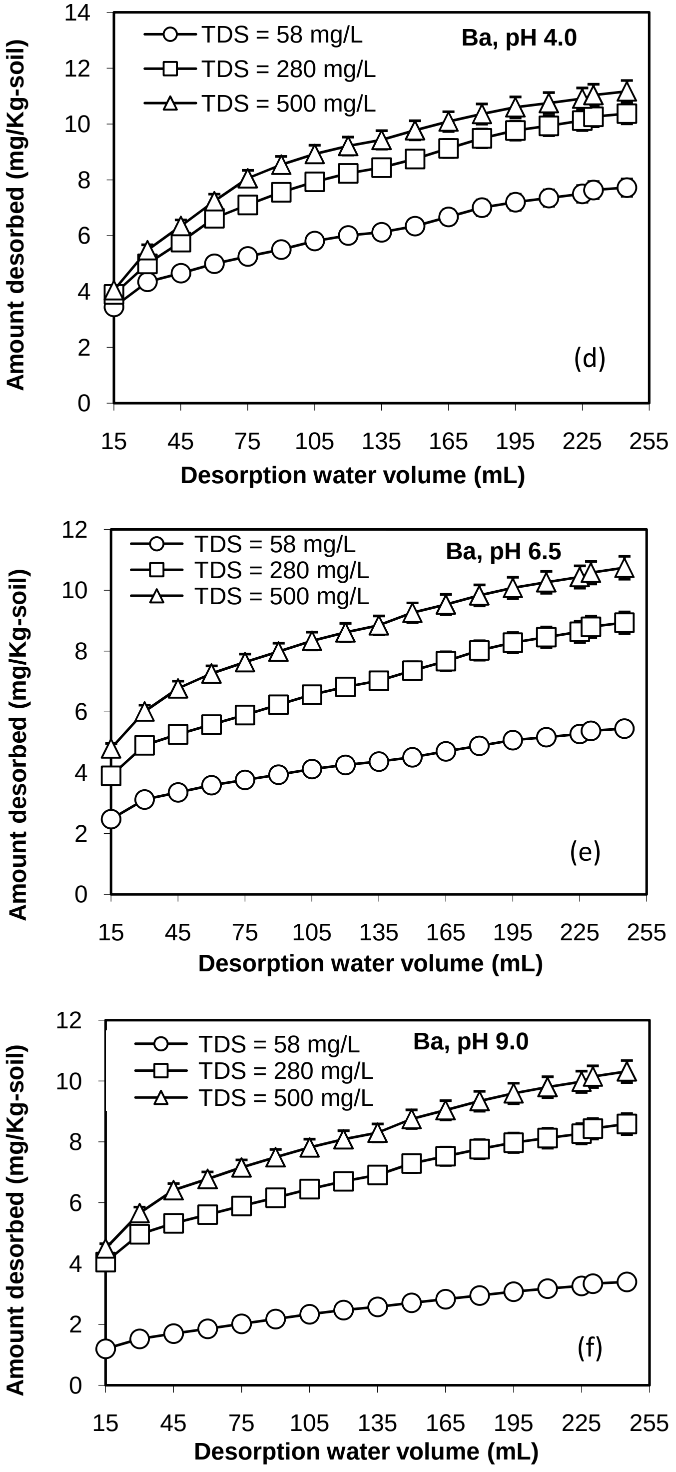

FIGURE 3.17. ***Continued.***

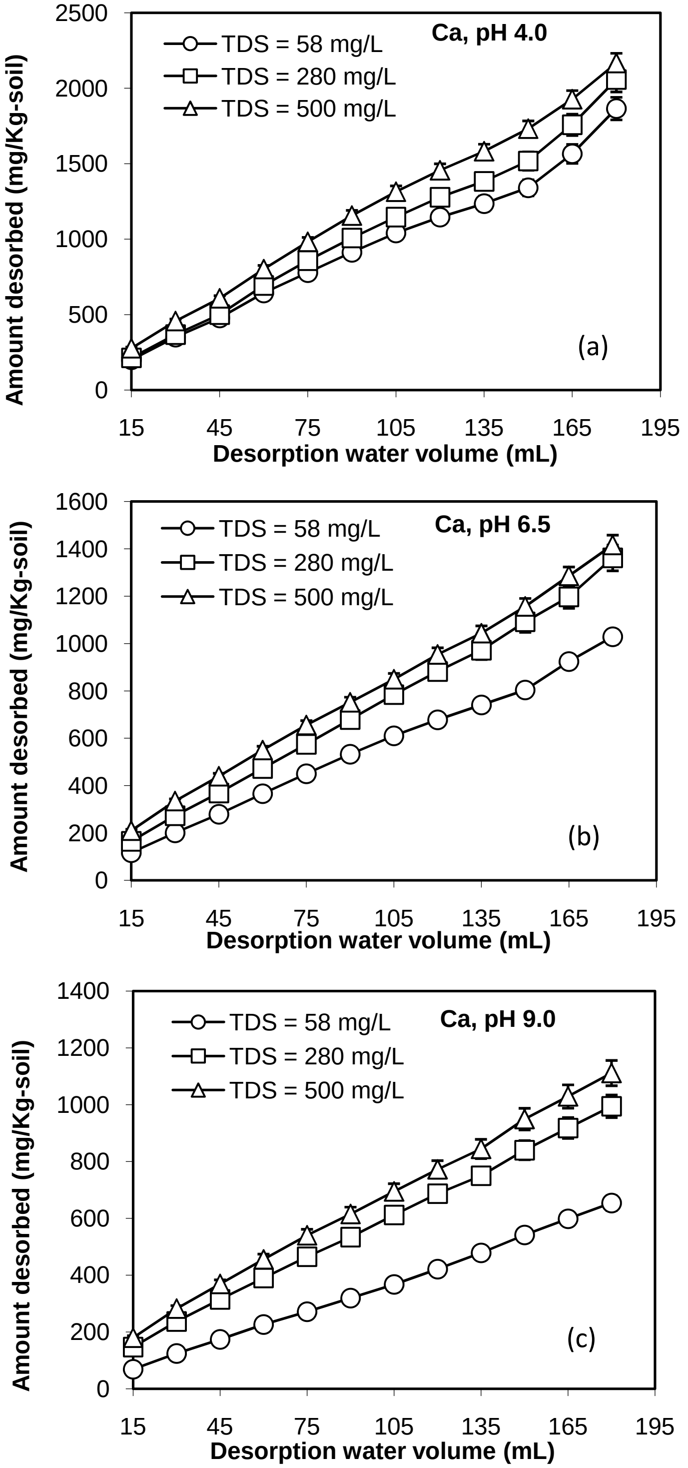

FIGURE 3.18. Effect of TDS on cumulative desorption of Ca from natural (a, b, and c) and artificially loaded (d, e, and f) S700.

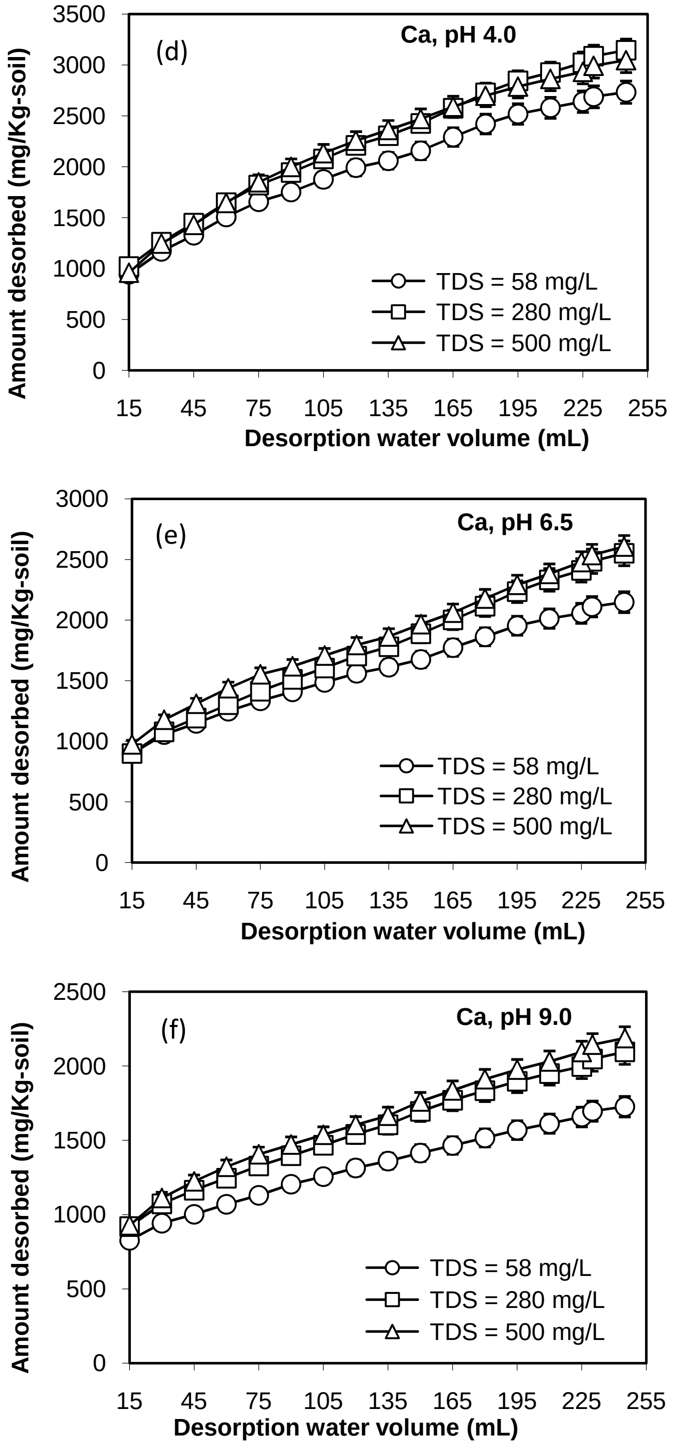

FIGURE 3.18. ***Continued*****.**

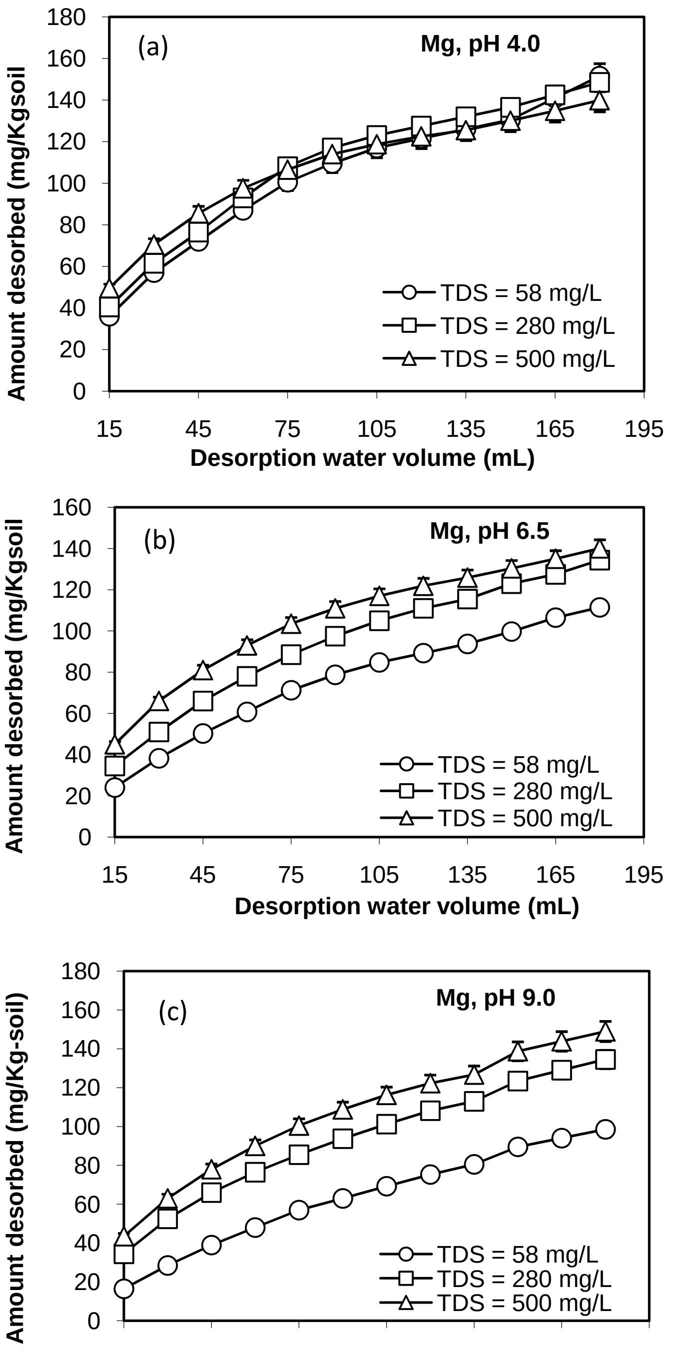

FIGURE 3.19. Effect of TDS on cumulative desorption of Mg from natural (a, b, and c) and artificially loaded (d, e, and f) S700.

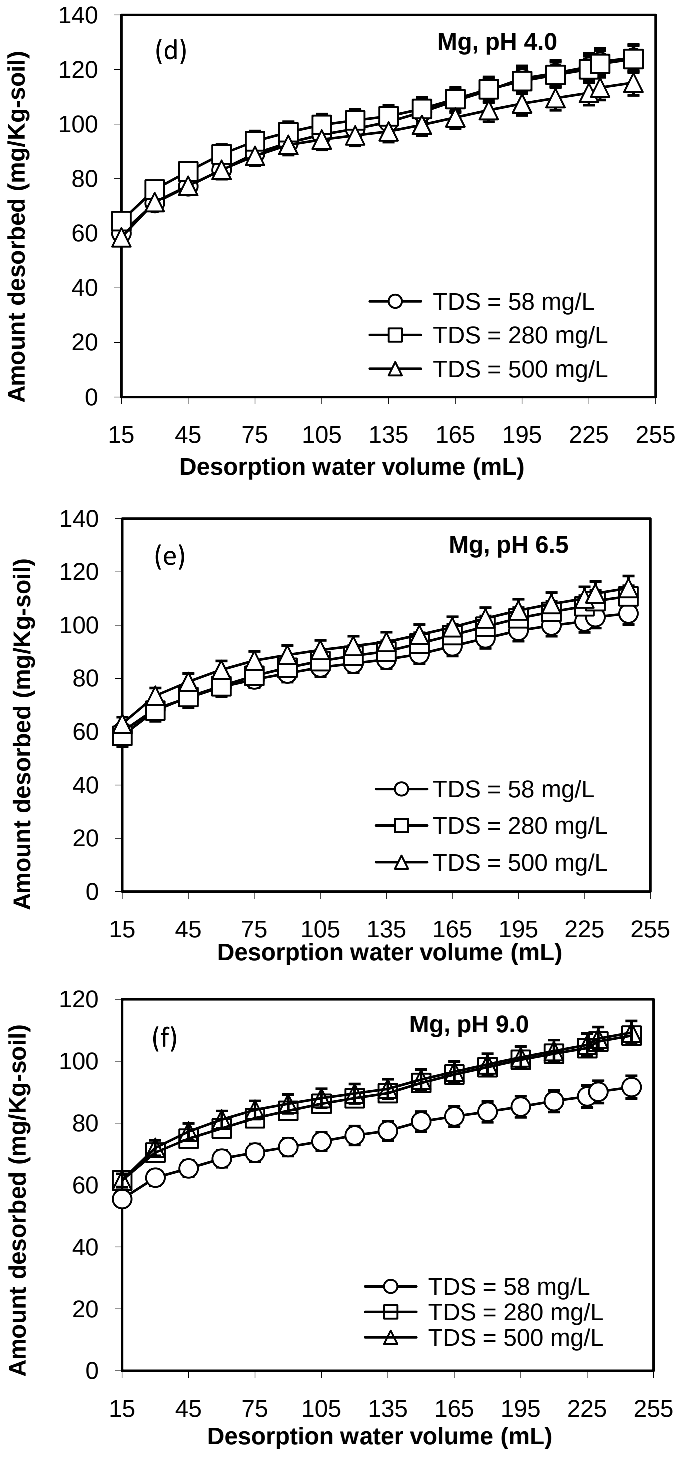

FIGURE 3.19. ***Continued*.**

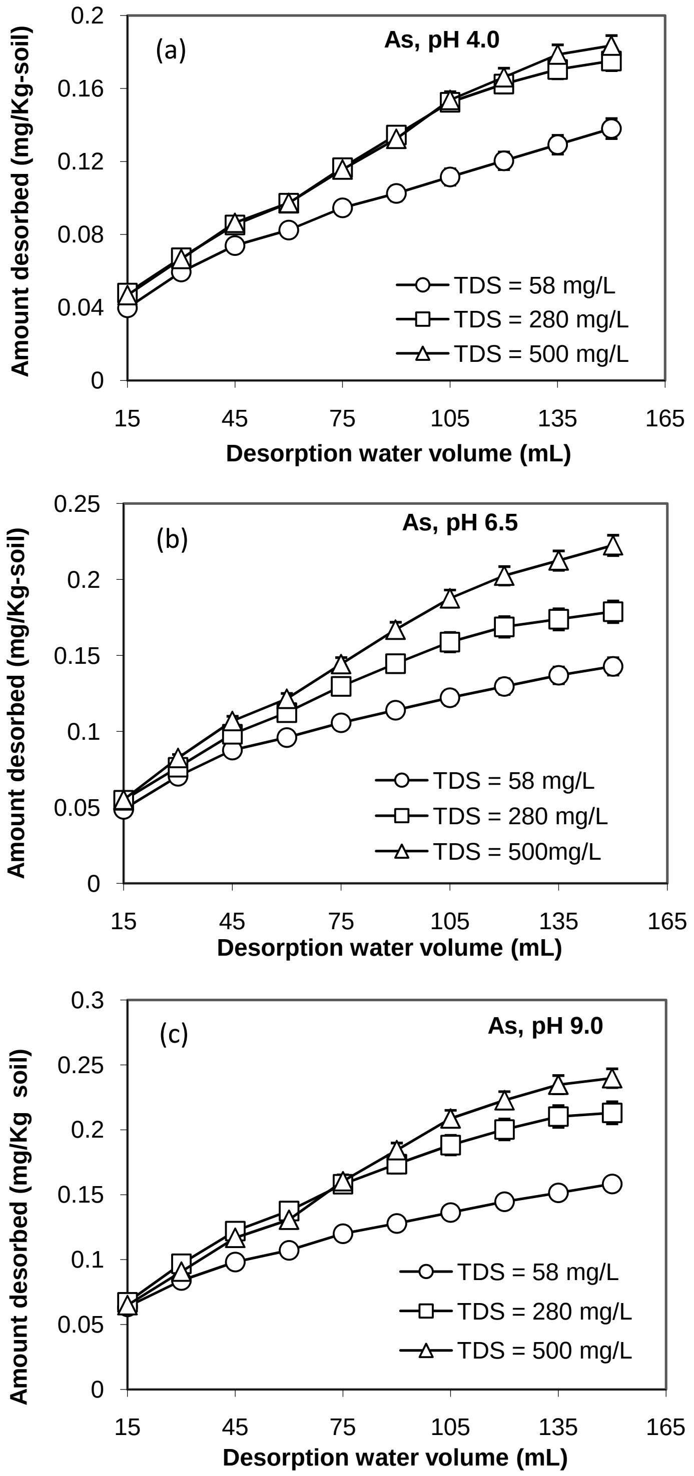

FIGURE 3.20. Effect of TDS on cumulative desorption of As from natural (a, b, and c) and artificially loaded (d, e, and f) S700.

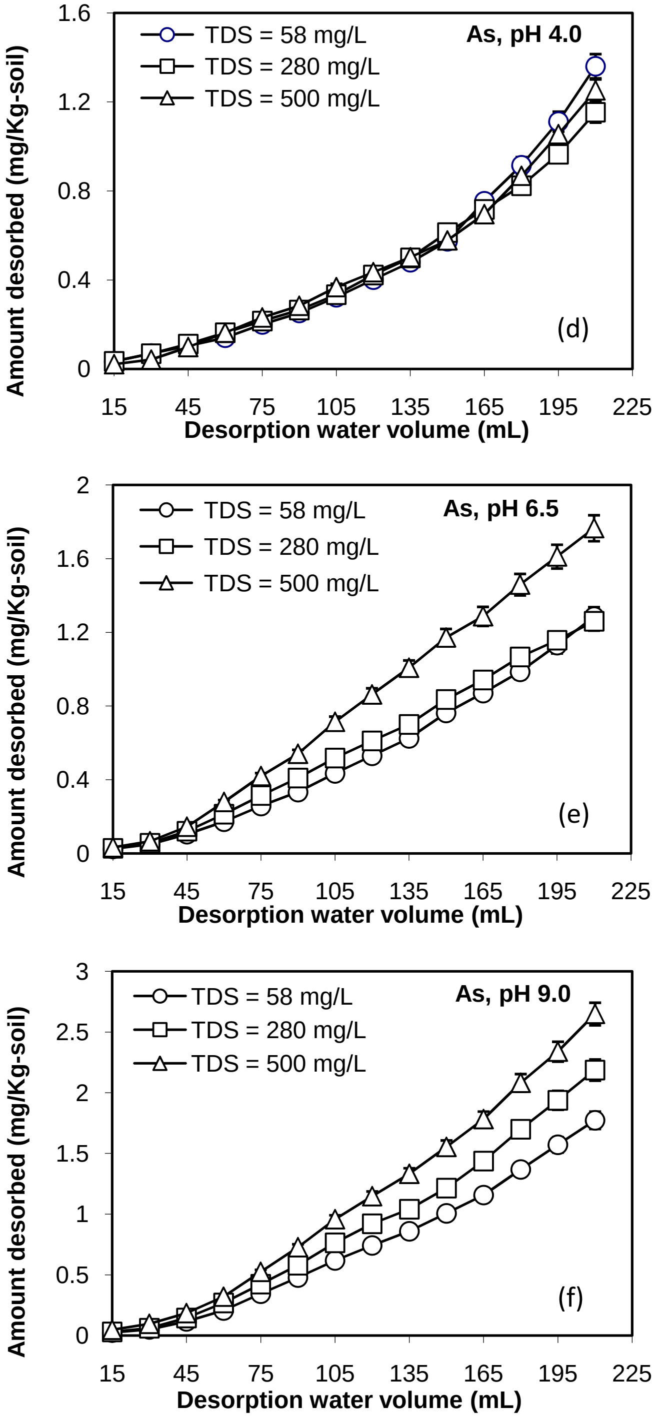

FIGURE 3.20. ***Continued*.**

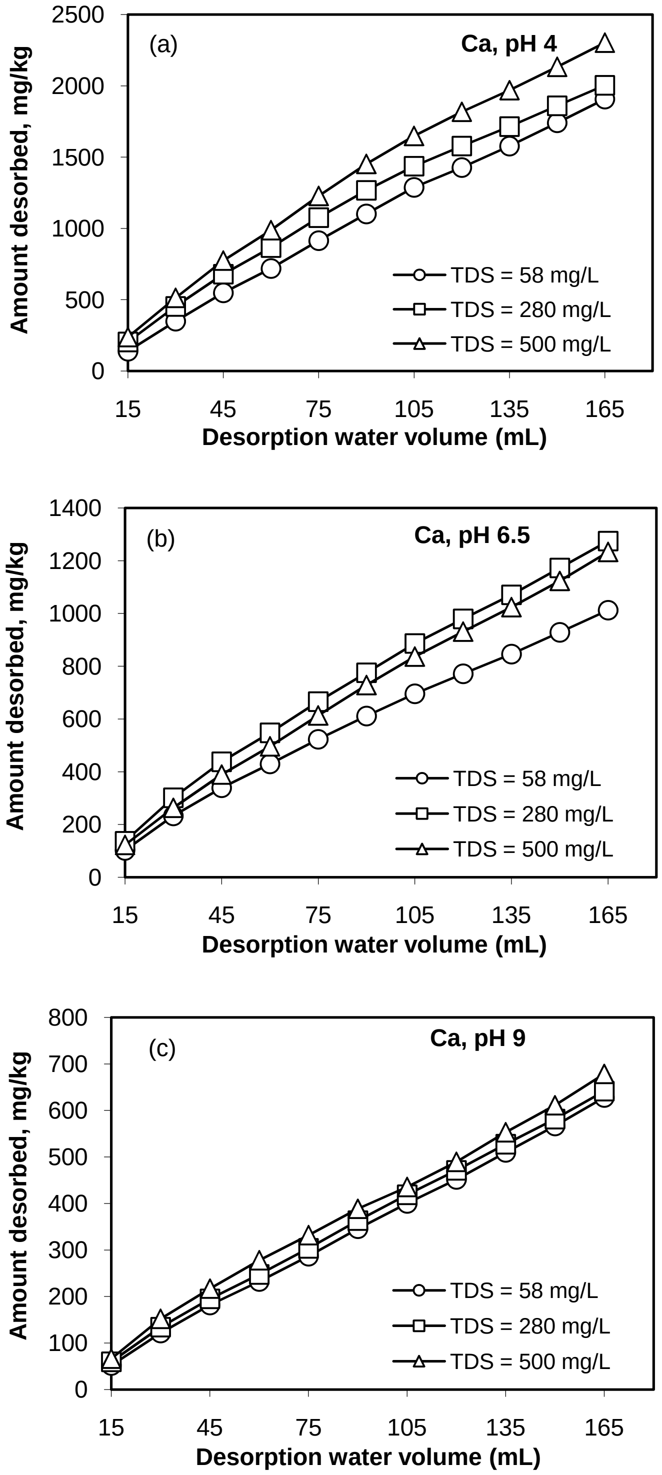

FIGURE 3.21. Effect of TDS on desorption of calcium from LHC30 in aerobic (a, b, and c) and anoxic (d, e, and f) conditions.

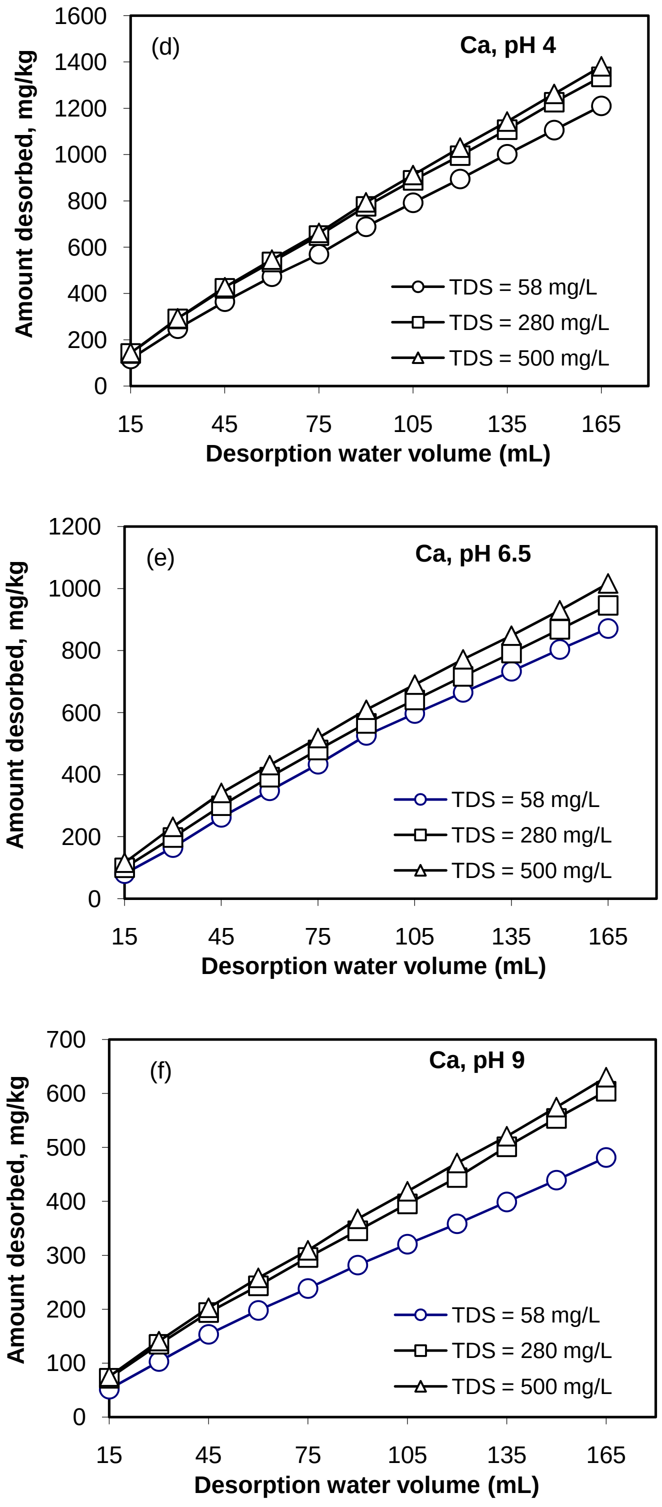

FIGURE 3.21. ***Continued*****.**

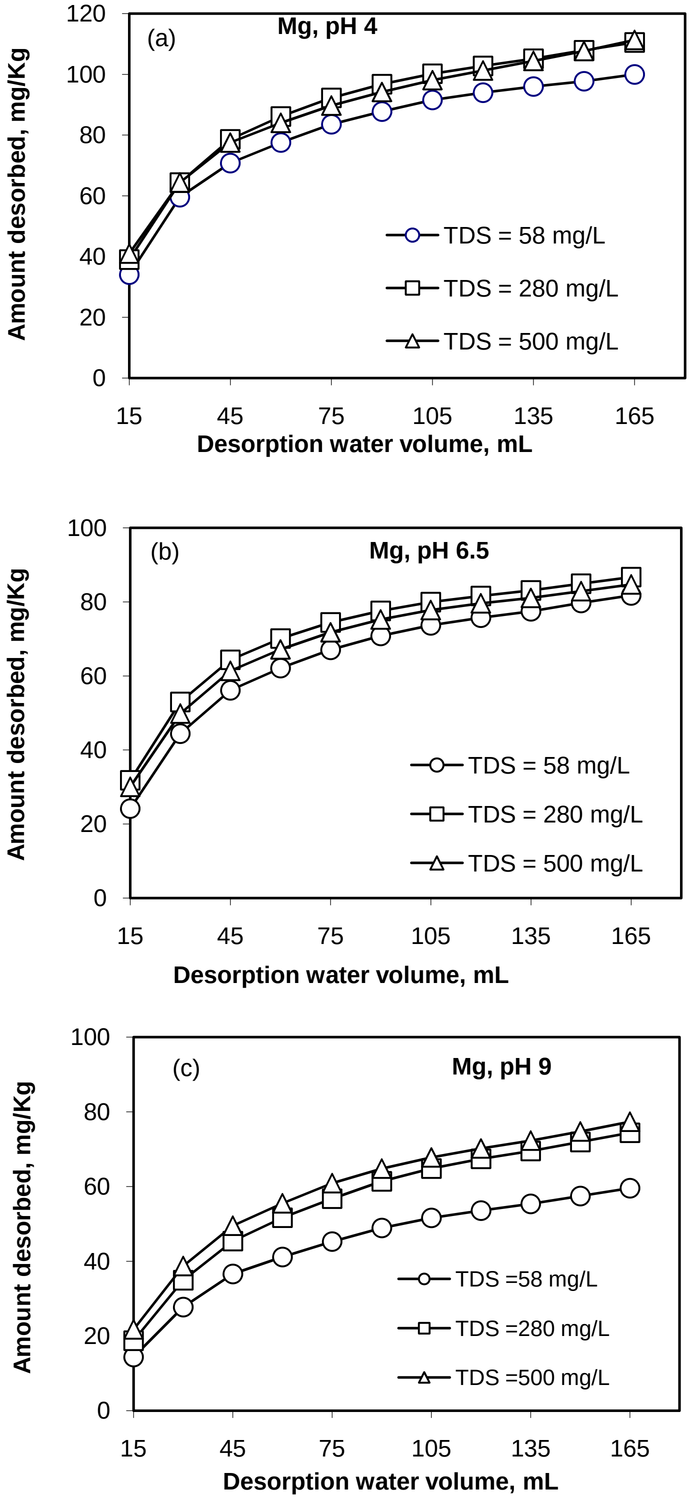

FIGURE 3.22. Effect of TDS on desorption of magnesium from LHC30 under aerobic (a, b, and c) and anoxic (d, e, and f) conditions.

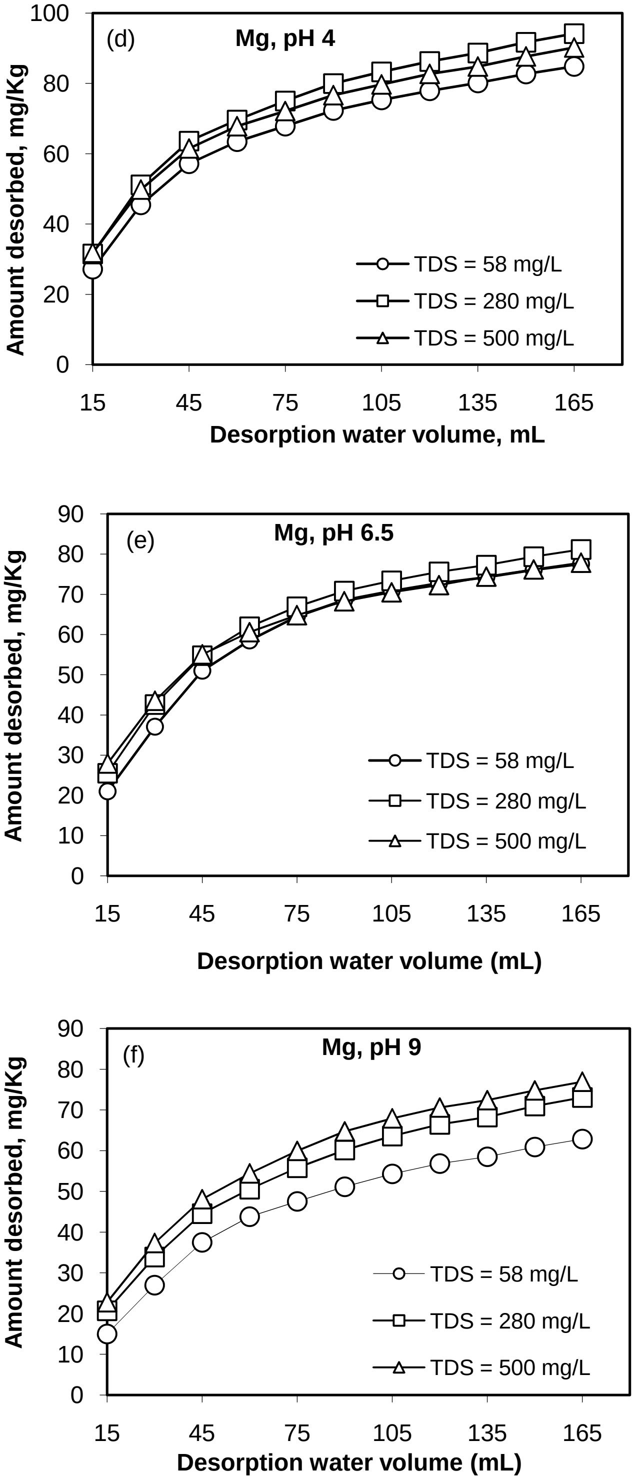

FIGURE 3.22. ***Continued.***

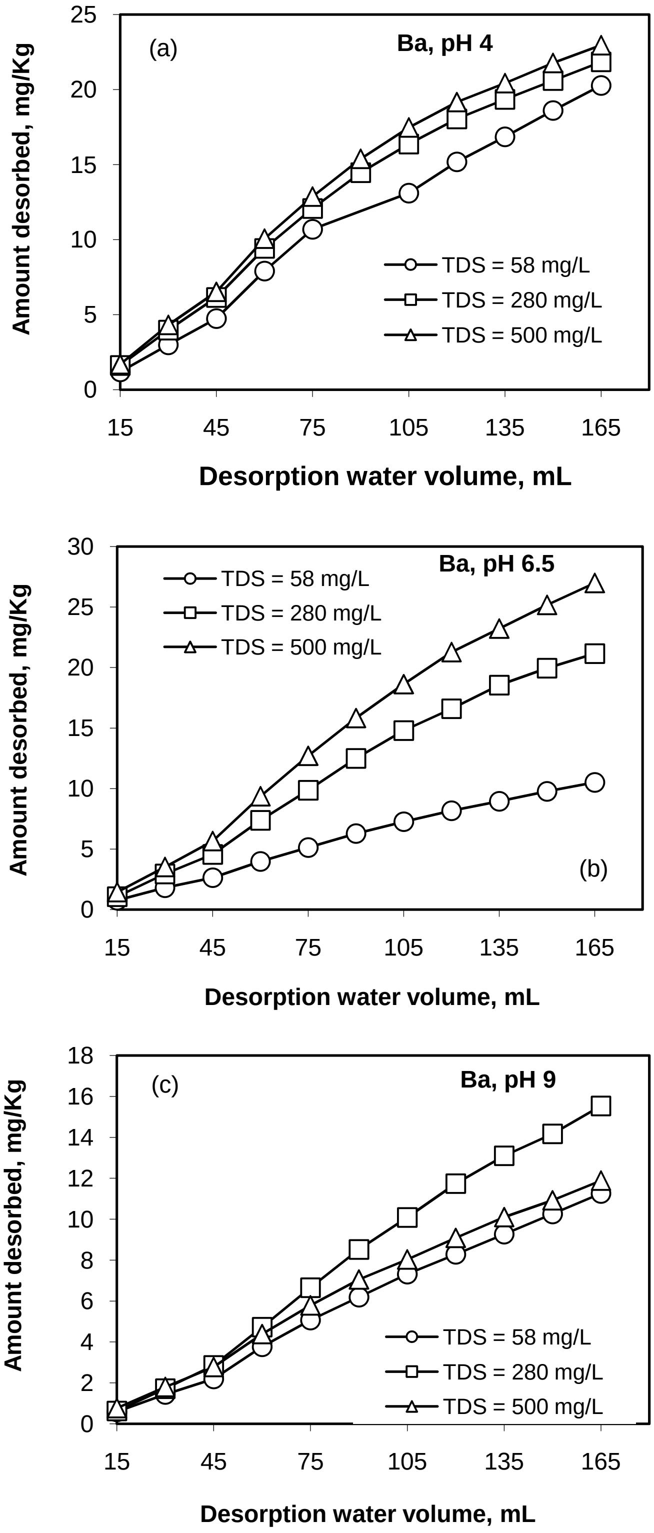

FIGURE 3.23. Effect of TDS on desorption of barium from LHC30 under aerobic (a, b, and c) and anoxic (d, e, and f) conditions.

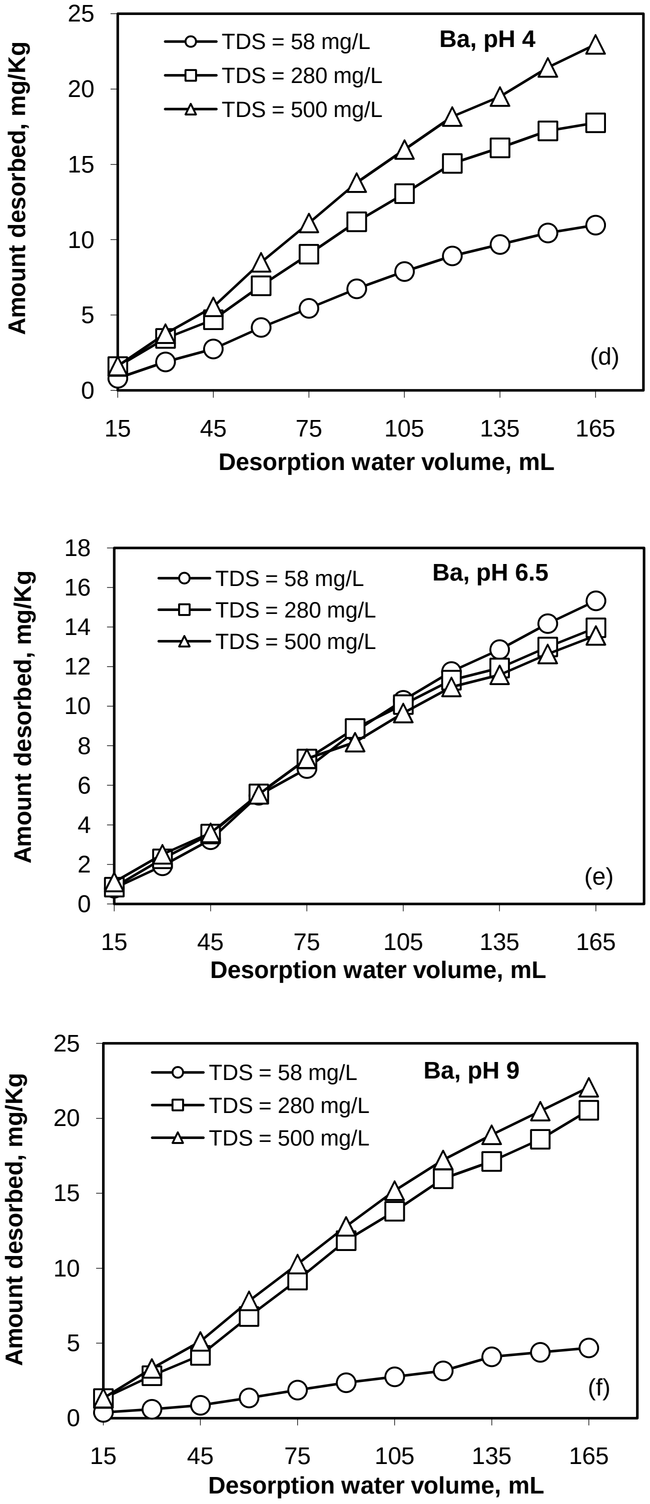

FIGURE 3.23. ***Continued.***

3.3.4 Effect of Ionic Composition

Based on the results presented above, it will be predicted that recharge water with higher TDS will cause more desorption of metal species. However, this prediction may not be true in practice because the ionic composition of the model recharge water used in the experiments reported above does not represent real recharge water. In these experiments, the TDS concentration was adjusted using NaCl alone. As a result, the recharge water contains mostly NaCl since the RO water contains very few other ions. In practice, the RO water often undergoes pH and alkalinity adjustment by lime addition before being used for recharge. Therefore, there is a significant amount of Ca and carbonate in the recharge water. Under such conditions, the common ion effect should be taken into consideration since carbonate mineral (namely, calcite) dissolution is a major mechanism responsible for leaching of As from the S400 and S700.

The effect of ionic composition was studied by adjusting the TDS level of the desorption solution and by using $CaCl_2$ instead of NaCl. Desorption equilibrium experiments were performed with the S400 at pH = 6.5 and with TDS of 50, 280, and 500 mg/L. Experimental results show that when $CaCl_2$ was used to adjust the TDS level of the desorption solution, a decrease instead of increase in aqueous-phase Ca concentration was observed, indicating a net adsorption instead of desorption due to the high concentration of Ca in the desorption solution.

Figure 3.24 compares the desorption of As for the two different desorption solutions. At the lowest TDS concentration, 58 mg/L, As desorption by the $CaCl_2$-augmented water was similar to that by the NaCl-augmented water. This phenomenon occurred because a very small amount of NaCl or $CaCl_2$ was added to adjust the solution pH from ~6 to 6.5. Hence, a very small amount of NaCl or $CaCl_2$ was added to bring the TDS level to 58 mg/L. The difference between the two desorption solutions was very small. At higher TDS concentrations, As desorption was significantly lower when $CaCl_2$ was used, and it decreased with increasing TDS (or $CaCl_2$) concentration. Considering that calcite is a primary mineral in the S400 soil, this finding is consistent with our hypothesis that part of the As released in desorption experiments with NaCl-augmented water is associated with calcite in the soil. This finding is also consistent with the soil analysis results, which show that a significant amount of As in the S400 soil sample is bound to carbonate (Figure 2.6b). When NaCl is used to adjust the TDS concentration of the desorption solution, the lack of Ca in the desorption solution causes dissolution of calcite in the S400 soil, resulting in the release of calcite-associated As. When a high concentration of $CaCl_2$ is used, the aqueous-phase Ca concentration exceeds the concentration in equilibrium with the soil. Therefore, adsorption or surface precipitation of Ca occurs (as shown in the decreasing aqueous-phase Ca concentration observed in the desorption experiments). As a result, desorption of As decreases with increasing $CaCl_2$ concentration in the desorption solution. It is anticipated that an increase in alkalinity will also result in a decrease in As desorption due to the reduced dissolution of calcite. This information can be used to guide surface infiltration operations to minimize As leaching: adding lime or soda ash to condition the RO-treated water can potentially mitigate As desorption.

On the other hand, desorption of Mg is significantly higher with $CaCl_2$-containing desorption solution than with NaCl (Figure 3.25). Desorption of Mg by both types of desorption solutions increases with increasing TDS levels. These results suggest that desorption of Mg is mainly through ion exchange. Ca has a higher selectivity than Na. Therefore, exchange of Mg by Ca is greater than that by Na.

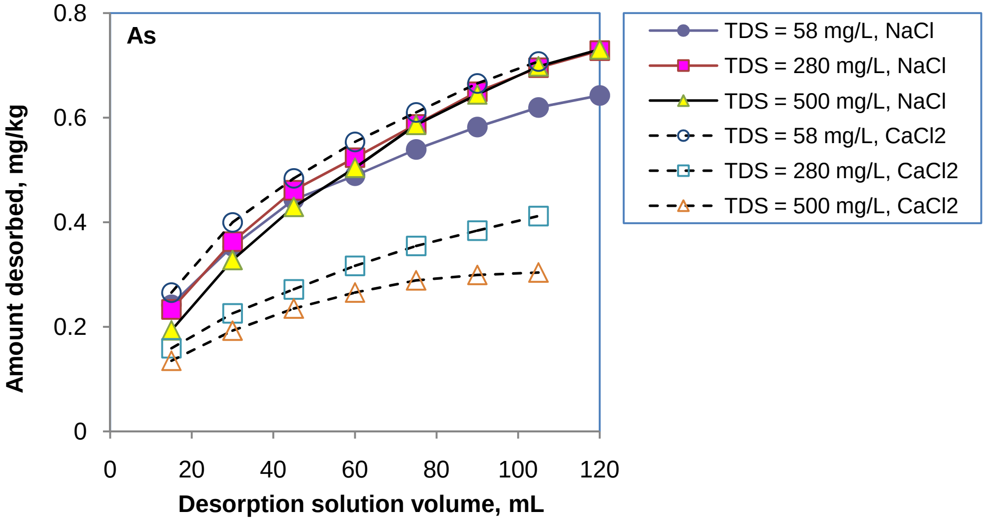

FIGURE 3.24. Effect of cationic composition of desorption solution on arsenic desorption.

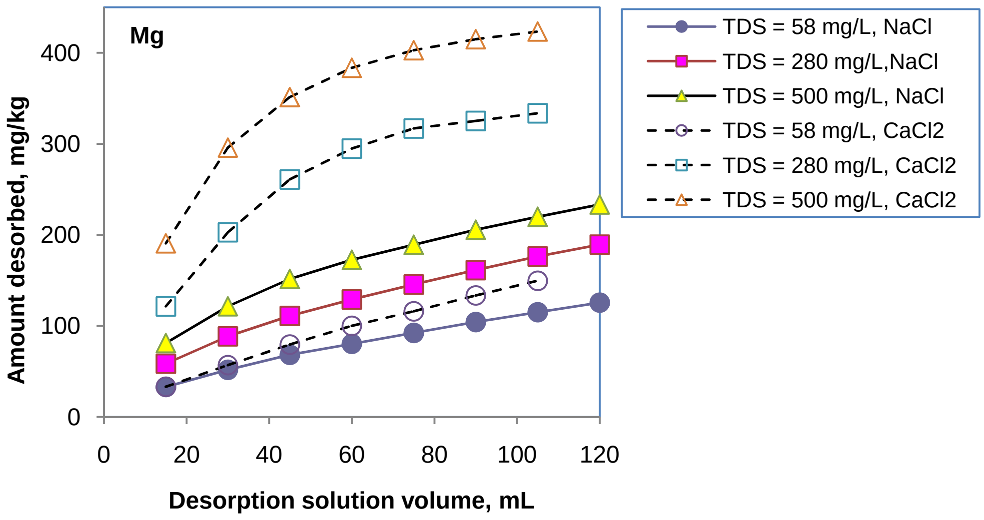

FIGURE 3.25. Effect of cationic composition of desorption solution on magnesium desorption.

3.3.5 Effect of Redox Potential

Desorption of both Ca and Mg from the LHC30 soil was found to be greater under aerobic conditions than that under anoxic conditions (see Figures 3.21 and 3.22). The impact of redox potential on Ba desorption, however, depends on the solution pH and the TDS level. At acidic pHs, namely, pH = 4, more desorption of Ba was observed under aerobic conditions. At higher pHs, no consistent trend was observed. The reason for the difference between the desorption behaviors under aerobic and anoxic conditions is unclear. A common reason for greater desorption under aerobic conditions is the oxidation and subsequent dissolution of iron sulfides. Although S was not identified in the elemental analysis of the soil samples from the IWWTP site (see Table 2.5), it may exist at trace concentration level in the form of FeS.

3.3.6 Effect of Microbiological Activity

The experiments reported above were all conducted under nonsterile conditions. Whether microbiological activity plays a role in the desorption of metals was unclear. Therefore, some desorption equilibrium experiments using natural and artificially loaded S400 were repeated with the addition of 1 mM NaN_3, a biocide commonly used in laboratory studies to inhibit microbial growth. The pHs tested were 4 and 9, and the TDS levels tested were 58 and 500 mg/L.

Figures 3.26 to 3.29 compare desorption results of three primary metals as well as of arsenic obtained from desorption equilibrium experiments with and without NaN_3. In general, no significant difference was found between the results obtained with and without NaN_3, indicating that microbiological activities did not play an important role in metal desorption under the conditions tested in this study. In a few cases, desorption in the presence of NaN_3 was greater: for example, As desorption at a pH of 4 and TDS of 58 mg/L and Ba desorption at pHs of 4 and 9 and TDS of 500 mg/L. It is noted that the concentration of NaN_3 is not included in the TDS values. The discrepancy observed may be partially due to the difference in TDS.

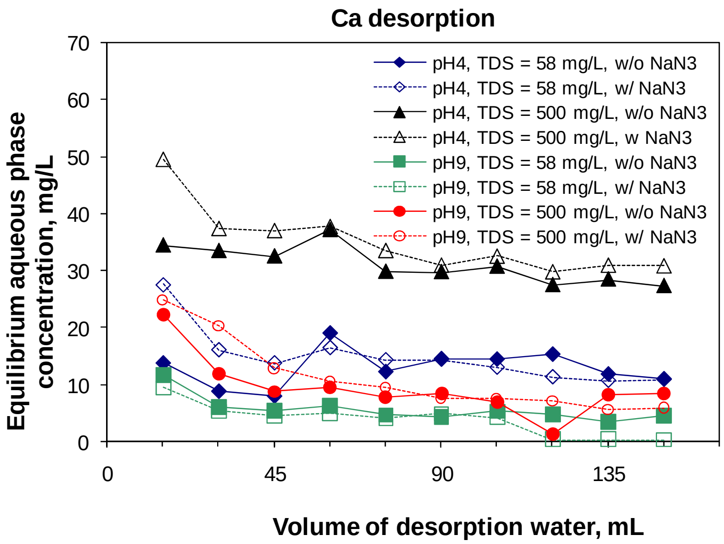

FIGURE 3.26. Calcium desorption in the presence and absence of biocide NaN_3.

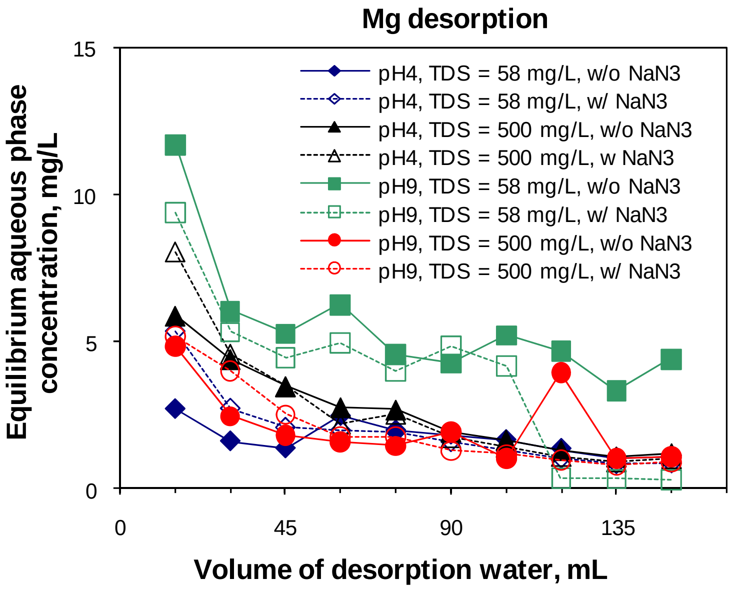

FIGURE 3.27. Magnesium desorption in the presence and absence of biocide NaN_3.

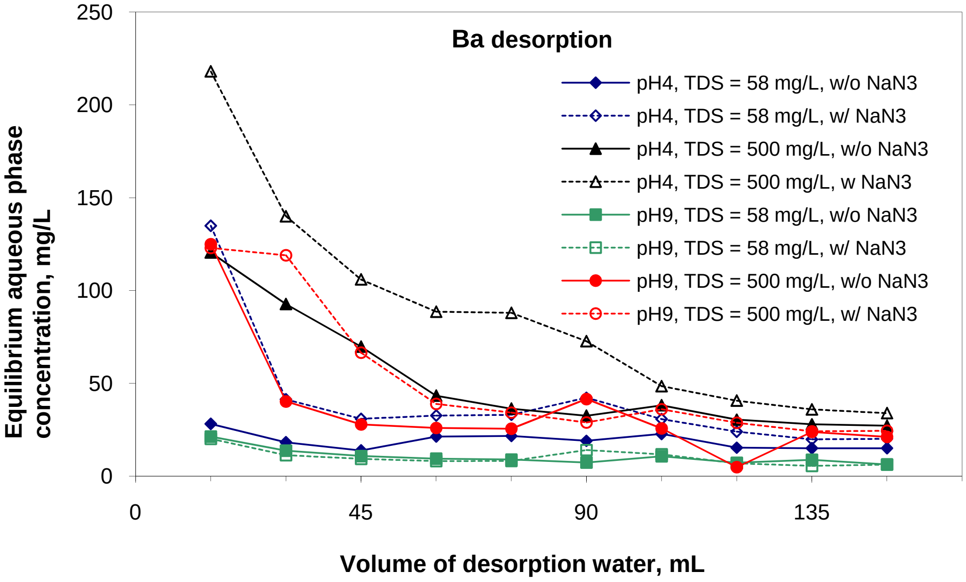

FIGURE 3.28. Barium desorption in the presence and absence of biocide NaN_3.

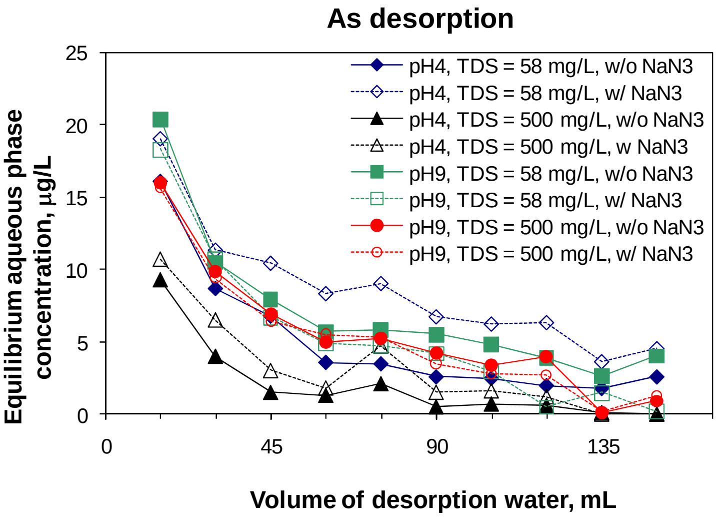

FIGURE 3.29. Arsenic desorption in the presence and absence of biocide NaN_3.

CHAPTER 4

DESORPTION KINETICS STUDY

In continuous-flow systems such as a surface infiltration basin, the rate of desorption is very important in determining the concentration profile of the desorbed metal, especially at high flow rates. In addition, kinetics studies can provide information on desorption mechanisms such as the nature of desorption sites. Therefore, kinetics studies were performed to investigate the effect of solution pH, TDS, and ionic composition on the rate of metal desorption. The desorption kinetics data were fitted with commonly used kinetics models to shed light on desorption reaction mechanisms. The vadose soil S400 and aquifer material LHC30 soil samples were used in the kinetics study.

4.1 EXPERIMENTAL SETUP

Batch desorption kinetics tests were conducted for both the S400 and LHC30 samples with a six-beaker jar test apparatus shown in Figure 4.1. The advantage of using this apparatus is that vigorous mixing can be provided so that surface reaction (namely, desorption) instead of mass transfer is the rate-limiting process. In addition, mixing conditions for each reactor are kept identical, and soil in each reactor is well homogenized.

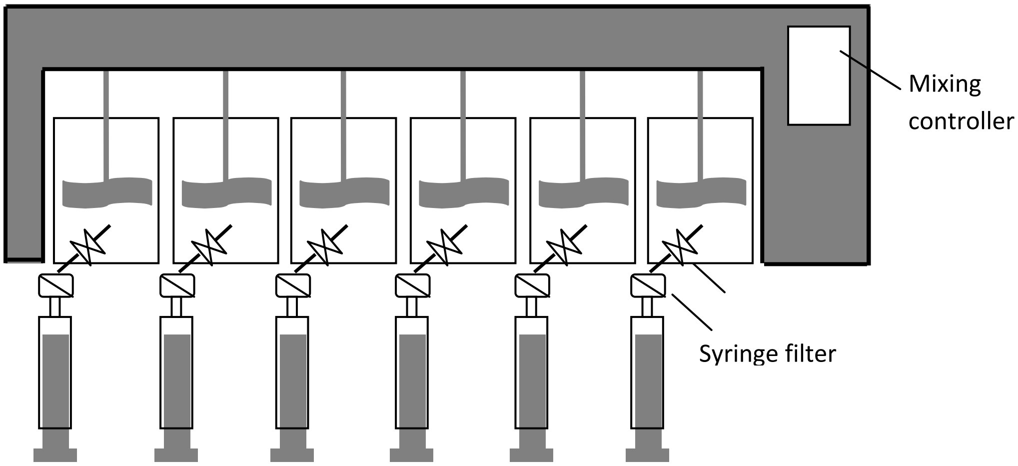

FIGURE 4.1. Schematic of jar test apparatus for batch desorption kinetics tests.

4.2 EXPERIMENTAL PROTOCOL

Aliquots of 66.7-g soil samples were weighed and transferred to the beakers. One liter of desorption solution was added to each jar to provide a water-to-soil ratio of 15, same as that used in the desorption equilibrium study. Vigorous mixing was provided immediately after the addition of desorption solution through Teflon-coated overhead propellers. At a predetermined time, samples were withdrawn through a 0.45-µm-pore-size low-binding PES syringe filter from the beakers. The membrane filters were replaced after each sampling. Because the soil-water mixture was uniformly stirred, it is assumed that the sampling procedure does not change the soil-to-water ratio in the reactor. Each sample was split into four aliquots for analysis of metal concentrations by ICP-AES and ICP-MS, two aliquots for each.

Previous research has found that desorption of some trace metals from natural sediment is usually biphasic, in which a rapid desorption process is followed by a process with a much lower rate. In order to capture kinetic information in both phases, samples were taken more frequently at the beginning (for example, every few minutes), and the sampling interval was increased to hours and days in the later phase.

Because S400 is a vadose soil sample, typically in an aerobic environment, and the sample had been exposed to air during sample collection, the kinetics experiments were conducted in ambient air for the S400 sample, namely, under aerobic conditions. Desorption kinetics of the LHC30 sample was investigated under anoxic conditions: batch reactors were set up in an anaerobic chamber purged with high-purity N_2. Desorption solutions were deoxygenated by purging with high-purity N_2 immediately before the experiment. An experimental protocol similar to that described above for aerobic conditions was followed.

Because the effect of pH on metal desorption has been found to be monotonic in the equilibrium study, desorption kinetics experiments were performed for both soil samples at only two pHs: pH = 4 and 9.

4.3 DESORPTION KINETICS FOR S400

Figures 4.2 to 4.5 present desorption kinetics data of S400. The results show that desorption of Ca, Mg, Ba, and As reached equilibrium within 24 h, consistent with the finding of our preliminary study before the desorption equilibrium study. The effects of solution pH and TDS observed in the kinetics experiments were also consistent with those found in the desorption equilibrium study.

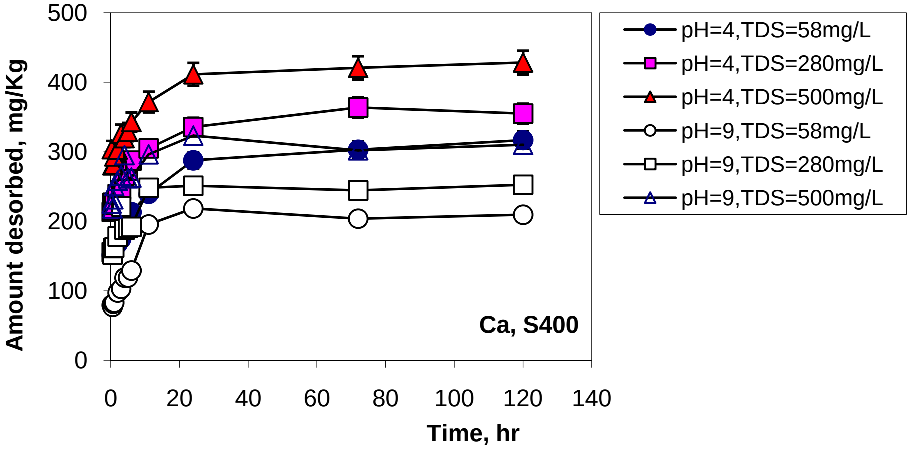

FIGURE 4.2. Calcium desorption kinetics of S400 under aerobic conditions.

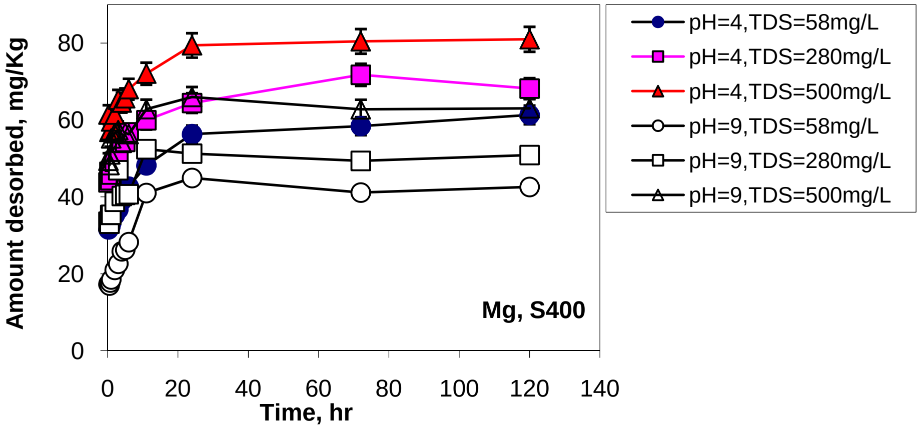

FIGURE 4.3. Magnesium desorption kinetics of S400 under aerobic conditions.

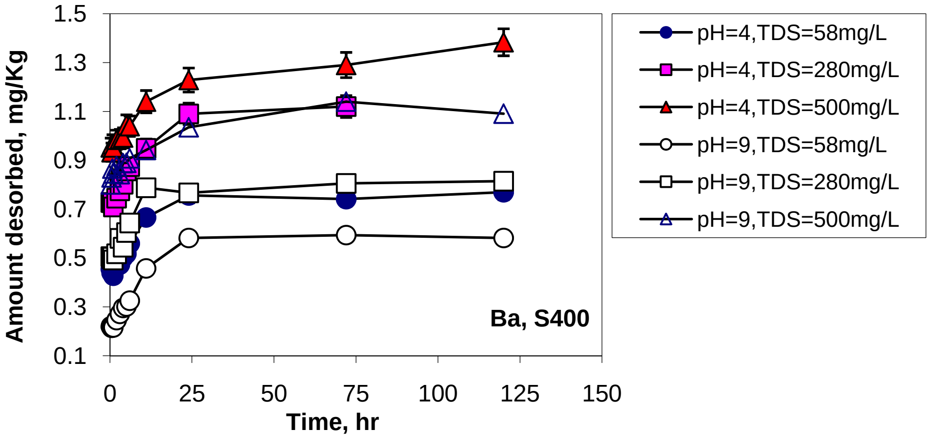

FIGURE 4.4. Barium desorption kinetics of S400 under aerobic conditions.

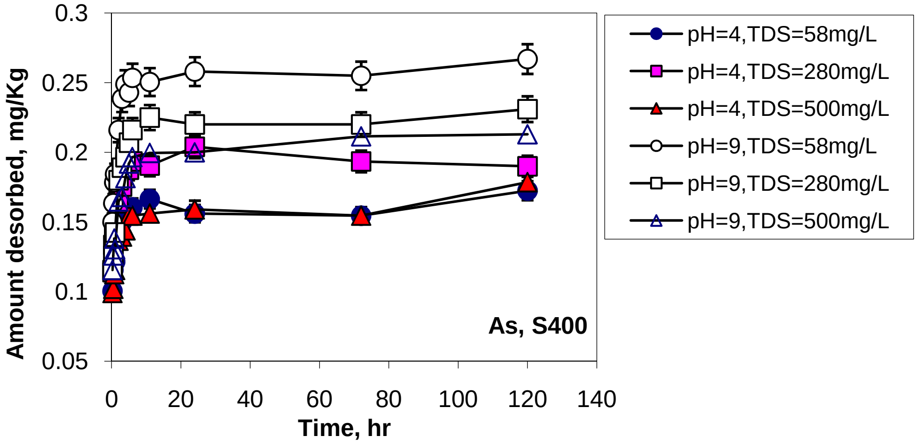

FIGURE 4.5. Arsenic desorption kinetics of S400 under aerobic conditions.

4.4 DESORPTION KINETICS FOR LHC30

Based on the results obtained with the S400 and the preliminary test results before the equilibrium study, kinetics experiments with LHC30 were run for 24 h. Results are shown in Figures 4.6 to 4.8. Consistent to the desorption equilibrium study results, no detectable As desorption was observed with LHC30. The effects of pH and TDS on desorption of Ca, Mg, and Ba were also consistent with those observed in the desorption equilibrium study: Desorption kinetics increased with decreasing pH and increasing TDS.

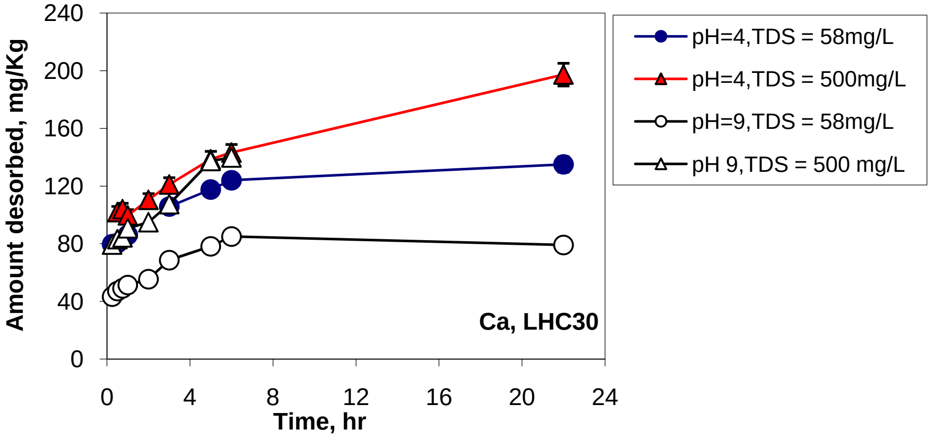

FIGURE 4.6. Calcium desorption kinetics of LHC30 under anoxic conditions.

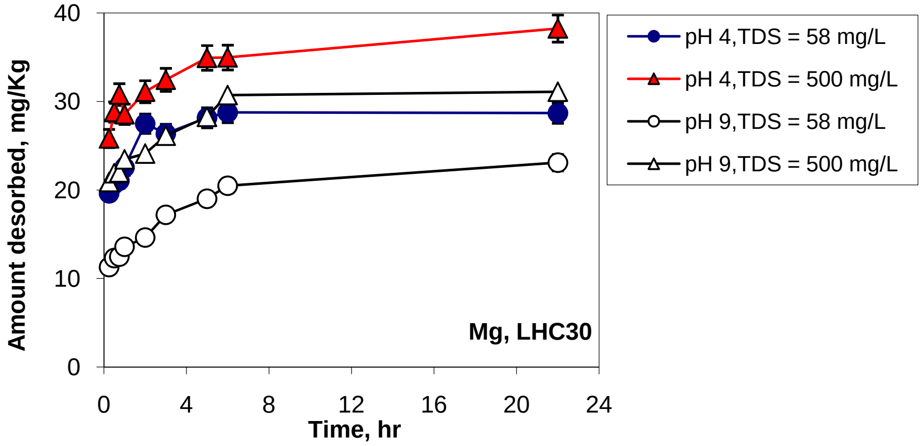

FIGURE 4.7. Magnesium desorption kinetics of LHC30 under anoxic conditions.

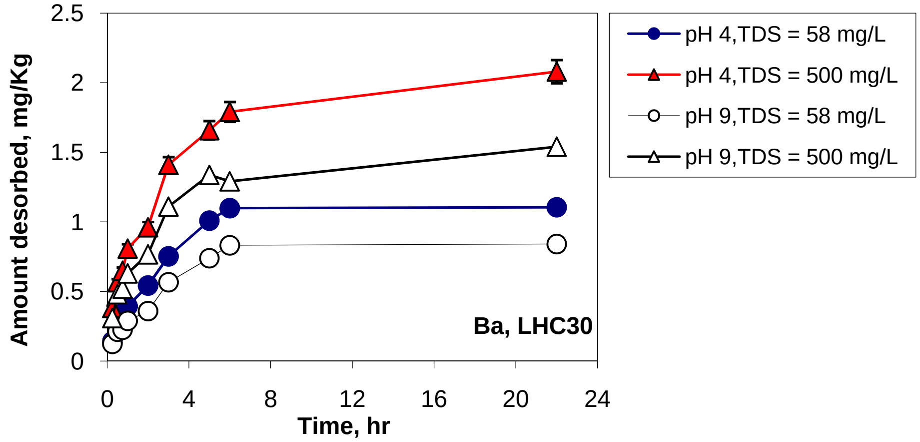

FIGURE 4.8. Barium desorption kinetics of LHC30 under anoxic conditions.

4.5 DESORPTION KINETICS MODEL

Batch desorption kinetics data were fitted with two kinetics models: a single-first-order-kinetics model and a two-first-order-reaction model. The single-first-order-reaction model did not fit the data very well. Therefore, modeling results are presented only for the two-first-order-reaction model.

Compared with the first-order-reaction model, the multiple-first-order-reaction model provides more information on the real physicochemical process of metal desorption in the natural environment, especially in the underground soil system (Fangueiro et al., 2005). It has been widely used by soil chemists. In this model, different first-order reactions are ascribed to discrete types of binding sites. It is assumed that there are multiple simultaneous first-order or pseudo-first-order reactions and their rates are independent. If the rate of desorption from a particular type of binding site follows first-order rate law, then for a batch system, the desorption rate is described by the following equation:

$$\frac{dQ_i}{dt} = k_i(Q_i^0 - Q_i) \qquad (4.1)$$

Q_i = amount of metal desorbed from site i at time t (mg/kg);

Q_i^0 = amount of metal desorbed from site i at equilibrium (mg/kg);

k_i = first-order-reaction rate constant for reactive site i (h^{-1}).

Metal adsorption onto and desorption from soil have been found to be nearly always biphasic with a fast reaction phase followed by a slow reaction phase (Yu and Klarup, 1994; Langford and Cook, 1995). In our study, we found those results to be true. A two-first-order-reaction model was therefore used to describe the desorption kinetics of different metals. Because of the vigorous mixing provided in the batch desorption experiments, we can assume that metal leaching kinetics is not mass-transfer-limited. For a metal desorbing from two sites, the overall desorption rate is the sum of the two-parallel-first-order reactions:

$$\frac{dQ}{dt} = \frac{dQ_1}{dt} + \frac{dQ_2}{dt} \qquad (4.2)$$

$$\frac{dQ_1}{dt} = k_1(Q_1^0 - Q_1) \qquad (4.3)$$

$$\frac{dQ_2}{dt} = k_2(Q_2^0 - Q_2) \qquad (4.4)$$

where Q_1^0 = the amount of metal associated with the fast desorption site (mg/kg);

k_1 = reaction rate constant for the fast desorption site (h^{-1});

Q_2^0 = the amount of metal associated with a slow desorption site (mg/kg);

k_1 = reaction rate constant for the slow desorption site (h^{-1}).

Given initial conditions of $Q_1(t=0)=0$ and $Q_2(t=0)=0$, the integrated form of the desorption rate law can be written as

$$Q = Q_1^0(1-\exp(-k_1 t)) + Q_2^0(1-\exp(-k_2 t)) \qquad (4.5)$$

The values of Q_1^0, Q_2^0, k_1, k_2 are determined by fitting the experimental data with Equation 4.5 using a nonlinear least-square-optimization method in MATLAB (FMINUNC).

Tables 4.1 to 4.4 summarize the kinetics parameters for Ca, Mg, Ba, and As desorption from S400 under various solution conditions. For Ca, Mg, and Ba, the amount of desorbable metal associated with the fast desorption sites, Q_1^0, increases with increasing TDS and decreasing pH, consistent with the observations from the desorption equilibrium study. On the other hand, the amount of desorbable metal associated with the slow desorption sites, Q_2^0, is not significantly affected by pH or TDS. This finding indicates that pH and TDS mainly affect the fast reaction sites. Another interesting point is that the desorption rate constant k_1 for the fast reaction sites is 3 orders of magnitude higher than that of the slow reaction site, k_2. The very large values of k_1 suggest that this step of desorption is almost instantaneous. This finding explains why the values of Q_1^0 are very close to the amount of metal desorbed measured at the first sampling point: 15 min.

The k_1 values for As desorption are significantly smaller than those for the three primary metals. No consistent trend was observed in Q_1^0 or Q_2^0 values of As when pH or TDS changed. This finding is consistent with the small impact of pH and TDS observed in the equilibrium study.

TABLE 4.1. Kinetics Model Parameters for Calcium Desorption from S400

pH	TDS (mg/L)	Q_1^0 (mg/kg)	k_1 (1/h)	Q_2^0 (mg/kg)	k_2 (1/h)	R[a]
4	58	148.65	126.43	162.69	0.075	0.996
4	280	212.09	126.43	144.20	0.103	0.994
4	500	282.49	126.43	143.18	0.088	0.989
9	58	66.71	126.43	147.28	0.117	0.983
9	280	150.79	126.43	100.26	0.153	0.940
9	500	225.60	126.43	80.10	0.159	0.926

[a] Correlation coefficient.

TABLE 4.2. Kinetics Model Parameters for Magnesium Desorption from S400

pH	TDS (mg/L)	Q_1^0 (mg/kg)	k_1 (1/h)	Q_2^0 (mg/kg)	k_2 (1/h)	R[a]
4	58	31.25	238.31	28.81	0.080	0.997
4	280	44.04	126.43	25.07	0.101	0.988
4	500	57.67	238.31	23.30	0.093	0.987
9	58	14.96	238.31	27.59	0.131	0.982
9	280	33.51	238.31	17.50	0.145	0.920
9	500	49.82	238.31	30.69	0.075	0.925

[a] Correlation coefficient.

TABLE 4.3. Kinetics Model Parameters for Barium Desorption from S400

pH	TDS (mg/L)	Q_1^0 (mg/kg)	k_1 (1/h)	Q_2^0 (mg/kg)	k_2 (1/h)	R[a]
4	58	0.41	423.88	0.35	0.091	0.986
4	280	0.69	423.88	0.44	0.083	0.994
4	500	0.94	423.88	0.41	0.053	0.989
9	58	0.19	423.88	0.41	0.084	0.992
9	280	0.47	423.88	0.34	0.118	0.974
9	500	0.83	423.88	0.29	0.052	0.983

[a] Correlation coefficient.

TABLE 4.4. Kinetics Model Parameters for Arsenic Desorption from S400

pH	TDS (mg/L)	Q_1^0 (mg/kg)	k_1 (1/h)	Q_2^0 (mg/kg)	k_2 (1/h)	R[a]
4	58	0.1023	9.8666	0.0660	0.4479	0.976
4	280	0.1185	9.2994	0.0851	0.3660	0.990
4	500	0.0903	40.1116	0.0673	0.4857	0.970
9	58	0.1359	19.1897	0.1248	0.5207	0.994
9	280	0.1083	13.5765	0.1198	0.3735	0.995
9	500	0.1112	13.8141	0.0959	0.3392	0.989

[a] Correlation coefficient.

Figures 4.9 and 4.10 compare the model fitting with the experimental results for As desorption from the S400 soil sample. It can be seen that the two-first-order-reaction models described the arsenic desorption kinetics well. Model fittings of the desorption kinetics data of other metals are not shown here. They all show good agreement with the experimental data.

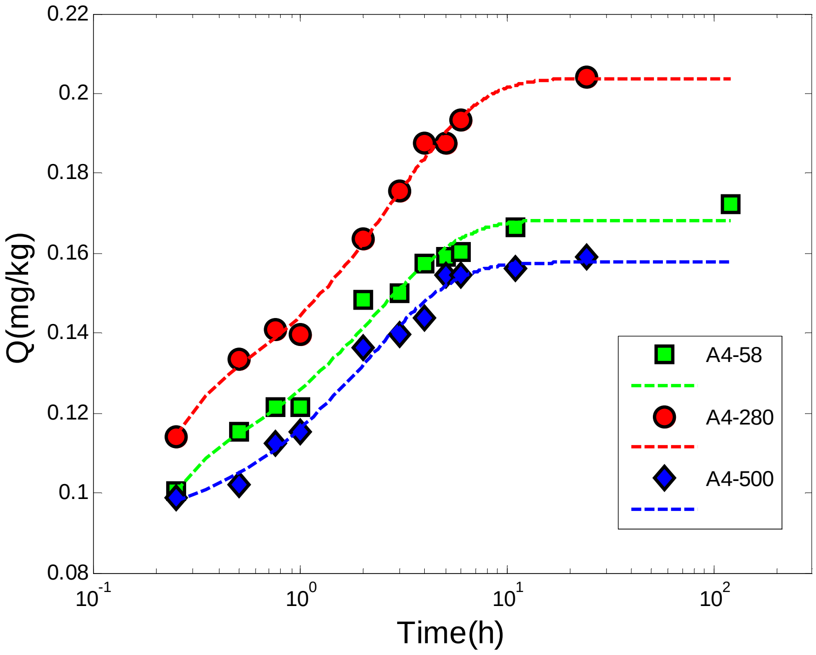

FIGURE 4.9. Model simulation and experimental measurement of arsenic desorption kinetics (S400, aerobic conditions, pH = 4). Symbols represent experimental data, and dotted lines represent model fitting results.

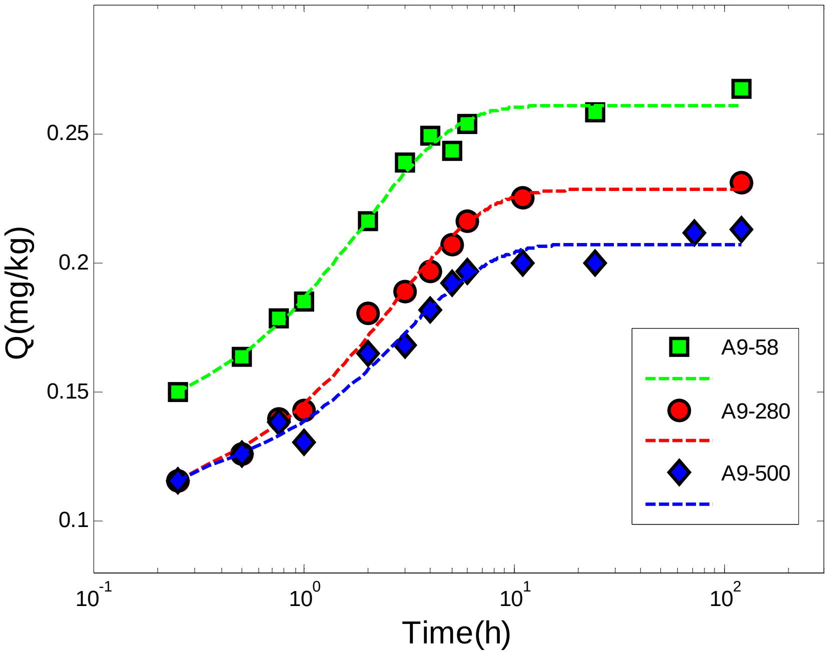

FIGURE 4.10. Model simulation and experimental measurement of arsenic desorption kinetics (S400, aerobic conditions, pH = 9). Symbols represent experimental data, and dotted lines represent model fitting results.

4.6 EFFECT OF SURFACE WATER BLENDING

To evaluate the strategy of surface water blending for control of metal leaching, desorption equilibrium and kinetics experiments were performed with the RO water and the CAP water mixed at different ratios. Relevant water quality parameters of the mixed waters are summarized in Table 4.5. For the S400 soil sample, desorption kinetics experiments were conducted under ambient conditions; for the LHC30 soil sample, experiments were performed under anoxic conditions with N_2 sparging throughout the experimental period.

TABLE 4.5. Measured Relevant Water Quality Parameters of the Mixed Waters

Variable Measured		RO:CAP Mixing Ratio				
Water quality		1:0	3:1	1:1	1:3	0:1
pH		6.2	8.2	8.1	8.1	7.8
TDS (ppm)		25.6	171	307	420	505.6
Metals (mg/L)	**K**	1.25	2.31	3.37	4.42	5.48
	Na	8.9	31.3	53.7	76.1	98.5
	Ca	0.24	18.7	37.4	55.2	74.6
	Mg	0.11	7.70	15.4	22.7	30.9
Metals (µg/L)	**Fe**	-	132	264	347	190
	Ba	-	39	72	100	135
	Cr	-	4	8	11	13.6
	As	-	1	1.8	3	3.9

Figure 4.11 compares the As desorption isotherms of the RO, the CAP, and the mixed waters. The desorption isotherms can be described by the Freundlich model (Equation 4.6) reasonably well. The Freundlich parameters for the RO, the CAP, and the mixtures are summarized in Table 4.6. Desorption of As in the CAP water was significantly lower than that in RO water, as indicated by the higher soil-phase concentrations (q) at the same equilibrium aqueous-phase concentration (C) over the concentration range tested. The CAP water contains significantly higher Ca^{2+} (74.6 mg/L) and alkalinity (110 mg/L as $CaCO_3$) than the RO water, which can greatly reduce the desorption of As associated with carbonate minerals—for example, calcite—in the S400 soil. This finding is consistent with the lower Ca desorption observed in the kinetics experiment (Figure 4.2).

$$q = KC^n \tag{4.6}$$

When the RO water was mixed with the CAP water, the Freundlich parameter n increased with the increasing percentage of the CAP water in the mixture. This finding suggests that the As desorption isotherms of the mixtures will cross each other; As desorption will decrease with the increasing percentage of CAP in the high concentration range (namely, low water-to-soil ratio) but will increase with the increasing percentage of CAP in the low concentration range (namely, high water-to-soil ratio). This finding can be clearly seen in Figure 5.11. The isotherm of the 1:3 RO/CAP lies above that of the 1:1 RO/CAP mixture for soil As concentrations greater than 3.4 mg/kg, suggesting that recharging using the 1:3 RO/CAP mixture will result in less As leaching than will recharging using the 1:1 RO/CAP mixture until the As content in the soil has been depleted to below 3.4 mg/kg. At lower As concentrations (q) in soil, As desorption is the lowest when the RO and CAP waters are mixed at a 1:1 ratio. With the percentage of the CAP water increasing, the As desorption isotherm approaches that of the CAP water.

These results suggest that blending the RO water with the CAP water can mitigate As desorption during the artificial recharge. Within a short time (namely, before significant depletion of soil As content), increasing the percentage of the CAP water is beneficial. However, careful study is needed to determine the blending ratio that minimizes As desorption for long-term operations.

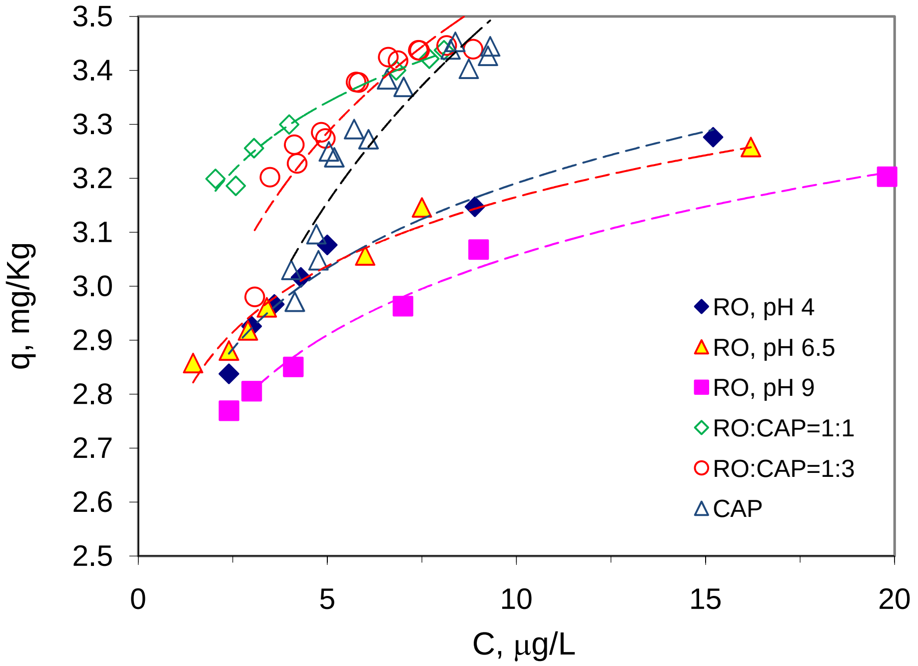

FIGURE 4.11. Arsenic desorption isotherms in the RO, CAP and mixed RO and CAP waters. Dotted lines represent Freundlich adsorption isotherm model fit.

TABLE 4.6. Freundlich Parameters of As Desorption Isotherms

Recharge Water		**Values for:**					
		RO, pH = 4	**RO, pH = 6.5**	**RO, pH = 9**	**RO: CAP = 1:1**	**RO: CAP = 1:3**	**CAP**
S400	K (mg/kg)(μg/L)$^{1/n}$	2.592	2.634	2.569	3.051	2.826	2.422
	n	0.089	0.0802	0.0758	0.0563	0.0981	0.1657

Figures 4.12 to 4.14 show desorption kinetics experimental data for S400 obtained with the mixed waters. Results for Mg are not shown because adsorption instead of desorption of Mg was observed, due to the relatively high concentration of Mg in the CAP water. Ca desorption in the mixed waters was significantly lower than that in the NaCl-augmented RO water, and

the amount desorbed decreased with the increasing percentage of the CAP water in the mixture. This finding was the result of two contradicting factors: on the one hand, the RO/CAP mixture had a higher pH than the RO water. In addition, the Ca and alkalinity concentrations of the mixture increased with the increasing percentage of the CAP water. Both factors reduced Ca desorption. On the other hand, the TDS concentration increased with the increasing percentage of the CAP water, which increased Ca desorption via ion exchange.

Ca desorption in the mixed water seemed to reach equilibrium more quickly than in the RO water. The aqueous concentration of Ca remained relatively stable after 1 h of mixing. This phenomenon might have occurred because the Ca associated with the slow desorption sites was not desorbing in the mixed water. With 75% of CAP water in the mixture, a slight decline in aqueous Ca concentration was observed. This result might have stemmed from the slow precipitation of Ca, since this mixture had the highest Ca and alkalinity concentration. Similar results were obtained for Ba.

Increasing the CAP water percentage from 25% to 50% did not seem to affect As desorption significantly. However, a further increase in CAP percentage to 75% resulted in notably lower As desorption (Figure 5.14), consistent with the results shown in Figure 5.11. The lower As desorption at higher percentage of the CAP water is also consistent with the much lower Ca desorption in this mixture, since part of the desorbable As is believed to be associated with calcite.

In the experiments using LHC30 soil, adsorption instead of desorption of Ca, Mg, and Ba was observed in all RO/CAP mixtures (data not shown). Similar to that observed with NaCl-augmented RO water, no desorption of trace metals of interest was found except for Zn. It was surprising to see a notable amount of Zn desorption from the LHC30 soil when it was exposed to the RO/CAP mixtures. Figure 4.15 presents Zn desorption kinetics data in the three mixtures tested. The desorption seemed to reach equilibrium within 15 min in the mixture containing 25% CAP water. With a higher percentage of the CAP water, however, it appeared that an adsorption phase followed the initial quick desorption. One possible explanation is that with a larger fraction of CAP water, the higher concentration of other cations caused more desorption of Zn due to ion exchange; meanwhile, the concentration of some cations, such as Ca^{2+}, Mg^{2+}, and Ba^{2+}, were higher than their respective equilibrium concentration in the aqueous phase. Zn released from the soil might have associated or coprecipitated with the newly formed surface precipitate of these metal cations, resulting in a decrease in its aqueous-phase concentration.

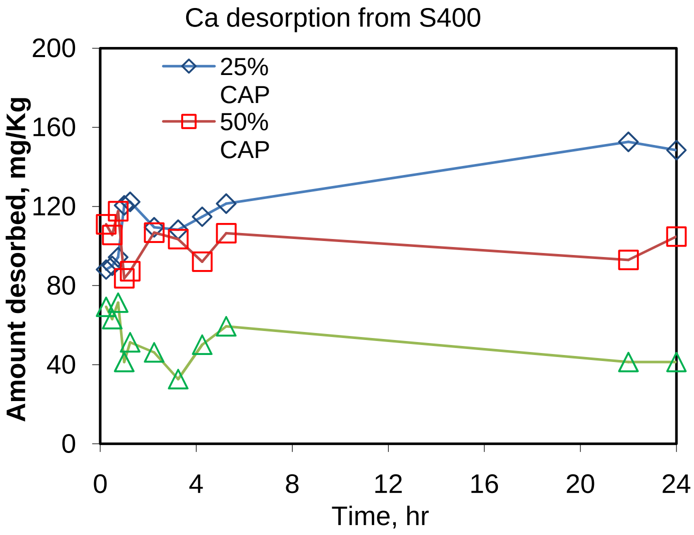

FIGURE 4.12. Calcium desorption kinetics of S400 in RO/CAP mixtures under aerobic conditions.

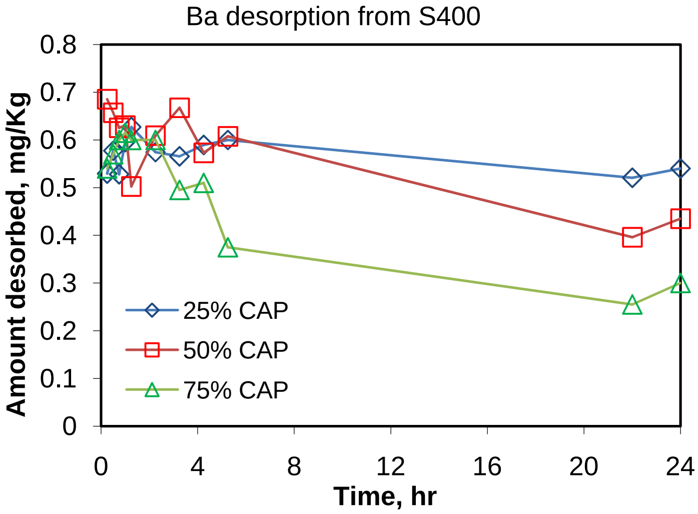

FIGURE 4.13. Barium desorption kinetics of S400 in RO/CAP mixtures under aerobic conditions.

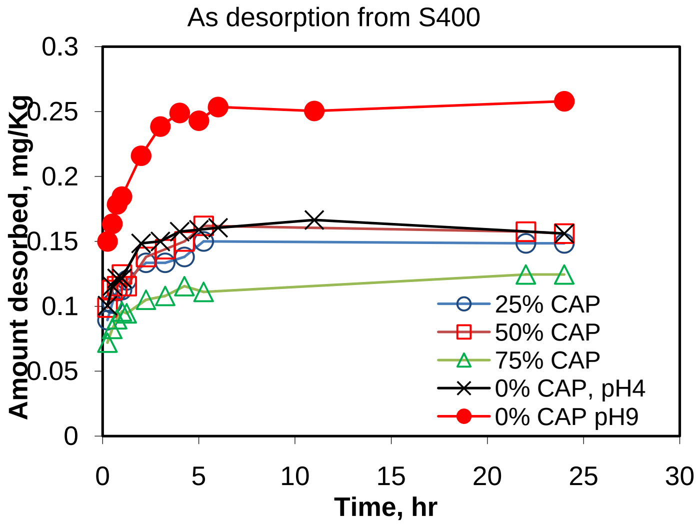

FIGURE 4.14. Arsenic desorption kinetics of S400 in RO/CAP mixtures under aerobic conditions.

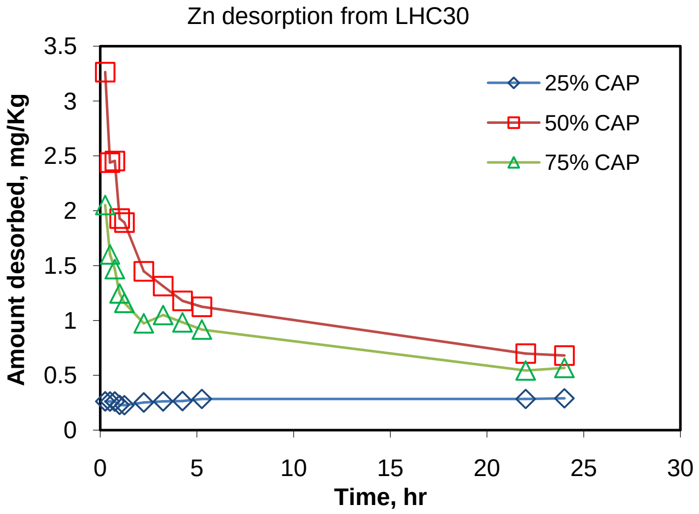

FIGURE 4.15. Zinc desorption kinetics of S400 in RO/CAP mixtures under anoxic conditions.

CHAPTER 5

CONTINUOUS-FLOW COLUMN EXPERIMENT STUDY

Continuous-flow column experiments were performed to investigate the dynamics of metal adsorption/desorption under simulated infiltration flow. Recharge waters made of the RO and the CAP waters at different mixing ratios were tested to assess surface water blending as a strategy to mitigate arsenic leaching from soil during surface infiltration operations.

5.1 CONTINUOUS-FLOW COLUMN EXPERIMENTAL SETUP

Based on the results from the batch desorption equilibrium study, the S400 soil sample was chosen for the column study because it had the highest desorption potential. The schematic diagram of a continuous-flow column apparatus is shown in Figure 5.1.

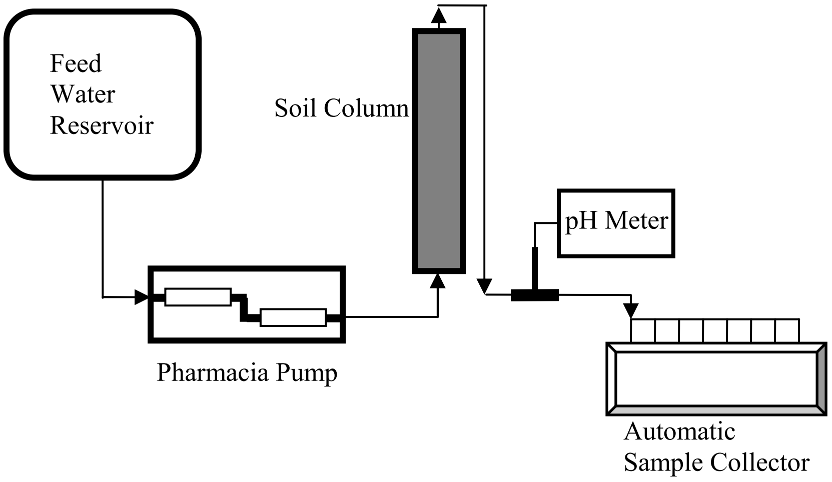

FIGURE 5.1. Schematic of column experimental setup.

5.1.1 Column Experiment Protocol

Small laboratory columns (15-cm height × 1.5-cm inside diameter) were dry-packed with the soil samples to achieve a porosity of 0.4. Dry packing instead of wet packing was chosen to avoid stratification of soil since the S400 is rich in fine clay and silt particles. The packed column was then saturated with the CAP water, which was used to approximate natural recharge water at the WCP site, at a flow rate of 5 ft/day. The desorption solution was then pumped through the soil column, and the effluent was collected at various time intervals using an autosampler. Samples were taken more frequently at the beginning to catch the effluent peak caused by the fast desorption reactions. Experiments were run continuously until the concentrations of all target metals become constant or below the detection limit.

5.1.2 Experimental Conditions

Experimental conditions used in the column experimental study are summarized in Table 5.1. To investigate surface water blending as a potential mitigation strategy, the RO water and two RO/CAP mixtures with RO:CAP ratios of 1:1 and 1:3 were used as model recharge waters. NaCl and NaOH were added to the RO water to adjust the solution pH to 9 and TDS to 58 mg/L so that the column experiment results could be compared to those from the desorption equilibrium and kinetics studies. A pH of 9 was selected to investigate the worst-case scenario because arsenic desorption increased with increasing pH. A typical infiltration rate in surface-spreading operations, 5 ft/day (12 mL/h), was used.

TABLE 5.1. Experimental Conditions for Column Experiments

	Experimental Variables					
Exp. ID	Soil Type	Recharge Water	pH	TDS (mg/L)	Flow Rate (ft/Day)	Redox Condition
1	S400	RO	9	58[a]	5	Aerobic
2	S400	CAP:RO=1:1	6.8	296	5	Aerobic
3	S400	CAP:RO=3:1	7.7	392	5	Aerobic

[a] TDS adjusted with NaCl;

RO and CAP mixed at different ratios.

5.2 METAL LEACHING BEHAVIOR IN CONTINUOUS-FLOW COLUMN EXPERIMENTS

Metal concentrations in the column effluent were shown in Figures 5.2 and 5.3 for different influent recharge waters.

With the RO water (pH = 9,TDS = 58 mg/L) as the influent recharge water, significant leaching of Ca, Mg, Ba, As, and Cr was detected in the effluent. Figure 5.2 shows the effluent concentrations of these metals as a function of time. Concentrations for all primary metals as well as Ba and Cr peaked within 1 h (a “washout” phenomenon) and then declined. The effluent concentration of As reached the highest level of 25.1 µg/L 2 h after the experiment started and dropped quickly afterward. It decreased to below our reporting limit of detection of 2 µg/L after 58 h. Although desorption of Cr was not observed in the equilibrium and kinetics studies, a notable concentration of Cr was detected in the effluent in the column experiment. This finding is attributed to the water-to-soil ratio in the column experiment being much lower than those used in the equilibrium and kinetics studies. Cr concentrations as high as 13.7 µg/L were detected in the effluent at the beginning of the experiment and stayed relatively stable at ~4 µg/L after 20 h.

When the RO water was blended with the CAP water at a 1:1 ratio, As, Cr, and Mn were detected at significant concentrations in the effluent (Figure 5.3). Similar to what was found with the RO water, the effluent As concentration peaked at 19.8 µg/L after ~2 h. However, the peak concentration was followed by a more gradual decrease in the As concentration. The effluent As concentration approached the influent concentration of 2.4 µg/L after ~100 h.

Effluent concentrations of Cr and Mn, on the other hand, stayed fairly stable after the initial increase in effluent concentration, both significantly higher than their influent concentration (8.5 and 0.05 µg/L for Cr and Mn, respectively).

Figure 5.4 shows the effluent concentration of different metals when the influent water contains 75% CAP water and 25% RO water. A similar As concentration profile was observed: the peak concentration, 13 µg/L, occurred at 2 h, followed by a gradual decline in concentration. The As concentration was still slightly above the influent concentration (2.7 µg/L) after 110 h. Cr and Mn exhibited unexpected behaviors: a small spike of Cr concentration was found in the first 8 h of the experiment. This event was followed by a stable effluent concentration equal to that in the influent, 9 µg/L until the 85th h, when the Cr concentration started to increase sharply to approximately 13 µg/L. Mn concentration events seemed to coincide with those of Cr: a high Mn concentration of 7 µg/L occurred in the effluent within the 1st h of the experiment even though the influent water did not contain detectable Mn. It quickly dropped to below the reporting limit of detection, followed by a continuous increase in concentration to 17 µg/L. This event occurred at the same time as when the Cr concentration spike was observed. After 80 h of gradual decrease, the effluent Mn concentration dropped sharply to approximately 4.3 µg/L and stabilized, the same time as when the Cr concentration increased sharply. These results suggest that the desorption of Cr is closely related to that of Mn. However, data collected from this study are not sufficient to reveal the mechanisms involved. Careful speciation studies of Cr and Mn are needed for better understanding of the observed phenomenon. Concentration events of Ca, Mg, and K were also found to coincide with each other, suggesting the interdependency of the desorptions of these metals.

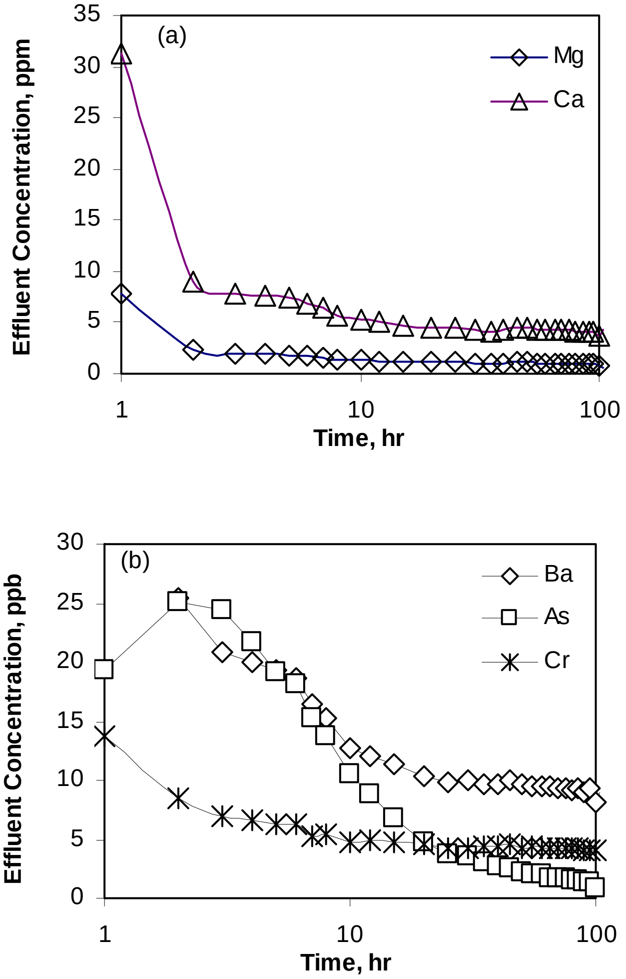

FIGURE 5.2. Effluent concentrations of primary (a) and trace (b) metals. Influent: RO, pH = 9, TDS = 58 mg/L.

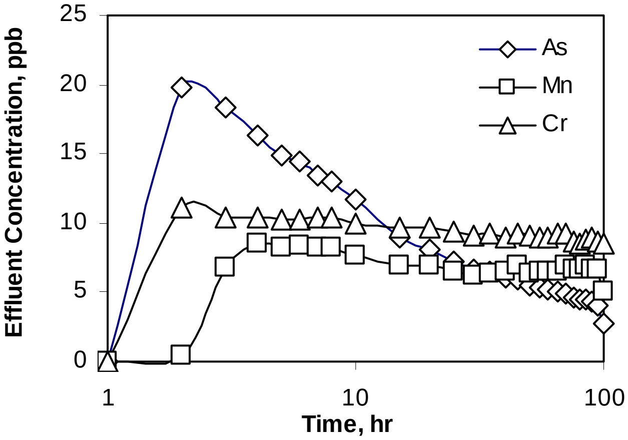

FIGURE 5.3. Effluent concentrations of trace metals. Influent: 1:1 RO/CAP mixture.

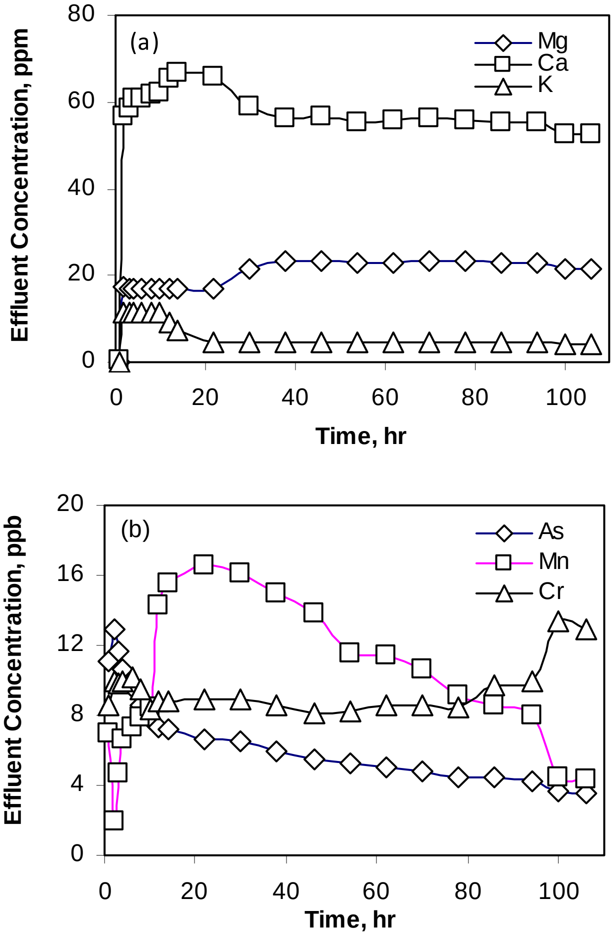

FIGURE 5.4. Effluent concentrations of primary (a) and trace (b) metals. Influent: 1:3 RO/CAP mixture.

Figure 5.5 compares the effluent concentrations of As, Cr, and Mn for the three different recharge waters. The effluent from the soil column receiving the RO water exhibited the highest peak concentration of arsenic: 25.1 μg/L. The peak As concentration decreased with the increasing per centage of the CAP water in the influent even through the influent As concentration increased at the same time.

The total amount of As, Cr, and Mn desorbed after 100 h of operation was compared in Table 5.2, with the metal concentrations in the influent water subtracted from those in the effluent. As expected, the total amount of As and Cr desorbed decreased with the increasing percentage of the CAP water in the recharge influent water. This finding is consistent with the results from the equilibrium and kinetics studies. However, the desorption of Mn was just the opposite: it increased with the increasing fraction of the CAP water, suggesting exchange/replacement of Mn by competing cations in the CAP water. The amount of As desorbed in the three experiments, 0.63, 0.47, and 0.36 mg/kg, was much smaller than the total As concentration in the soil, 3.5 mg/kg, although the effluent concentration at the end of each experiment was almost the same as the influent concentration. In addition, the effluent As concentrations were much lower than the concentration in equilibrium with the remaining As concentrations in the soil. This finding indicates that a notable fraction of desorbable As was associated with the slow reaction site, consistent with the observation from our kinetics study. A lower recharging rate may result in higher As concentrations in the effluent.

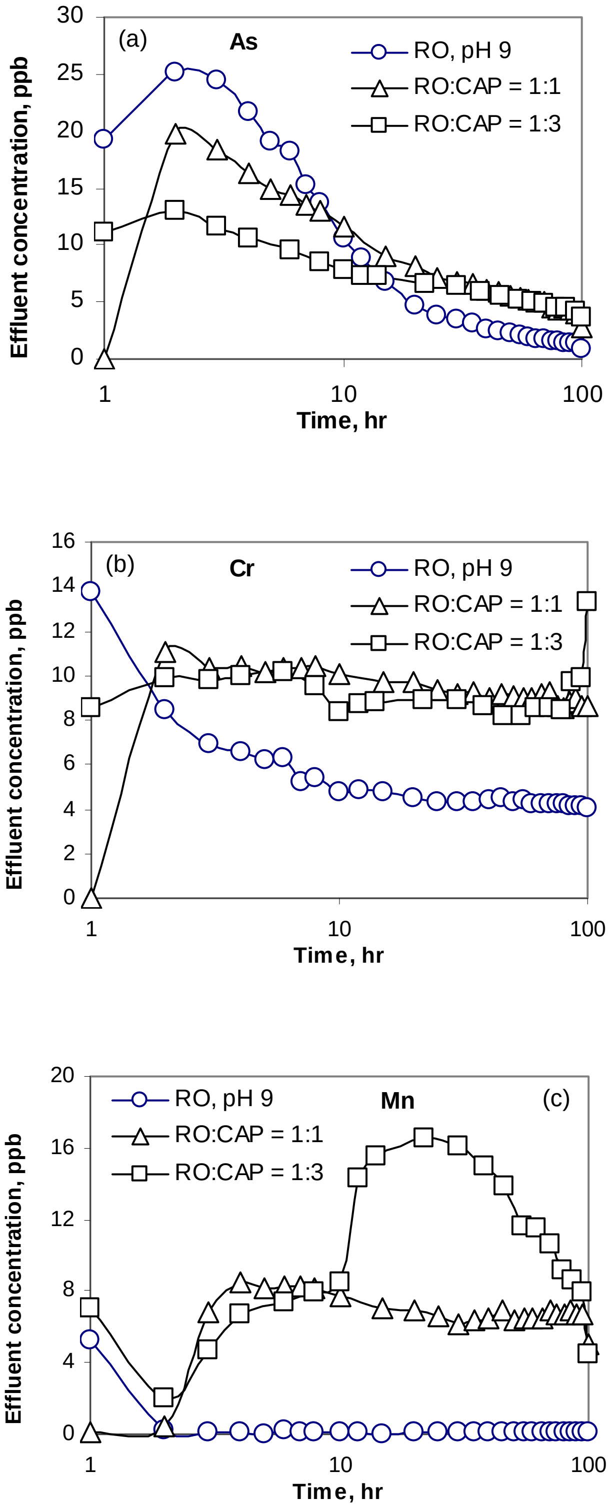

FIGURE 5.5. Comparison of effluent concentrations of As (a), Cr (b), and Mn (c) for the three recharge waters.

TABLE 5.2. Total Amount of Trace Metal Desorbed after 100 h

	Metal Desorbed (mg/kg)		
Influent Water	As	Cr	Mn
RO, pH = 9	0.63	1.35	0.03
RO:CAP = 1:1	0.47	0.08	0.74
RO:CAP = 1:3	0.36	0.02	1.33

Based on the above discussion, blending the low-ionic-strength RO water with high-ionic-strength water such as a surface water may be an effective strategy for mitigating leaching of heavy metals such as As and Cr from soil during surface infiltration operations. However, potential increased desorption of other metals such as Mn needs to be carefully evaluated before application of this method.

CHAPTER 6

GROUNDWATER FLOW AND REACTIVE TRANSPORT MODELS

6.1 DESCRIPTION OF THE MODELS: MODFLOW AND RT3D

The hydrology of the area surrounding the Scottsdale Water Campus was evaluated using the modular three-dimensional finite-difference groundwater flow (MODFLOW) model to assess the impact of the artificial recharge on the groundwater elevations and the Reactive Transport in Three Dimensions (RT3D) model to assess contaminant (arsenic) transport. MODFLOW was developed by McDonald and Harbaugh (1984). MODFLOW is a physically based model that applies Darcy's law for the movement of fluids in saturated porous media and allows for a wide range of inputs utilizing multiple layers on irregularly shaped regimens. Simulations can be carried out in steady and unsteady states. By providing initial conditions and hydraulic properties, the model generates head values for each cell in the finite element grid.

Contaminant advection, dispersion, and adsorption to aquifer material were simulated using the RT3D model (Clement, 1997). The RT3D model describes the reactive flow and transport of multiple mobile and/or immobile species. This is done by solving the three-dimensional reactive advection dispersion equation that governs these processes:

$$\frac{\partial C}{\partial t} = \left[D_x \frac{\partial^2 C}{\partial x^2} + D_y \frac{\partial^2 C}{\partial y^2} + D_z \frac{\partial^2 C}{\partial z^2} \right] - \left[\bar{v}_x \frac{\partial C}{\partial x} + \bar{v}_y \frac{\partial C}{\partial y} + \bar{v}_z \frac{\partial C}{\partial z} \right] + r \qquad (6.1)$$

where D_i is the coefficient of hydrodynamic dispersion along the i axis (meters^2/day), C is the contaminant aqueous-phase concentration (milligrams/liter), $\bar{v}_i$ is the seepage velocity along the i axis (meters/day), and r are all the reactions that occur in the aqueous and solid phases (milligrams/liter-day).

RT3D uses the solvers for advection and dispersion from the 1997 Department of Defense version of MT3D. It is a generalized multispecies version of the U.S. Environmental Protection Agency (EPA) transport code, MT3D. The transport equation considers changes in concentration due to advection (water flow), dispersion, molecular diffusion, and external sources/sinks and reactions on the water/solid phase. Groundwater velocity and distribution required to calculate transport by RT3D were obtained by using MODFLOW to model the site hydrogeological characteristics. RT3D was chosen as the platform for our simulations because the program has a modular architecture, it is in the public domain, it can be interfaced with a postprocessing program such as the Groundwater Modeling System (GMS) (Jones, 2000), and it is widely used. RT3D has been previously validated by comparing the code results against various numerical and analytical solutions (Clement et al., 2000; Sun and Clement, 1999; Sun et al., 1998).

The Department of Defense GMS, which is a pre- and postprocessor, was used to integrate data input and output with both MODFLOW and RT3D models. GMS provides a graphical user interface for site characterization, model conceptualization, grid generation, geostatistics, and post-data processing. Data input files for MODFLOW are entered through GMS. These input files are then read and executed by MODFLOW, and the output generated is then used by RT3D to calculate transport processes. MODFLOW utilizes a site map to develop a conceptual model for analysis. The conceptual model utilizes Geographical Information System (GIS) tools to develop a representative model for the site in question. The locations of sources and sinks, layer parameters, site boundaries and all other data necessary for simulation can be defined at the conceptual model level. After completion of the conceptual model, a grid model is generated with all cell-by-cell assignments performed automatically.

6.2 APPROACH

Our approach in this study is to first use MODFLOW to model the hydrogeological characteristics of the site at steady-state simulations. With the groundwater distribution over our domain, we used RT3D to simulate contaminant transport from site sources. One of the main advantages of RT3D is that it has a user-defined reaction option that can be used to simulate any type of user-specified reaction kinetics (Clement et al., 1998). This capability allows the development of custom sorption and reaction modules without changing the coded flow and transport processes.

The focus of this work, desorption of arsenic from the soil matrix to the aqueous phase, was calculated using a user-defined desorption kinetics module. The built-in adsorption kinetics module option in RT3D in a GMS environment considers only adsorption to soil particles. It does not have the equations to take into account the amount of contaminant desorbed from the soil to the aqueous phase. The custom module created for this study incorporates the desorption kinetics equations, which comprise a system of ordinary differential equations that must be solved at each grid block and each time step after the advection and dispersion terms are calculated by RT3D.

6.3 CONCEPTUAL MODFLOW MODEL

The Northeast Valley Aquifer, Scottsdale, AZ, was selected for our model simulation. It is noted that this location was used simply to provide the groundwater flow field for our metal transport model simulation. The parameters and recharge conditions used in our model simulation do not represent those at the actual recharge site of the WCP.

A three-dimensional domain was used to simulate flow in the Northeast Valley Aquifer. The model domain of the groundwater flow model developed for the cities of Scottsdale and Phoenix by AMEC was utilized for the Northeast Valley Aquifer Management (NEAM) Study (AMEC Earth and Environmental, 2005). The upper half of the model domain of the NEAM study, right above E. Mt. View Rd., where the groundwater elevation is almost constant at 920 ft, was selected as the domain for this modeling exercise. The model domain covers a map area of 6.5 mi × 7.5 mi between *x* coordinates 4,412,271 m and 4,422,733 m and *y* coordinates 3,719,510 m and 3,731,465 m. On the basis of the geological cross-sections, the hydrogeology is schematized in three layers, but the upper two layers were divided into eight and three sublayers, respectively, for the thorough analysis of the transport phenomena in the vadose zone and in the aquifer. The first layer, which includes eight sublayers, is the recharge zone by surface infiltration. Layers 9 to 12 are open to the water table.

The study area is located in the Sonoran Desert and experiences long, hot summers and short, mild winters. Precipitation is approximately 7.66 in. per year. The McDowell Mountains are located to the north and east of the study area. No perennial streams flow through the area.

Simulations in MODFLOW-GMS were performed by using hydraulic and topographical data from the NEAM study (AMEC Earth and Environmental, 2005). The first layer consists of unconsolidated coarse-grained deposits (sand and gravel) with minor finer-grained silt and sand deposits. The first layer had a uniform hydraulic conductivity of 35 ft/day, and the thickness averages approximately 300 ft (ranges from 200 to 600 ft). A storage coefficient (S) and a specific yield (Sy) of 0.1 and an effective porosity (EP) of 0.2 were used in the first layer. The second layer is a (semi)confined aquifer with an average thickness of 500 ft (ranges from 300 to 900 ft) and a hydraulic conductivity of 6 ft/day. The second layer consists of unconsolidated, fine-grained silt and clay deposits with interbedded silt and sand deposits. It becomes coarser-grained to the north, where it consists of relatively massive silt and sand deposits that are difficult to distinguish from the first layer deposits in localized areas (AMEC Earth and Environmental, 2005). The third layer consists of heterogeneous deposits of weakly to strongly cemented silt, clay, sand, and gravel. Values of S = 0.005, Sy = 0.09, and EP = 0.1 were used for the storage and porosity. The thickness of this layer is highly variable near the McDowell Mountains because of shallow, undulating bedrock, and the minimum thickness of this layer is approximately 100 to 400 ft in localized areas (AMEC Earth and Environmental, 2005). A horizontal hydraulic conductivity of 12 ft/day was used for the third layer. A value of 1/10 of the horizontal hydraulic conductivity was used to calculate the vertical hydraulic conductivities.

Figure 6.1 displays the MODFLOW conceptual model base map. In this figure, the thick solid lines in the southern boundary of the model domain indicate the constant head boundaries, which will be described in more detail in the next section.

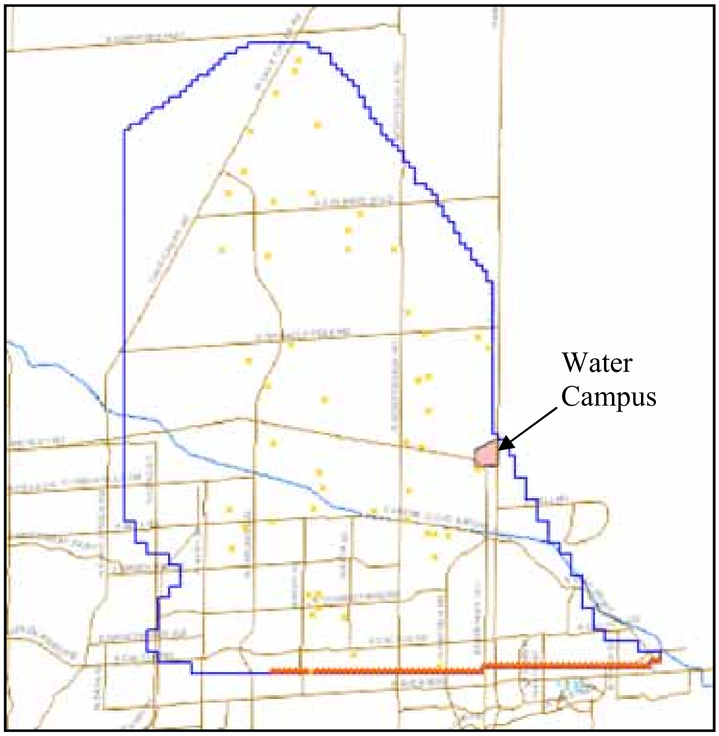

FIGURE 6.1. Model domain.

6.3.1 Boundary Conditions

Boundary conditions defined in the conceptual model are “Well” and “Specified Head Boundaries.” As in the NEAM study by AMEC (2005), cells along the northern boundary representing the Lake Pleasant underflow were simulated with a specified flux boundary, where injection wells pumped into Layer 3 (sublayer 12). The southern boundary was simulated as the specified head boundary, with 920 ft as the specified head, which was the groundwater elevation calculated by the NEAM study.

6.3.2 Recharge

All recharge was modeled as vadose zone recharge to the first layer. For Scottsdale’s reclaimed water, recharge of all reclaimed water was assumed to take place at the Scottsdale WCP. A recharge rate of 0.4 ft/day was used to represent recharge in the WCP. Using lower recharge rates causes the cells in the first layer to be dry. In order to investigate desorption of arsenic from subsurface soil to the aqueous phase, it was necessary to saturate the soil column with water. This recharge rate was sufficient to saturate the first layer. The recharge water had zero arsenic concentration.

6.4 RESULTS

6.4.1 MODFLOW Simulation Results

The conceptual model is translated into a MODFLOW model with cell sizes of 660 ft, namely, 52 columns and 60 rows. The PCG2, preconditioned conjugated gradient solver was used with a head and residual convergence criteria of 0.001; the model was set up as a steady-state simulation.

In the steady-state simulations, for the second and third layers (sublayers 9 to 12) the piezometric water level was obtained. However, in the first layer (sublayers 1 to 8), dry cells occurred except for the recharge zone, since the water table was located in the second model layer. Dry cells in the first eight sublayers were deactivated because of the numerical instability that they caused in the model simulations. The water table in the second and the third layers varied between 920 ft and 1620 ft. The lowest water table positions occurred on the southern boundary. The head increased northward, with the maximum around the Water Campus recharge location. The head distribution and velocities were similar to those reported in the NEAM study (AMEC Earth and Environmental, 2005), only with higher heads.

6.4.2 RT3D Simulation Results

Reactive transport was simulated with RT3D, which uses the head solution from MODFLOW as input. The transport-modeling domain is the same as that used for flow modeling. The initial concentration of arsenic in the aquifer was assumed to be zero for simplification.

The initial arsenic concentrations and the desorption equilibrium parameters for the three soil layers used in the model simulations are shown in Tables 6.1 and 6.2. It is noted that because of the limited desorption equilibrium experiments performed, the desorption isotherm parameters determined using the S400 soil sample were used for most cases except for layers at a depth of >550 ft, when 100% RO water was used.

TABLE 6.1. Arsenic Content of Soil Samples at WCP

Model Layers	Depth (ft)	Initial As Concn in Soil (mg/kg)
Layers 1 to 5	0–200	1.3
Layers 6 to 10	200–500	3.5
Layers 10 to 11	>500	2.1

TABLE 6.2. Freundlich Parameters for Different Soil Layers

		Constant Values for:			
Depth (ft)	**Constant**	**RO: CAP = 1:0**	**RO: CAP = 1:1**	**RO: CAP = 1:3**	**RO: CAP = 0:1**
0–200	K	2.634	3.051	2.826	2.422
	n	0.0202	0.0563	0.0981	0.1657
200–550	K	2.634	3.051	2.826	2.422
	n	0.0802	0.0563	0.0981	0.1657
>550	K	2.007[a]	2.039	2.826	2.422
	n	0.0202[a]	0.0219	0.0981	0.1657

[a] Determined with the S700 soil sample.

The model simulations were performed for the RO water and the CAP water mixed at different ratios: RO:CAP = 1:0, RO:CAP = 1:1, RO:CAP = 1:3, and RO:CAP = 0:1. Figures 6.2 and 6.3 show the horizontal spread of the arsenic plume for each scenario at 3000 days and 18,000 days after the recharge water was introduced. It should be noted that several assumptions were made in the model simulation, which do not necessarily represent the actual condition and recharge activities at the Northeast Valley Aquifer:

- The initial arsenic concentration in the aquifer was assumed to be zero. The actual groundwater in this aquifer contains a significant amount of arsenic.
- Arsenic desorption equilibrium parameters were based in most cases on the S400 soil sample, which has the highest arsenic desorption capacity. Soil at other depths has significantly less arsenic desorption capacity.
- Arsenic distribution in the soil phase was based on analyses of soil samples taken at three different depths from only one well location and was assumed to be uniform for each depth throughout the study site. The actual distribution may be much more heterogeneous.
- Recharge was assumed to occur at the surface layer. The WCP site uses vadose zone recharge and deep-well aquifer recharge.

The model run for RO:CAP ratio of 1:0 represents the worst-case scenario. The initial concentration of arsenic in RO water is zero, but since the desorption of arsenic in RO water is the highest among the other scenarios, the arsenic concentration in water reaches 34.6 µg/L, the concentration at equilibrium with the arsenic concentration of 3.5 mg/kg in the vadose zone soil, and can be found in the aquifer approximately 500 ft under the infiltration zone in 500 days (Figure 6.4). The arsenic plume with a front concentration of 34.6 µg/L travels 2.4 mi horizontally in the aquifer in 50 years. The plume with a concentration of 10 µg/L travels 2.8 mi horizontally in 50 years (Figures 6.2 and 6.4 and Table 6.3).

The plume simulated for the recharge water with an RO:CAP ratio of 1:1 has lower concentrations throughout the 50-year simulation period, and at the end of the 50-year simulation, the 10-µg/L arsenic concentration travels about 2.5 mi horizontally from the infiltration zone (Figure 6.2).

The arsenic concentrations never reach 10 µg/L for the other two scenarios where the recharge water contains a higher ratio of the CAP water (Figure 6.3). The plume with a maximum concentration of 5 µg/L travels about 2.8 mi horizontally at the end of the 50-year simulation for both cases.

These results suggest that mixing high-ionic-strength recharge water (CAP water in this case) with the low-ionic-strength reclaimed RO water can serve as a potential mitigation strategy. Arsenic concentrations in the aquifer decrease when the fraction of the high-ionic-strength reclaimed water is increased from 0 to 100%. For short-term operation, the fraction of the high-ionic-strength water can be gradually reduced with depletion of the heavy metal contents of the soil.

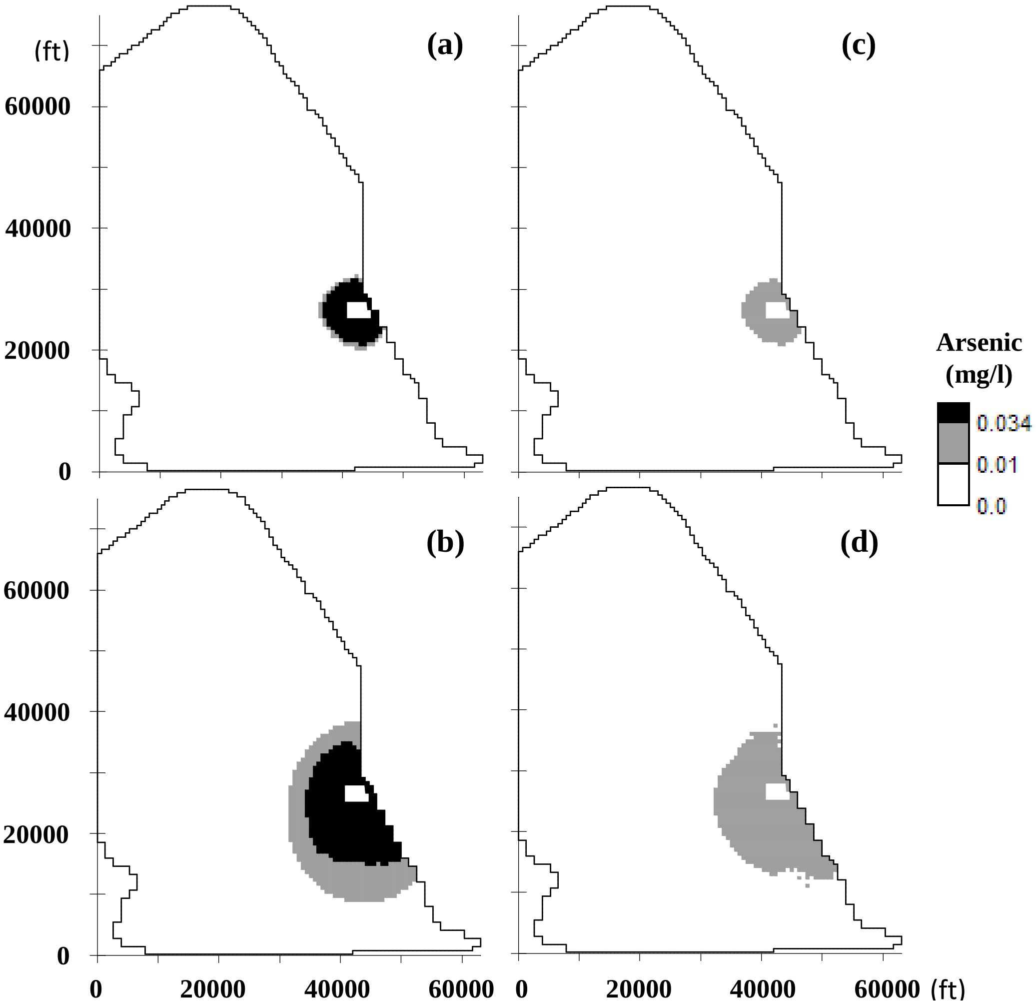

FIGURE 6.2. Arsenic concentration contours (mg/L) for worst-case scenarios (above 10 µg/L): (a) RO:CAP = 1:0 at 3000 days, (b) RO:CAP = 1:0 at 18,000 days, (c) RO:CAP = 1:1 at 3000 days, and (d) RO:CAP = 1:1 at 18,000 days.

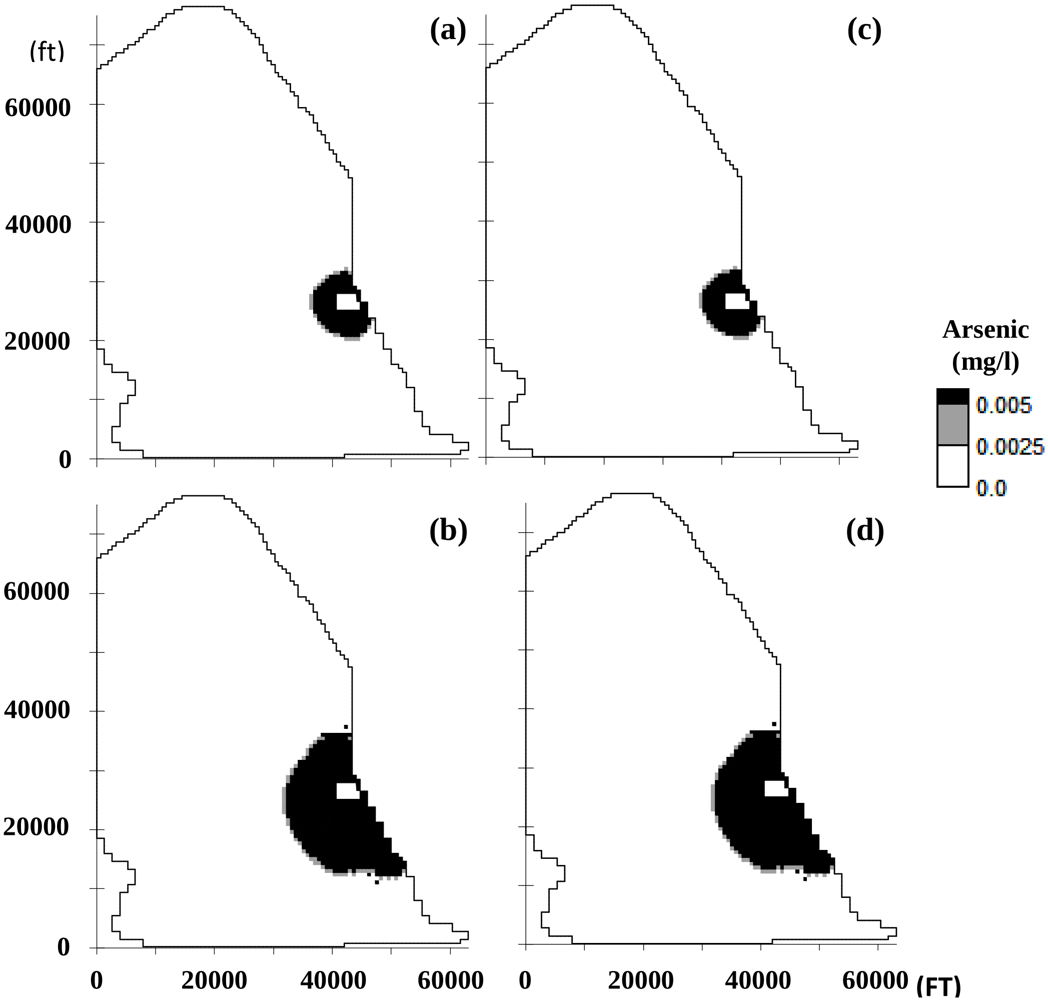

FIGURE 6.3. Arsenic concentration contours (mg/L) for best-case scenarios (below 10 µg/L): (a) RO:CAP = 1:3 at 3000 days, (b) RO:CAP = 1:3 at 18,000 days, (c) RO:CAP = 0:1 at 3000 days, and (d) RO:CAP = 0:1 at 18,000 days.

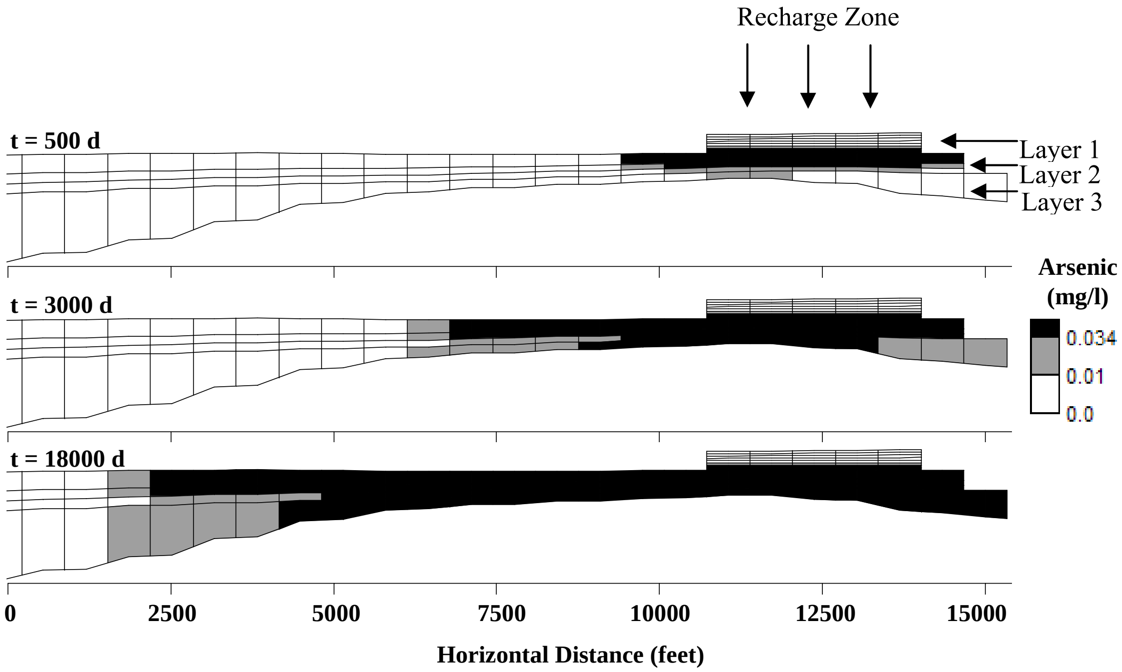

FIGURE 6.4. Lateral arsenic concentration profiles for RO:CAP = 1:0 scenario at 500, 3000, and 18,000 days of simulation.

TABLE 6.3. Maximum Arsenic Concentration in Water and Horizontal Distance of the 10-µg/L Contour

Scenario	Maximum Arsenic Concentration in Water (ug/l)	Horizontal travel distance (miles) of the 10 ug/l contour			
		500 days	3000 days	10000 days	18000 days
RO:CAP=1:0	34.6	0.2	1.0	1.9	2.8
RO:CAP=1:1	11.5	0.1	0.8	1.7	2.5
RO:CAP=1:3	8.9	0.0	0.0	0.0	0.0
RO:CAP=0:1	9.2	0.0	0.0	0.0	0.0

APPENDIX I

SUMMARY OF SOIL AND GROUNDWATER SAMPLING

SOIL SAMPLING

Soil sampling was performed by using a hollow-stem auger drilling rig operated by Yellow Jacket Drilling Services, based in Phoenix, AZ. A clean 8-in. auger was used to advance the borehole located in the southwest corner of the parking lot south of the main office building and east of the wastewater percolation pond. The boring was advanced initially to 20 ft bgs without collecting samples. Beginning at 20 ft bgs a sampler sleeve was lowered through the hollow augers, hammered 1 ft into the undisturbed soil below the augers, and retrieved for sample collection. The augers were then advanced 1 ft into the subsurface and the process repeated to a total depth of 36 ft. Each sample collection returned two 2-in.-diameter by 6-in.-lemgth undisturbed core samples contained in brass sleeves. The samples were sealed with square Teflon sheets, capped, labeled, and put on ice. A general description of subsurface stratigraphy was obtained through analysis of the cuttings returned when advancing the augers (see attached boring log SB-1).

GROUNDWATER SAMPLING

On August 23, 2007, a groundwater sample was collected from MW-5B located adjacent to McCulloch Blvd., approximately 500 ft from the eastern border of the Lake Havasu City WWTP, and more than 1000 ft from the nearest wastewater infiltration pond. The well is installed to a total depth of approximately 30 ft with a screened interval from 25 to 30 ft bgs. The static water level measured 24.45 ft below the top of the casing prior to purging. Field measurements for pH, specific conductivity, and temperature were taken periodically (every 5 gal) throughout purging (see Appendix 1 for groundwater sampling record). After roughly 35 gal was purged, a 20-L sample was taken in the supplied container and put on ice.

SAMPLE SHIPPING

At the conclusion of the sampling program, the samples were repacked in ice in order to remove any excess water and reduce shipping weight. Ice was packed in double-bagged Ziplocs to prevent any melt water from entering the samples during shipping. Soil and groundwater samples were shipped in separate coolers via FedEx Priority Overnight to the offices of GSI Environmental. Upon arrival, the samples were then transported from GSI's office to Rice University on the same day.

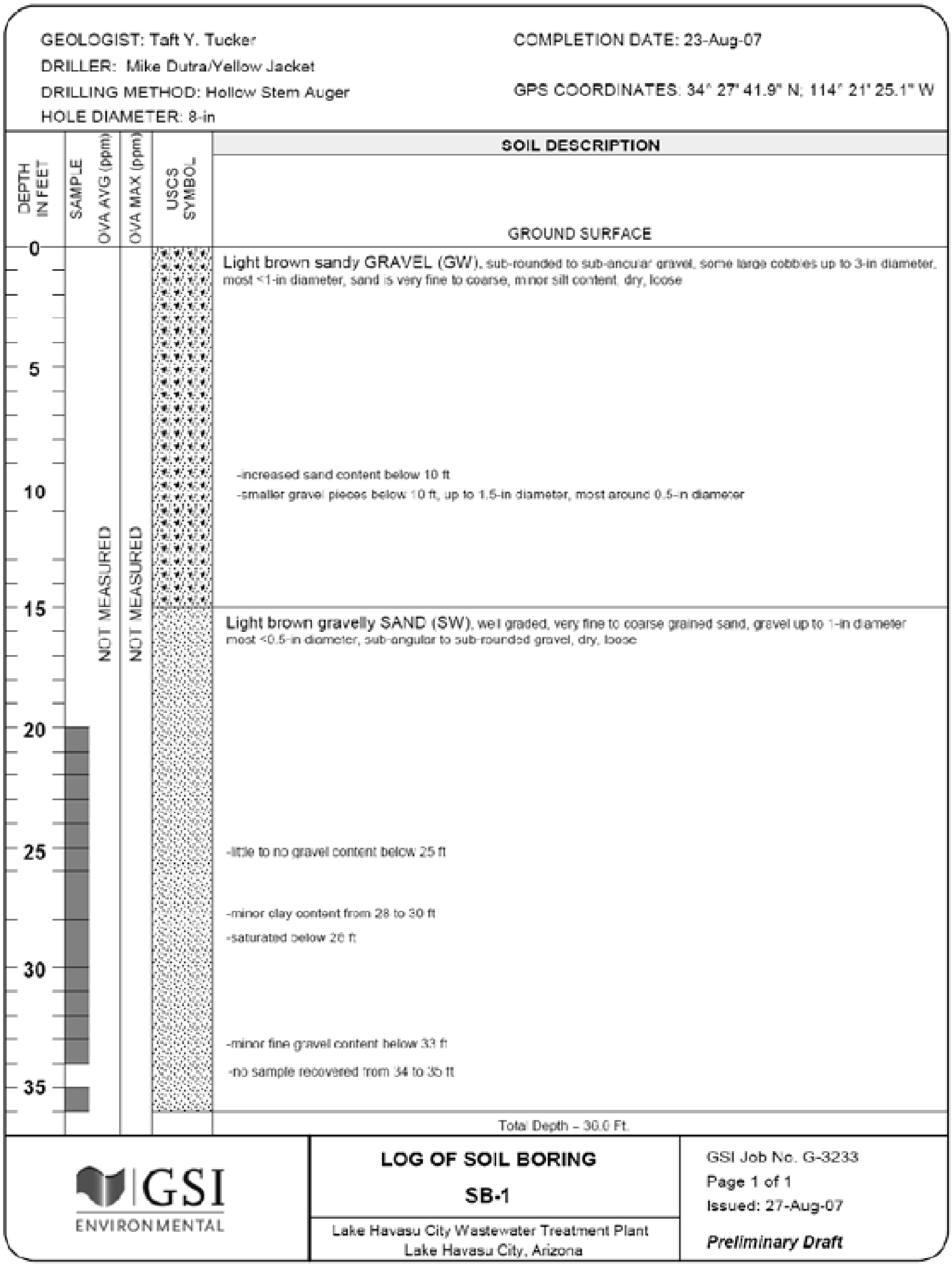

GEOLOGIST: Taft Y. Tucker
DRILLER: Mike Dutra/Yellow Jacket
DRILLING METHOD: Hollow Stem Auger
HOLE DIAMETER: 8-in

COMPLETION DATE: 23-Aug-07

GPS COORDINATES: 34° 27' 41.9" N; 114° 21' 25.1" W

DEPTH IN FEET	SAMPLE	OVA AVG (ppm)	OVA MAX (ppm)	USCS SYMBOL	SOIL DESCRIPTION
					GROUND SURFACE
0		NOT MEASURED	NOT MEASURED	GW	**Light brown sandy GRAVEL (GW),** sub-rounded to sub-angular gravel, some large cobbles up to 3-in diameter, most <1-in diameter, sand is very fine to coarse, minor silt content, dry, loose
10					-increased sand content below 10 ft -smaller gravel pieces below 10 ft, up to 1.5-in diameter, most around 0.5-in diameter
15				SW	**Light brown gravelly SAND (SW),** well graded, very fine to coarse grained sand, gravel up to 1-in diameter most <0.5-in diameter, sub-angular to sub-rounded gravel, dry, loose
25					-little to no gravel content below 25 ft
					-minor clay content from 28 to 30 ft -saturated below 28 ft
					-minor fine gravel content below 33 ft -no sample recovered from 34 to 35 ft
					Total Depth – 30.0 Ft.

GSI ENVIRONMENTAL

LOG OF SOIL BORING

SB-1

Lake Havasu City Wastewater Treatment Plant
Lake Havasu City, Arizona

GSI Job No. G-3233
Page 1 of 1
Issued: 27-Aug-07

Preliminary Draft

APPENDIX II

XRD DATA OF SOIL SAMPLES

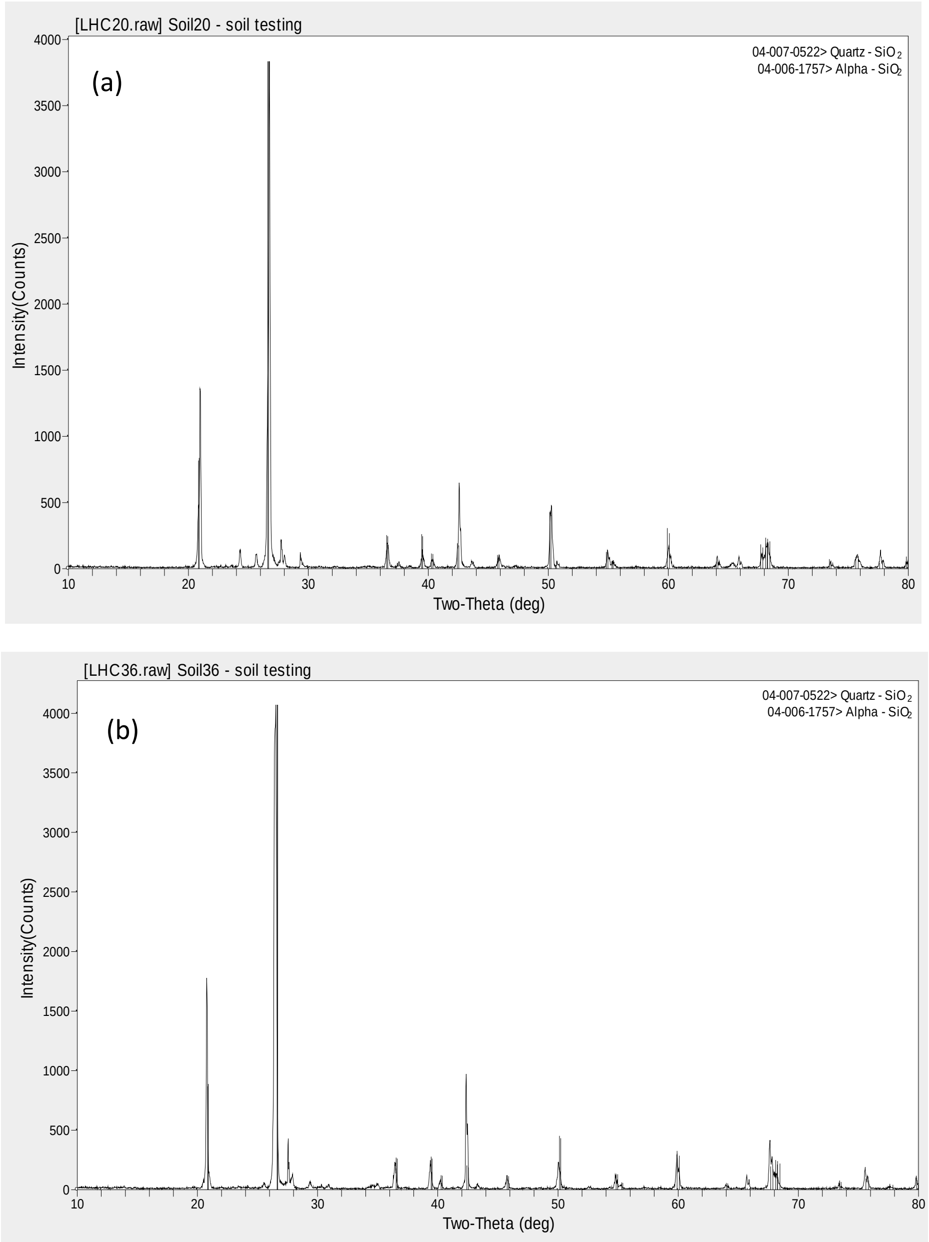

FIGURE A-1. XRD of soil samples collected at 20' (a) and 36' (b) at the IWWTP site.

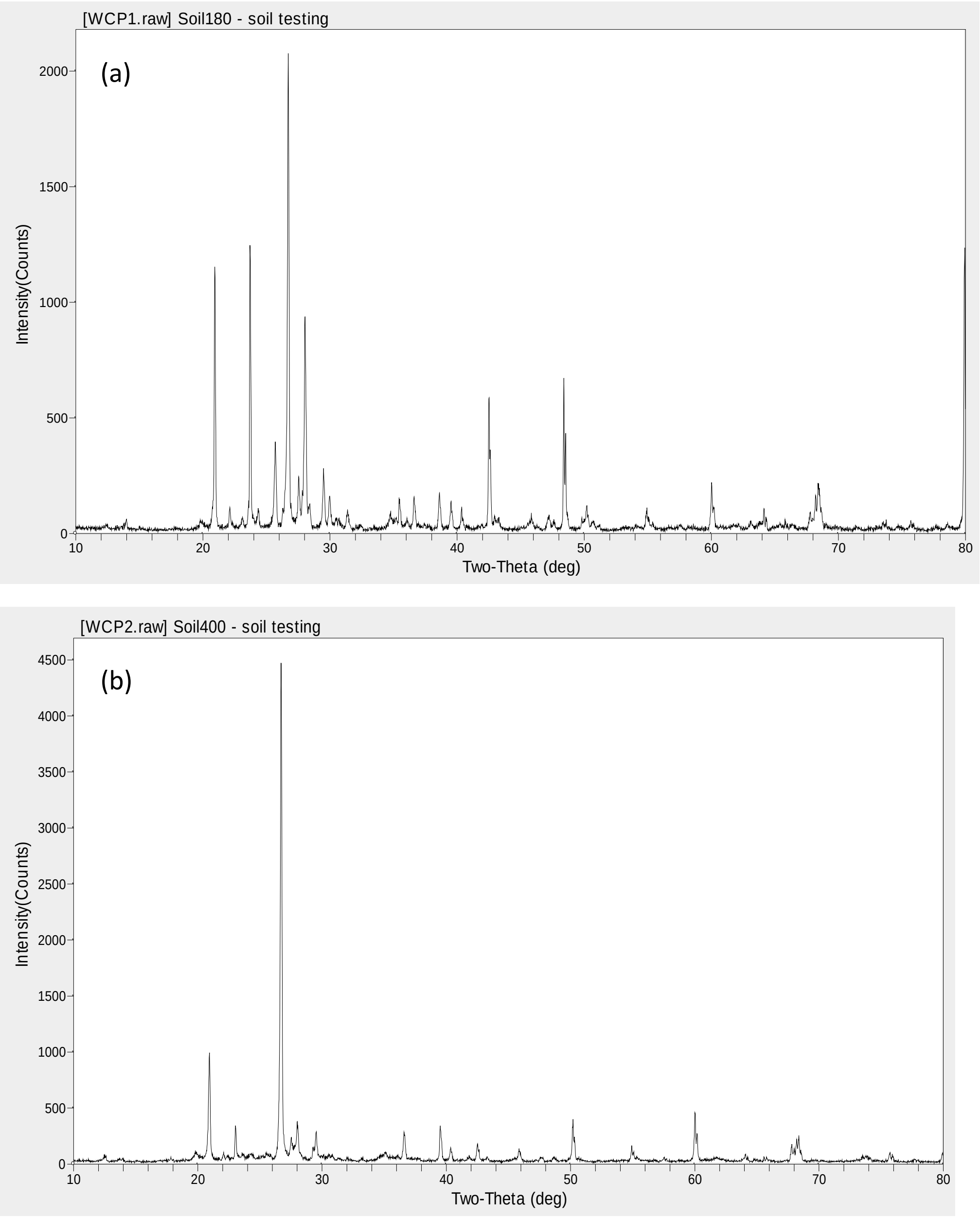

FIGURE A-2. XRD of soil samples collected at 180' (a), 400' (b), 550' (c), and 700' (d) at the WCP site.

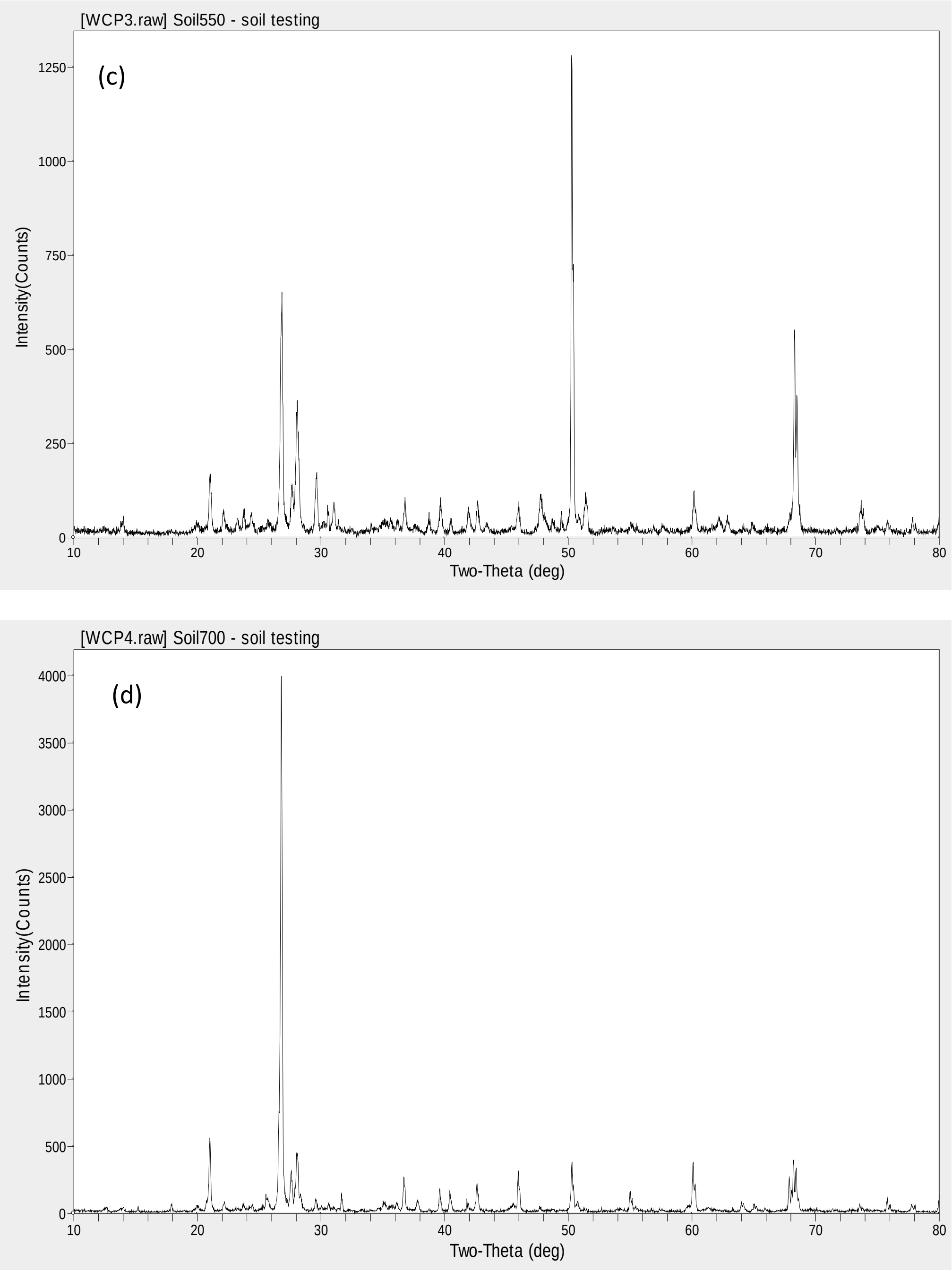

FIGURE A-2. ***Continued*****.**

APPENDIX III

SEM/EDAX DATA OF SOIL SAMPLES

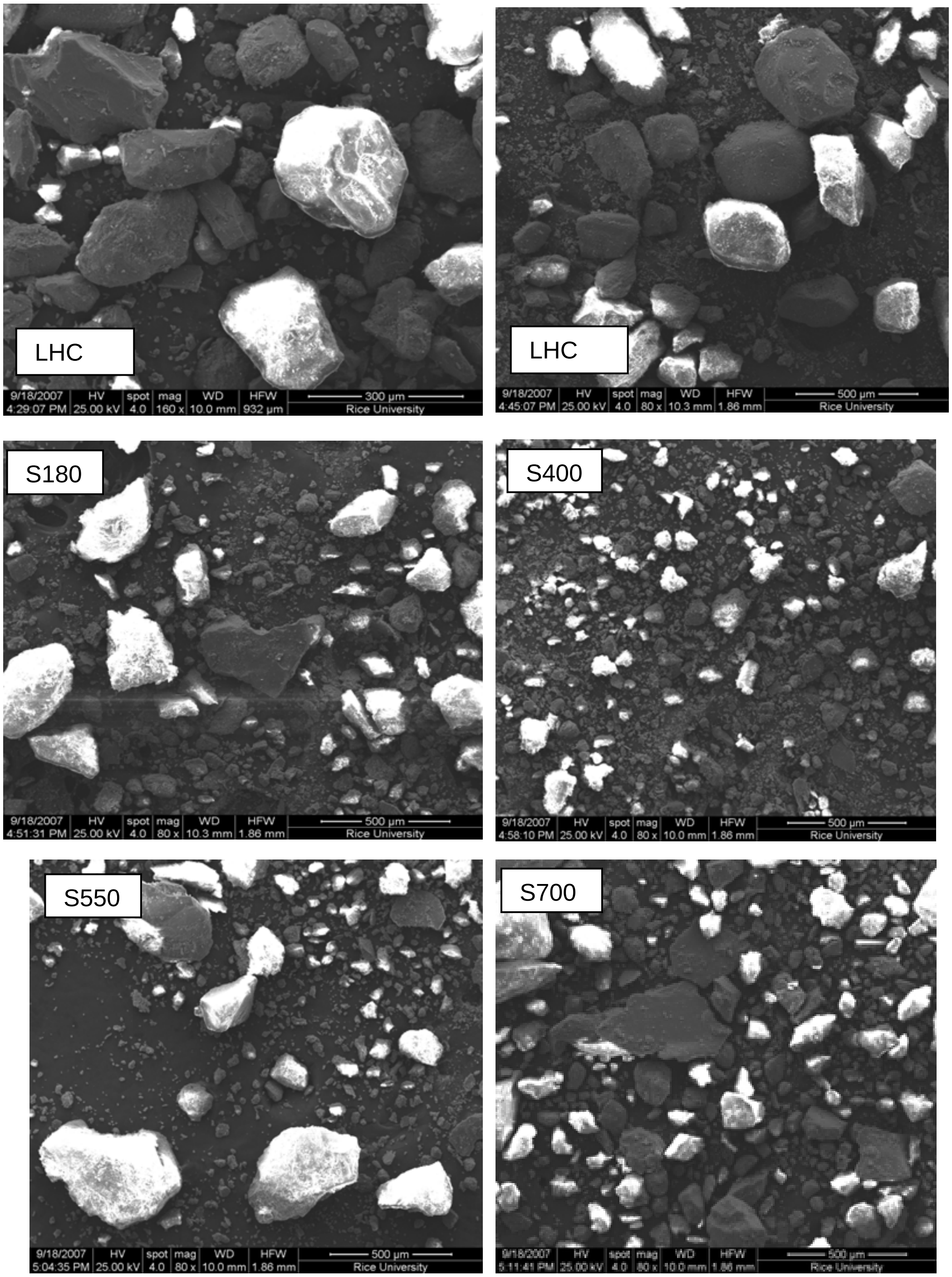

FIGURE A-3. SEM images of soil samples.

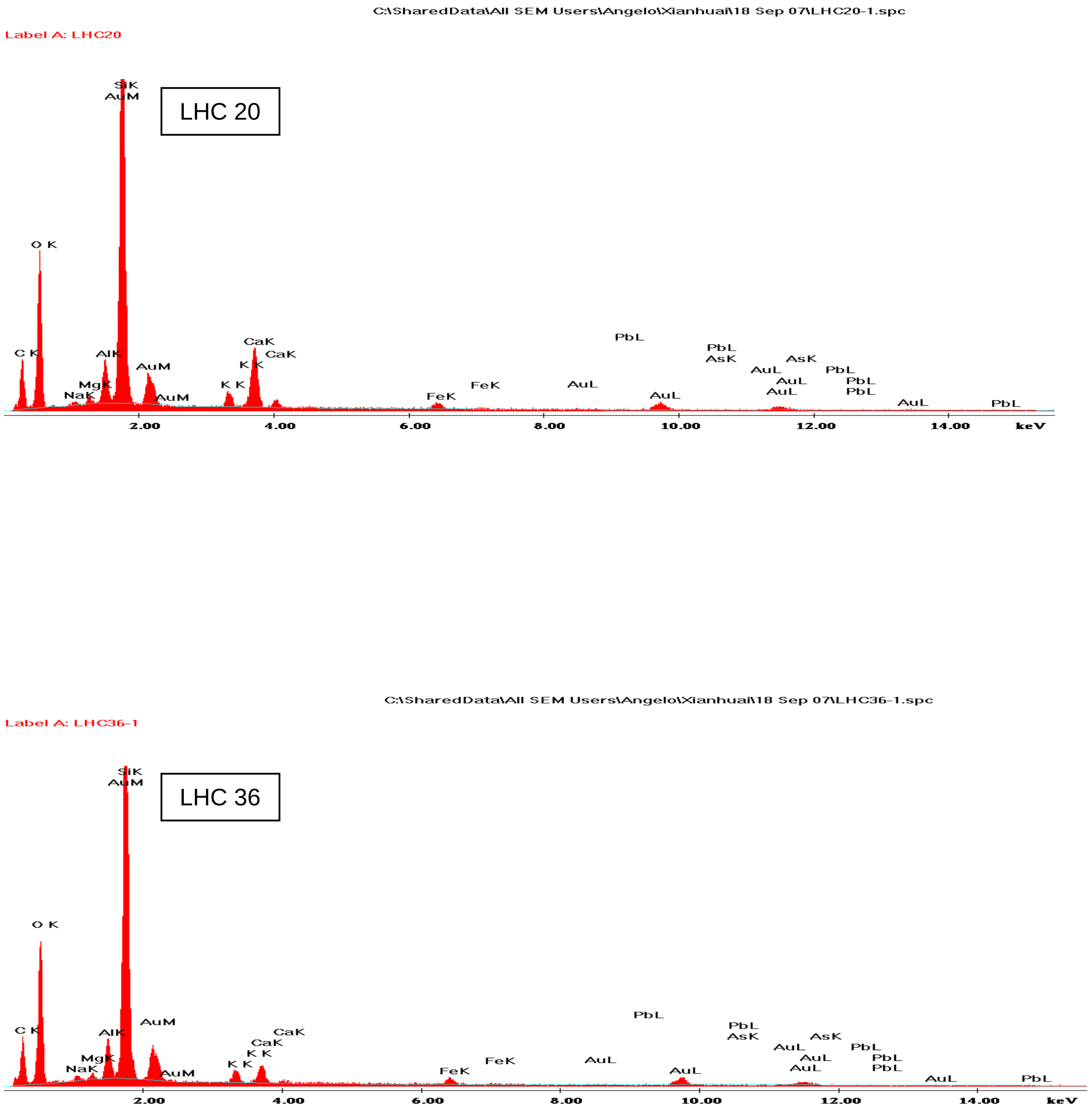

FIGURE A-4. EDAX analysis of soil samples.

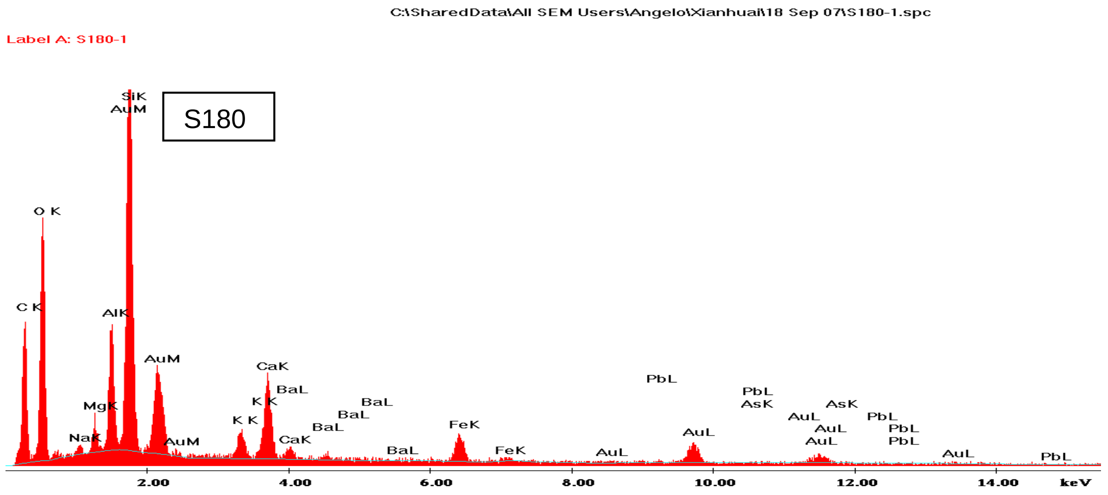

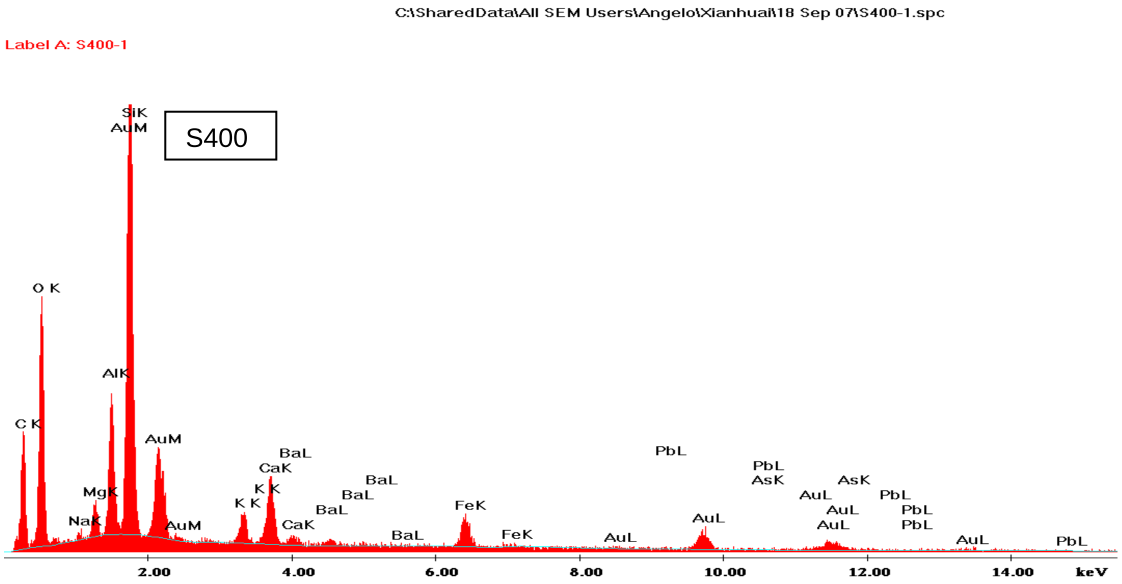

FIGURE A-4. ***Continued.***

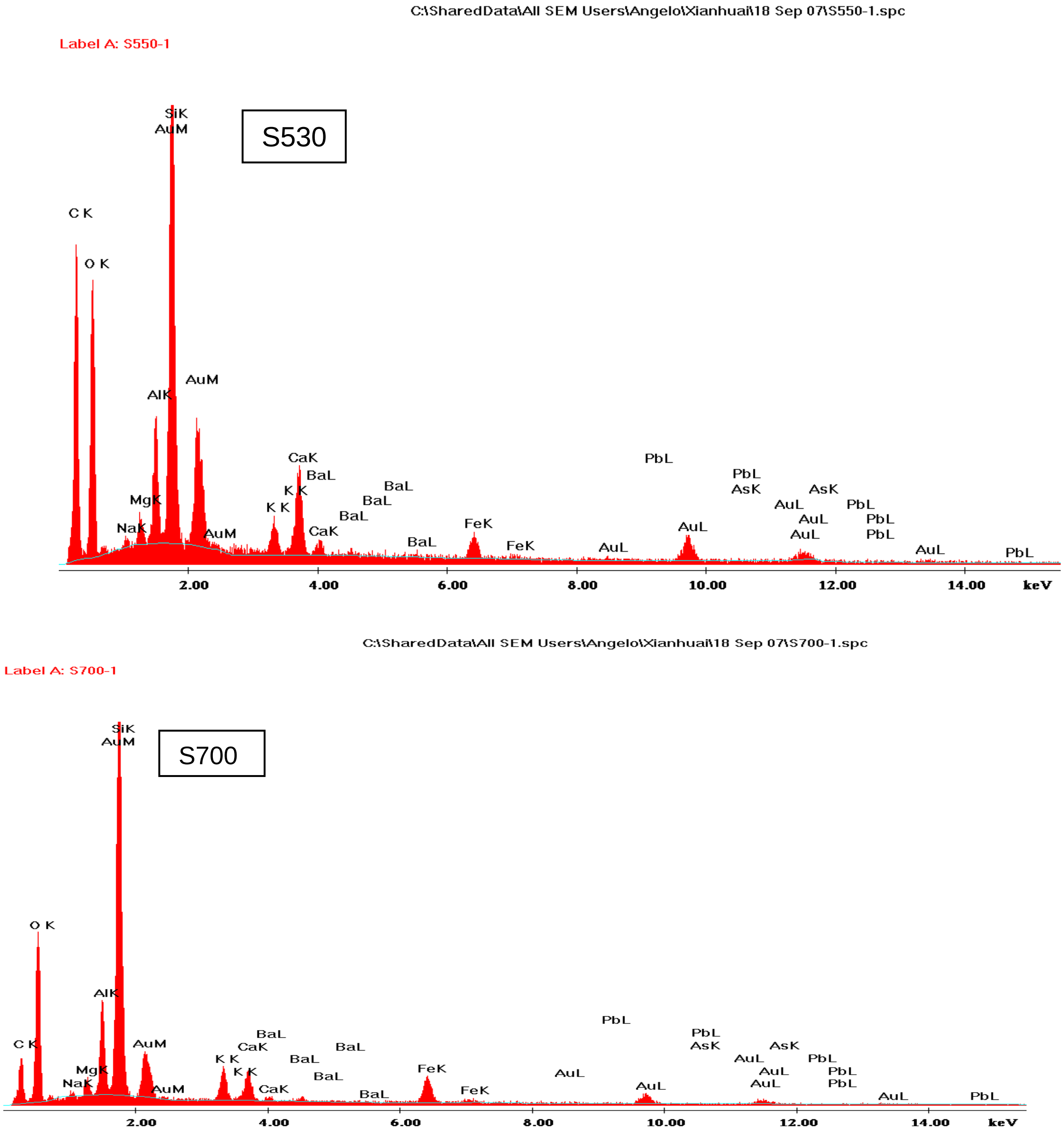

FIGURE A-4. ***Continued.***

REFERENCES

Agbenin, J. O.; Olojo, L. A. Competitive adsorption of copper and zinc by a Bt horizon of a savanna Alfisol as affected by pH and selective removal of hydrous oxides and organic matter. *Geoderma* **2004**, *119,* 85–95.

Allen, H. E., Ed. *Metal Contaminated Aquatic Sediments;* Ann Arbor Press, Inc.: Chelsea, MI, 1995; p 292.

Alloway, B. J. *Heavy Metals in Soils;* John Wiley & Sons: New York, 1990.

AMEC Earth and Environmental. *Northeast Valley Aquifer Management Study;* AMEC Earth and Environmental: Calgary, Alberta, Canada, February 2005.

Anderson, M. C.; Ferguson, J. F.; Gavis, J. Arsenate adsorption on amorphous aluminum hydroxide. *J. Colloid Interface Sci*. **1976,** *54,* 391–399.

Ang, W. S.; Lee, S; Elimelech, M. Chemical and physical aspects of cleaning of organic-fouled reverse osmosis membranes. *J. Membr. Sci*. **2006,** *272,* 198–210.

Arias, M. Adsorption and desorption of copper and zinc in the surface layer of acid soils. *J. Colloid Interface Sci.* **2005,** *288,* 21–29.

Backstrom, M.; et al. Mobilisation of heavy metals by deicing salts in a roadside environment. *Water Res*. **2004,** *38,* 720–732.

Baker, L. A.; Qureshi, T.; Wyman, M. Sources and fate of arsenic in the Salt and Verde Rivers, Arizona. *Water Resour. Res.* **1998,** *34,* 1543–1552.

Banin, A.; et al. Geochemical Processes in Recharge Basin Soils Used for Municipal Effluents Reclamation by the Soil-Aquifer Treatment (SAT) System. In *Management of Aquifer Recharge for Sustainability;* Dillon, P. J., Ed.; A. A. Blakema: Rotterdam, The Netherlands, 2002; pp 327–332.

Ben-Dor, E.; Banin, A. Determination of organic matter content in arid-zone soils using a simple “loss-on-ignition” method. *Commun. Soil Sci. Plant Anal*. **1989,** *201,* 1675–1695.

Benjamin, M. M.; Leckie, J. O. Multiple-site adsorption of Cd, Zn, and Pb on amorphous iron oxyhydroxide. *J. Colloid Interface Sci*. **1981,** *79,* 209–221.

Bermond, A.; Yousfi, I.; Ghestem, J. P. Kinetic approach to the chemical speciation of trace metal in soils. *Analyst* **1998,** *123,* 785–789.

Bordas, F.; Bourg, A. C. M. Effect of complexing agents (EDTA and ATMP) on the remobilization of heavy metals from a polluted river sediment. *Aquat. Geochem.* **1998,** *4,* 201–214.

Bose, P.; Reckhow, D. A. Modeling pH and ionic strength effect on proton and calcium complexation of fulvic acid: a tool for drinking water-NOM studies. *Environ. Sci. Technol.* **1997,** *31,* 765–770.

Boulegue, J.; Lord, C. J.; Church, T. M. Sulfur speciation and associated trace metals (Fe, Cu) in the porewaters of Great Marsh, DE. *Geochim. Cosmochim. Acta* **1982,** *46,* 453–464.

Bouwer, H. *Groundwater Hydrology;* McGraw-Hill: New York, 1978; p 480.

Bouwer, H.; Chaney, R. L. Land treatment of wastewater. *Adv. Agron*. **1974,** *26,* 133–176.

Bradbury, M. H.; Baeyens, B. Modelling the sorption of Zn and Ni on Ca-montmorillonite. *Geochim. Cosmochim. Acta* **1999,** *63,* 325–336.

Carlson, R. R.; et al. Rapid infiltration treatment of primary and secondary effluent. *J.—Water Pollut. Control Fed.* **1982,** *54,* 270–280.

Cengiz, S.; Karaca, A. C.; Cakır, I.; Uner, H. B.; Sevindik, A. SEM–EDS analysis and discrimination of forensic soil. *Forensic Sci. Int*. **2004,** *141,* 33–37.

Clement, T. P. *RT3D: a Modular Computer Code for Simulating Reactive Multi-Species Transport in 3-Dimensional Groundwater Aquifers;* PNNL-SA-11720; Pacific Northwest National Laboratory: Richland, WA, 1997.

Clement, T. P.; Sun, Y.; Hooker, B. S.; Petersen J. N. Modeling multi-species reactive transport in groundwater aquifers. *Ground Water Monit. Rem.*, **1998**. 18, 2, 79- 92.

Clement, T. P.; Johnson, C. D.; Sun, Y.; Klecka, G. M.; Bartlett, C. Natural attenuation of chlorinated solvent compounds: Model development and field-scale application. *J. Contam. Hydrol.,* **2000**. 42, 113-140.

Crook, J., *Water Reclamation*, in *Encyclopedia Physical Science and Technology*, R.A. Meyer, Eds. Academic Press: San Diego, CA, **1992**, 559-589.

Davis, J. A.; Kent, D. B. Mineral-Water Interface Geochemistry. In *Reviews in Mineralogy*, Hochella, M. F., White, A. F., Eds.; Mineralogical Society of America: Washington DC, 1990; pp 177–260.

Elprince, A. M.; Sposito, G. Thermodynamic derivation of equations of the Langmuir type for ion equilibria in soils. *Soil Sci. Soc. Am. J.* **1981,** *45,* 277–282.

Fangueiro, D.; Bermond, A.; Santos, E.; Carapuc, H.; Duarte, A. Kinetic approach to heavy metal mobilization assessment in sediments: choose of kinetic equations and models to achieve maximum information. *Talanta* **2005,** *66,* 844–857.

Filella, M.; Town, R. M. Heterogenity and lability of Pb(II) complexation by humic substances: practical interpretation tools. *Fresenius' J. Anal. Chem.* **2001,** *370,* 413–418.

Gardner, L. R. Organic versus inorganic trace metal complexes in sulfidic marine waters—some speculative calculations based on available stability constants. *Geochim. Cosmochim. Acta* **1974,** *38,* 1297–1302.

Ghosh, A.; Sáez, A. E.; Ela, W. Effect of pH, competitive anions and NOM on the leaching of arsenic from solid residuals. *Sci. Total Environ*. **2006,** *363,* 46–59.

Giblin, A. E.; Valiela, I.; Luther, G. W. Trace metal solubility in salt marsh sediments contaminated with sewage sludge. *Estuar. Coastal Shelf Sci.* **1986,** *23,* 477–498.

Glaus, M. A.; Hummel, W.; Van Loon, L. R. Trace metal-humate interations: I. Experimental determination of conditional stability constants. *Appl. Geochem*. **2000,** *15,* 953–973.

Griffin, R. A.; Shimp, N. F. *Attenuation of Pollutants in Municipal Landfill Leachate by Clay Mineral;* EPA-600/2-78-157; U.S. Environmental Protection Agency, U.S. Government Printing Office: Washington, DC, 1978.

Haley, S. M.; Tappin, A. D.; Bond, P. R.; Fitzsimons, M. F. A comparison of SEM-EDS with ICP-AES for the quantitative elemental determination of estuarine particles. *Environ. Chem. Lett*. **2006,** *4,* 235–238.

Han, F. X.; Banin, A. Long-term transformations and redistribution of potentially toxic heavy metals in arid-zone soils. I. Under saturated conditions. *Water Air Soil Pollut.* **1997,** *95,* 399–423.

Harter, R. D. Competitive sorption of cobalt, copper, and nickel ions by a calcium saturated soil. *Soil Sci. Soc. Am. J.* **1992,** *56,* 444–449.

Harter, R. D.; Lehmann, R. G. Use of kinetics for the study of exchange reactions in soils. *Soil Sci. Soc. Am. J.* **1983,** *47,* 666–669.

Hickey, M. G.; Kittrick, J. A. Chemical partitioning of cadmium, copper, nickel, and zinc in soils and sediments containing high levels of heavy metals. *J. Environ. Qual*. **1984,** *13,* 372–376.

Hingston, F. J.; Posner, A. M.; Quick, J. P. Competitive adsorption of negatively charged ligands on oxide surfaces. *Discuss. Faraday Soc.* **1971,** *52,* 334–342.

Johnson, J. S.; Baker, L. A.; Fox, P. Geochemical transformations during artificial groundwater recharge: soil-water interactions of inorganic constituents. *Water Res.* **1999,** *33,* 196–206.

Jones, N.L., GMS v3.1 Reference Manual, Environmental Modeling Research Laboratory, Brigham Young University, Provo, Utah, **2000**.

Kelly, W. R. Arsenic in glacial aquifers: sources and geochemical controls. *Ground Water* **2005,** *43,* 518–530.

Kjoller, C.; Postma, D.; Larsen, F. Groundwater acidification and the mobilization of trace metals in a sandy aquifer. *Environ. Sci. Technol.* **2004,** *38,* 2829–2835.

Lance, J. C.; Rice, R. C.; Gilbert, R. G. Renovation of sewage water by soil columns flooded with primary effluent. *J.—Water Pollut. Control Fed.* **1980,** *52,* 381–388.

Langford, C. H.; Cook, R. L. Kinetic versus equilibrium studies for the speciation of metal complexes with ligands from soil and water. *Analyst* **1995,** *120,* 591–596.

Lin, C. Y.; Shacahr, Y.; Banin, A. Heavy metal retention and partitioning in a large-scale soil-aquifer treatment (SAT) system used for wastewater reclamation. *Chemosphere* **2004,** *57,* 1047–1058.

Lion, L. W.; Altmann, R. S.; Leckie, J. O. Trace-metal adsorption characteristics of estuarine particulate matter: evaluation of contributions of Fe/Mn oxide and organic surface coatings. *Environ. Sci. Technol.* **1982,** *16,* 660–676.

Lippold, H.; Muller, N.; Kupsch, H. Effect of humic acid on the pH-dependent adsorption of terbium(III) onto geological materials. *Appl. Geochem.* **2005,** *20,* 1209–1217.

McDonald, M. G., Harbaugh, A. W. A Modular Three-Dimensional Finite-Difference Ground-Water Flow Model. *Techniques of Water-Resources Investigations of the United States Geological Survey;* TWRI 6-A1; U.S. Government Printing Office: Washington, DC, 1984.

McLean, J. E.; Bledsoe, B. E. Behavior of Metals in Soils. *Ground Water Issue;* EPA/540/S-92/018, U.S. Environmental Protection Agency, U.S. Government Printing Office: Washington, DC, 1992.

Morel, F. M. M.; Hering, J. G. *Principles and Applications of Aquatic Chemistry;* Wiley-Interscience: New York, 1993; p 608.

Murray, J. W. Interaction of metal-ions at manganese dioxide solution interface. *Geochim. Cosmochim. Acta* **1975,** *39,* 505–519.

National Research Council. *Groundwater Recharge Using Waters of Impaired Quality;* National Academy Press: Washington, DC, 1994.

Nelson, D. W.; Sommers, L. E. A rapid and accurate procedure for estimation of organic carbon in soil. *Proc. Indiana Acad. Sci.* **1975,** *84,* 456–462.

Page, A. L., Miller, R. H., Keeney, D. R., Eds. *Methods of Soil Analysis,* 2nd ed.; American Society of Agronomy: Madison, WI, 1982; Vol. 9, p 1159.

Patrick, W. H., Jr.; Mahapatra, A. K. Transformation and availability of nitrogen and phosphorus in water-logged soils. *Adv. Agron.* **1968,** *20,* 323–359.

Pierce, M. L.; Moore, C. B. Adsorption of arsenite on amorphous iron hydroxide from dilute aqueous solution. *Environ. Sci. Technol.* **1980,** *14,* 214–216.

Polemio, M.; Rhoades, J. D. Determining cation exchange capacity: a new procedure for calcareous and gypsiferous soils. *Soil Sci. Soc. Am. J.* **1977,** *41,* 524–528.

Prado, A. G. S.; Airoldi, C. Humic acid-divalent cation interactions. *Thermochim. Acta* **2003,** *405,* 287–292.

Rice, R. C.; Bouwer, H. Soil-aquifer treatment using primary effluent. *J.—Water Pollut. Control Fed.* **1984,** *56,* 84–88.

Righi, D.; Elsass, F. Characterization of soil clay minerals: decomposition of X-ray diffraction diagrams and high-resolution electron microscopy. *Clays Clay Miner.* **1996,** *44,* 791–800.

Schmitt, D.; Muller, M. B.; Frimmel, F. H. Metal distribution in different size fractions of natural organic matter. *Acta Hydrochim. Hydrobiol.* **2000,** *28,* 400–410.

Shuman, L. M. Chemical Forms of Micronutrients in Soils. In *Micronutrients in Agriculture* Mortvedt, J. J., et al., Eds.; The Soil Science Society of America Book Series No. 4; Soil Science Society of America: Madison, WI, 1991; pp 113–144.

Simon, P. *Tapped Out: The Coming World Crisis in Water and What We Can Do about It;* 2nd ed.; Welcome Rain: New York, 1998.

Sparks, D. L. *Kinetics of Soil Chemical Processes;* Academic Press: San Diego, CA, 1989.

Streck, T.; Richter, J. Heavy metal displacement in a sandy soil at the field scale: II. Modeling. *J. Environ. Qual*. **1997,** *26,* 49–56.

Sun, Y.; Clement, T. P. A decomposition method for solving coupled multispecies reactive transport problems. *Transp. Porous Media* **1999,** *37,* 327–346.

Sun, Y.; Petersen, J. N.; Clement, T. P.; Hooker, B. S. Effects of reaction kinetics on predicted concentration profiles during subsurface bioremediation. *J. Contam. Hydrol.* **1998**, *31,* 359–372.

Todd, D. K. *Groundwater Hydrology,* 2nd ed.; Wiley: New York, 1980.

Treweek, G. P. Pretreatment Processes for Groundwater Recharge. In *Artificial Recharge of Groundwater;* Asano, T., Ed.; Butterworth: Boston, MA, 1985; pp 205–248.

Weng, C. H. Chromium leaching behavior in soil derived from chromite ore processing waste. *Sci. Total Environ*. **1994,** *154,* 71–86.

Yu, J.; Klarup, D. Extraction kinetics for copper, zinc, iron, and manganese from contaminated sediment using disodium ethylenediaminetetraacetate. *Water Air Soil Pollut.* **1994,** *75,* 205–225.

Zhou, P.; Yan, H.; Gu, B. H. Competitive complexation of metal ions with humic substances. *Chemosphere* **2005,** *58,* 1327–1337.

Advancing the Science of Water Reuse and Desalination

WATEREUSE FOUNDATION

1199 North Fairfax Street, Suite 410
Alexandria, VA 22314 USA
(703) 548-0880
Fax (703) 548-5085
E-mail: Foundation@WateReuse.org
www.WateReuse.org/Foundation